N74-12555

NASA CR-112238

NON-CLASSICAL ADHESIVE-BONDED JOINTS IN PRACTICAL AEROSPACE CONSTRUCTION

TECHNICAL REPORT

by

L. J. HART-SMITH

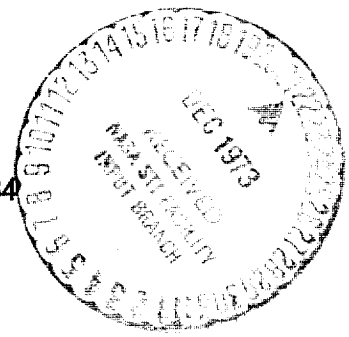

Prepared under Contract NAS1-11234
Douglas Aircraft Company
McDonnell Douglas Corporation
3855 Lakewood Blvd
Long Beach, California 90846

January 1973

for

Langley Research Center
Hampton, Virginia 23366

NATIONAL AERONAUTICS AND SPACE ADMINISTRATION

NASA CR 112238

NON-CLASSICAL ADHESIVE-BONDED JOINTS IN PRACTICAL AEROSPACE CONSTRUCTION

TECHNICAL REPORT

by

L. J. HART-SMITH

Prepared under Contract NAS1-11234
Douglas Aircraft Company
McDonnell Douglas Corporation
3855 Lakewood Blvd
Long Beach, California 90846

JANUARY 1973

for

Langley Research Center
Hampton, Virginia 23366

NATIONAL AERONAUTICS AND SPACE ADMINISTRATION

ABSTRACT

Solutions are derived for adhesive-bonded joints of non-classical geometries. Particular attention is given to bonded doublers and to selective reinforcement by unidirectional composites. Non-dimensionalized charts are presented for the efficiency limit imposed on the skin as the result of the eccentricity in the load path through the doubler. It is desirable to employ a relatively large doubler to minimize the effective eccentricity in the load path. The transfer stresses associated with selective reinforcement of metal structures by advanced composites are analyzed. Reinforcement of bolt holes in composites by bonded metal doublers is covered quantitatively. Also included is the adhesive joint analysis for shear flow in a multi-cell torque box, in which the bond on one angle becomes more critical sooner than those on the others, thereby restricting the strength to less than the total of each maximum strength when acting alone. Adhesive plasticity and adherend stiffness and thermal imbalances are included. A simple analysis/design technique of solution in terms of upper and lower bounds on an all-plastic adhesive analysis is introduced. This is far simpler than the more precise elastic-plastic adhesive analysis and, in most cases is of adequate accuracy. An analysis of tapered-lap bonded joints is included and this shows how to alleviate the peel-stress problem characteristic of thick uniform double-lap joints. The tapered-lap joints remain fully efficient for thicknesses above which the uniform double-lap joint becomes inefficient. Illustrative examples are included throughout the text.

KEYWORD DESCRIPTORS

Bonded Joints
Adhesive Stresses and Strains
Bonded Doublers
Selective Reinforcement
Tapered-Lap Joints
Peel Stresses
Bolt-Hole Reinforcement
Advanced Composite Joints

FOREWORD

This report was prepared by the Douglas Aircraft Company, McDonnell Douglas Corporation, Long Beach, California under the terms of Contract NAS1-112234. One summary report (NASA CR 2218) and four technical reports (NASA CR 112235, -6, -7, and -8) cover the work, which was performed between November 1971 and January 1973. The program was sponsored by the National Aeronautics and Space Administration's Langley Research Center, Hampton, Virginia. Dr. M. F. Card and Mr. H. G. Bush were the Contracting Agency's Technical Monitors.

CONTENTS

ILLUSTRATIONS

SYMBOLS

A,B,C,F	=	Integration constants
A	=	Cross-sectional area of adherend (in.^{2})
D	=	Flexural rigidity of adherends (lb in.^{2})
d	=	Length of elastic zone in adhesive bond (in.)
E	=	Young's modulus (longitudinal) for adherend (psi)
E_c, E_c'	=	Adhesive peel (transverse tension) modulus (psi)
e	=	Edge distance (in.)
G	=	Adhesive shear modulus for elastic-plastic representation (psi)
G_1, G_2, etc.	=	Adherend in-plane shear moduli (psi)
k	=	Bending stress coefficient
k	=	Load sharing factor (Figure 12)
k_b	=	$D / [Et^3 / 12(1 - \nu^2)]$ = bending stiffness factor for composite adherends
L, ℓ	=	Overlap (length of bond) (in.)
M	=	Bending moment in adherend (lb in. / in.)
P	=	Applied direct load on entire joint (lb / in.)
S	=	Shear stress resultant (in-plane) in adherend (lb / in.)
s	=	Co-ordinate in plane of adhesive layer (in.)
T	=	Temperature (°F)
ΔT	=	Temperature change ($T_{operating} - T_{cure}$) (°F)
t	=	thickness of adherend (in.)
V	=	Transverse shear force on adherend (lb / in.)
w	=	Transverse deflection of adherend (in.)
w	=	Width of bond-line (in.)
x	=	Axial (longitudinal) co-ordinate parallel to direction of load (in.)

α = Coefficient of thermal expansion (/°F)

γ = Adhesive shear strain

γ_e = Elastic adhesive shear strain

γ_p = Plastic adhesive shear strain

δ = Axial (longitudinal) and in-plane (shear) displacement of adherend (in.)

ξ,ζ = Axial co-ordinates (different origin and/or sense from x) (in.)

η = Thickness of adhesive layer (in.)

λ = Exponent of elastic shear stress distribution ($in.^{-1}$)

ν = Poisson's ratio for adherend(s)

ξ = $\sqrt{(P/D)}$ = Bending stiffness parameter ($in.^{-1}$)

σ_c = Peel stresses in adhesive (psi)

$\sigma_{max},\sigma_{avg}$ = Maximum and average adherend stresses (psi)

τ = Adhesive shear stress (psi)

τ_{av} = Average adhesive shear stress (psi)

τ_p = Plastic adhesive shear stress (psi)

SUBSCRIPTS

a,c = Adhesive (cement)

c,m = Composite and metal adherends

n = Property normal to plane of adherends

r = Residual value (due to thermal mismatch)

t,c,s = Tension, compression and shear with respect to applied load

u,t = Uniform and tapered adherends

d,s = Doubler and skin, respectively

1,2, to 7 = Regions into which joint is subdivided for purposes of analysis

SUMMARY

It is not usual to find adhesive bonded joints in aerospace structures which conform precisely to the geometry and load conditions of the classical classes of joints on which tests are performed. The objective of this report is to apply to practice some of the analysis/design capability developed by the elastic-plastic formulation of the classical (double-lap, single-lap, stepped-lap, and scarf) joints. Particular attention is devoted to bonded doublers, with a range of end support conditions. Non-dimensionalized charts are presented for the efficiency limit imposed on the skin as the result of the eccentricity in the load path through the doubler. It is desirable to employ a relatively large doubler to minimize the effective eccentricity in the load path. In addition, consideration is given to the selective reinforcement of metal structures by unidirectional composites and of composites by bonded metal doublers around bolt holes. In the former case, the key issue is the load transfer at the end of the composite reinforcement while, in the latter case, the usual problem is that of load transfer between the metal doubler and the composite part. Also to be found in this report is an analysis of the bond stress and strain distributions for shear flow in a multi-cell torque. A technique of alleviating the peel-stress problem for thick uniform double-lap joints is described and analyzed. The optimum tapering of the outer adherends is shown to eliminate the peel problem while adding 24 per cent to the bond shear strength.

Adhesive plasticity and adherend stiffness and thermal imbalances are accounted for. A simple analysis/design technique of solution in terms of upper and lower bounds on an all-plastic adhesive analysis is introduced. This is far simpler than the more precise elastic-plastic adhesive analysis and, in most cases, is of adequate accuracy. Indeed, in many cases such solutions are simpler than a perfectly-elastic method. Consequently, analytical solutions can be obtained for a far graeter range of joint configurations and complex load conditions than is possible with more precise methods.

Illustrative examples are included throughout the text to explain how to employ the analyses derived.

1. INTRODUCTION

It is unusual in the design of aircraft and space vehicles to encounter an adhesive-bonded joint of precisely one of the classical families of analysis such as the double-lap joint, the single-lap joint, the scarf joint, and the stepped-lap joint. It is even more unusual to encounter simultaneously a pure form of load application, such as tensile lap shear which is the basic test condition. The differences in load capacities for compressive lap-shear and in-plane shear are discussed in companion reports (References 1, 2, and 3).

The purpose of this report is to apply the basic analysis techniques established in References 1, 2, and 3 for double-lap single-lap, and scarf and stepped-lap joints, respectively, to joint configurations more frequently encountered in aerospace practice.

Perhaps the most numerous applications of adhesive bonding are to be found in the form of bonded edge doublers for flush mechanical attachments. Such applications share many of the governing equations for unsupported single-lap joints. The limiting characteristic is usually not that of adhesive shear or peel but of the non-uniform load distribution across the thickness of the main sheet just outside of the doubler. It has long been known that the doubler must be flexible in bending at its tip to diffuse load transfer gradually. This is why feathered edges and fingered doublers are so widely employed. The analyses here confirm the need for such procedures and provide a rational basis for design.

Another application, of growing importance in the form of metal structures selectively reinforced with advanced filamentary composites, is that of a bonded-on area doubler, usually unidirectional unless it is thick. Such doublers are quite distinct from edge doublers inasmuch as the latter serve principally to reduce a stress level locally while the former are more of the principal load path type of structure. As such it is usual to minimize the eccentricities in the load path, to provide moment-resistant supports, and aim for the much higher efficiencies of double-lap joints. The key problem with this class of bonded structure is usually that of load transfer at the ends. If the area of the bonded-on doubler is too large in proportion to the bond

area, the weak link will be the shear capacity of the adhesive at the ends of the doubler.

A common problem in composite structures is that of bonded metal doublers in an area of mechanical attachments. An analysis technique and illustrative example are provided.

The fourth class of non-classical adhesive-bonded joints is concerned with the transfer of in-plane shear loads. The pure form of this problem, from one member to another, is covered in References 1 and 3. (The single-lap case is governed by the analyses of Reference 1 for this situation.) The analytically more challenging problem arises in multi-cell torque boxes, such as aircraft wings. The best known illustrative example is that of a wing skin to spar web attachment, with a change in skin shear flow at the intersection. The boundary conditions for each leg of such a joint differ from those of a single-transfer joint, but the governing equations are of the same form. A related problem also covered by the analysis in this report (with appropriate boundary conditions) is that of the shear flow between a spar (beam) web and a concentrated cap.

Approximate analysis techniques for combined loading on joints are suggested. These are based on the concept of the maximum adhesive shear strain being the square rooot of the sum of the squares of orthogonal strain components.

In the more complicated joint configurations it does not prove practical to perform precise elastic-plastic analyses. It is quite effective to obtain simpler solutions in terms of upper and lower bounds by means of perfectly-plastic adhesive analyses. The simplification arises from the elimination of the "boundary" conditions at each of the elastic-to-plastic transitions. This simplification is even more powerful than just a reduction in number of boundary conditions because the location of such transitions is not known at the start of an analysis and, furthermore, it shifts as the load intensity is changed. (See References 1, 2, and 3). Further justification for this technique is provided by the fact that, for ultimate static load, the upper and lower bounds are quite close together for the ductile adhesives used in subsonic commercial aircraft structures. Even though such bounds are further apart for the brittle adhesives needed for high-temperature zones on supersonic aircraft, they

represent a considerable improvement over the blanket application of a uniform shear stress developed from single-lap shear tests. This report, in conjunction with the companion References 1, 2, and 3 provides all the background and techniques necessary for a more precise elastic-plastic analysis if ever needed.

The report concludes with a description of a powerful technique to obtain peel-stress relief for thick uniform double-lap adherends. This consists of tapering the outer adherends to make them flexible at the tip in order to prevent the peel stresses from ever developing. This technique has been used in practice for a considerable time. By means of the fully-plastic analysis method outlined above, it was possible to determine the optimum proportions to not only achieve peel-stress relief but also to simultaneously maximize the shear transfer capacity of the tapered-lap bonded joint.

2. ADHESIVE-BONDED DOUBLERS

One of the most frequent applications of adhesive bonding in aircraft structures is that of bonded edge doublers. Two important applications are the build up in thickness to permit the use of flush fasteners in thin gage sheet metal and the fingered or feathered-edge doublers around panels subjected to accoustic fatigue loads. In either case, the bond itself is not usually the limiting element in the strength of the structure. The adhesive shear load can usually be developed in about half an inch or so of plastic zones (while the overlaps are typically very much greater) and typical design practice excludes substantial differences in thickness at the edge of the doubler (and thereby minimizes any potential peel-stress problems). The dominant limiting feature is the eccentricity in load path when a doubler can be fitted on one side only of the structure as is the case for external skins. The relevant analyses are akin to those for the single-lap joint (Reference 2).

2.1 Adherend Stresses in Adhesive-Bonded Doublers

It is customary to make fingered doublers less thick than the skin to which they are bonded (typically 0.6 times as thick or one skin gage less if very thin). Therefore, with reference to the single-lap joint analysis of Reference 2, equation (152) is of interest here rather than the moment at the other end of the single-lap joint which dominates that analysis. The distance (c - e) in equation (152) of Reference 2 refers to the distance between the point of inflexion (M = 0) and the edge of the doubler and may consequently be less than the total overlap. Here, the end-support condition selected for analysis is that of the skin/doubler combination being built in. Also, the analysis of Reference 2 is adapted to provide for simply-supported ends. A comparison of the two sets of answers so derived indicates that the former is related to the latter by a factor of 2 (to some five or six significant figures) in the extent of the overlap. Other end-support conditions can therefore be analyzed by interpolation.

The geometry governing the present analysis is defined in Figure 1. The load is assumed to be reacted at the neutral axis of the skin/doubler combination. It is easily shown that this stiffness "centroid" is located at a distance from the middle of adherend 4 of

$$EC_4 = \frac{\frac{1}{2}(t_1 + t_4 + 2\eta)}{\left(1 + \frac{E_4 t_4}{E_1 t_1}\right)} \quad . \tag{1}$$

Throughout the adherend 4, outside the overlap, the longitudinal stress resultant (force per unit lateral width) is uniform, at the value P of the applied load. The stress couple M_4, per unit width, is then defined by the equilibrium equation

$$M_4 = P\left[\frac{(t_1 + t_4 + 2\eta)}{(\ell_4 + \ell_d)\left(1 + \frac{E_4 t_4}{E_1 t_1}\right)}\left(\frac{x_4}{2}\right) - w_4\right] \quad \text{for } -\ell_4 \leq x_4 \leq 0. \tag{2}$$

The classical theory for the infinitesimal deformation of thin, cylindrically

bent plates then yields

$$\frac{d^2w_4}{dx_4^2} = -\frac{M_4}{D_4} = -\frac{P}{D_4}\left[\frac{(t_1 + t_4 + 2\eta)}{(\ell_4 + \ell_d)\left(1 + \frac{E_4t_4}{E_1t_1}\right)}\left(\frac{x_4}{2}\right) - w_4\right] \quad , \tag{3}$$

whence

$$w_4 = A_4 \cosh(\xi_4 x_4) + B_4 \sinh(\xi_4 x_4) + \frac{(t_1 + t_4 + 2\eta)}{(\ell_4 + \ell_d)\left(1 + \frac{E_4t_4}{E_1t_1}\right)}\left(\frac{x_4}{2}\right) \quad , \tag{4}$$

where

$$\xi_4^2 = \frac{P}{D_4} = \frac{12P(1 - \nu_4^2)}{(k_b)_4 E_4 t_4^3} \quad . \tag{5}$$

The assumption of negligible moment restraint at $x_4 = 0$ (or, equivalently, that ℓ_4 is so large in comparison with ℓ_d that the precise nature of the end condition is immaterial) prescribes that

$$A_4 = 0 \quad . \tag{6}$$

The behavior of regions 2 and 3 (Figure 1) is governed by precisely the same equations as for the single-lap joint analysis (Reference 2), with the exception that, here, at $s = 0$ the boundary conditions differ. The equations are set up simply as

$$\left.\begin{aligned} \frac{dM_2}{ds} - V_2 + \tau\left(\frac{t_1 + \eta}{2}\right) = 0 \\ \frac{dM_3}{ds} - V_3 + \tau\left(\frac{t_4 + \eta}{2}\right) = 0 \end{aligned}\right\} , \tag{7}$$

$$\left.\begin{aligned} \frac{dT_2}{ds} + \tau = 0 \\ \frac{dT_3}{ds} - \tau = 0 \end{aligned}\right\} , \tag{8}$$

$$\left.\begin{aligned} \frac{dV_2}{ds} + \sigma_c &= 0 \\ \frac{dV_3}{ds} - \sigma_c &= 0 \end{aligned}\right\}, \tag{9}$$

$$\left.\begin{aligned} \frac{d^2w_2}{ds^2} &= -\frac{M_2}{D_1} = -\frac{12M_2(1-\nu_1^2)}{(k_b)_1 E_1 t_1^3} \\ \frac{d^2w_3}{ds^2} &= -\frac{M_3}{D_4} = -\frac{12M_3(1-\nu_4^2)}{(k_b)_4 E_4 t_4^3} \end{aligned}\right\}. \tag{10}$$

As in Reference 2 it is necessary to use the approximations

$$w_2 \simeq w_3 \quad , \qquad \frac{dw_2}{ds} \simeq \frac{dw_3}{ds} \tag{11}$$

while maintaining the distinction between the higher derivatives. From the equations above,

$$\frac{d^2(w_2 + w_3)}{ds^2} = -\frac{M_2}{D_1} - \frac{M_3}{D_4} \quad , \tag{12}$$

$$\frac{d^3(w_2 + w_3)}{ds^3} = -\frac{V_2}{D_1} + \frac{\tau}{D_1}\left(\frac{t_1 + \eta}{2}\right) - \frac{V_3}{D_4} + \frac{\tau}{D_4}\left(\frac{t_4 + \eta}{2}\right) \quad , \tag{13}$$

$$\frac{d^4(w_2 + w_3)}{ds^4} = \frac{\sigma_c}{D_1} - \frac{\sigma_c}{D_4} + \left(\frac{t_1 + \eta}{2D_1} + \frac{t_4 + \eta}{2D_4}\right)\frac{d\tau}{ds} \quad , \tag{14}$$

$$\frac{d^2(w_2 - w_3)}{ds^2} = -\frac{M_2}{D_1} + \frac{M_3}{D_4} \tag{15}$$

and, since for an adhesive obeying a linear elastic law in tension (peeling)

$$\frac{\sigma_c}{E_c} = \frac{(w_3 - w_2)}{\eta} \quad , \tag{16}$$

$$\frac{d^4(w_2 - w_3)}{ds^4} = -\left(\frac{1}{D_1} + \frac{1}{D_4}\right)\frac{E_c}{\eta}(w_2 - w_3) + \left(\frac{t_1 + \eta}{2D_1} - \frac{t_4 + \eta}{2D_4}\right)\frac{d\tau}{ds} \quad . \tag{17}$$

Equations (14) and (17) indicate coupling between the shear and peel stresses in the adhesive. In order to obtain an explicit solution expeditiously, an

approximate solution will be adopted with sufficient integration constants to satisfy the dominant boundary conditions. The simplest such solution, used also in Reference 2, is

$$\frac{1}{2}(w_2 + w_3) \simeq A_{23}s^3 + B_{23}s^2 + C_{23}s + F_{23} \quad . \tag{18}$$

The conditions at $s = 0$ for a built-in end of the skin/doubler combination permit the setting of

$$C_{23} = F_{23} = 0 \quad . \tag{19}$$

(For simply-supported ends, the corresponding relations would be

$$B_{23} = F_{23} = 0 \quad . \quad) \tag{20}$$

As in Reference 2, it is assumed that

$$\frac{dw_2}{ds} \simeq \frac{dw_3}{ds} \qquad \text{at} \quad s = 0 \quad \text{and} \quad s = \ell_d \tag{21}$$

but that the distinction between the second derivatives is of paramount importance since

$$\frac{d^2w_3}{ds^2} = \frac{M_o}{D_4} \quad , \qquad \frac{d^2w_2}{ds^2} \equiv 0 \qquad \text{at} \quad s = \ell_d \quad . \tag{22}$$

(Note the sign convention for positive values of M_o, the critical moment in the adherend.) The pertinent boundary conditions, at $s = \ell_d$, $x_4 = -\ell_4$ are

$$w_4 = -B_4\sinh(\xi_4\ell_4) - \left[\frac{t_1 + t_4 + 2\eta}{\ell_4 + \ell_d}\right]\frac{1}{\left(1 + \dfrac{E_4t_4}{E_1t_1}\right)}\left(\frac{\ell_4}{2}\right)$$

$$= \frac{1}{2}(w_2 + w_3) = A_{23}(\ell_d)^3 + B_{23}(\ell_d)^2 \quad , \tag{23}$$

$$\frac{dw_4}{dx_4} = B_4\xi_4\cosh(\xi_4\ell_4) + \left[\frac{t_1 + t_4 + 2\eta}{\ell_4 + \ell_d}\right]\frac{1}{\left(1 + \dfrac{E_4t_4}{E_1t_1}\right)}\frac{1}{2}$$

$$= \frac{1}{2}\frac{d(w_2 + w_3)}{ds} = 3A_{23}(\ell_d)^2 + 2B_{23}(\ell_d) \quad , \tag{24}$$

$$\frac{d^2w_4}{dx_4^2} = \frac{M_o}{D_4} = -B_4\xi_4^2\sinh(\xi_4\ell_4)$$

$$= \frac{1}{2}\left(\frac{d^2(w_2 + w_3)}{ds^2} - \frac{d^2(w_2 - w_3)}{ds^2}\right) = 6A_{23}(\ell_d) + \frac{M_o}{2D_4} \tag{25}$$

and, for sufficiently large $\xi_4\ell_4$,

$$\sinh(\xi_4\ell_4) \simeq \cosh(\xi_4\ell_4) \simeq \frac{1}{2}e^{(\xi_4\ell_4)} \quad . \tag{26}$$

By a process of elimination it is established that

$$M_o\left[1 + \frac{1}{2}(\xi_s\ell_d) + \frac{1}{24}(\xi_s\ell_d)^2\right] = \frac{Pt_d}{2}\frac{\left(1 + \frac{t_s}{t_d} + \frac{2\eta}{t_d}\right)}{\left(1 + \frac{E_s t_s}{E_d t_d}\right)}\left(1 - \frac{\ell_d}{2(\ell_s + \ell_d)}\right) \tag{27}$$

$$\simeq \frac{Pt_d}{2} \quad . \tag{28}$$

Equation (27) holds for built-in ends. It follows from equation (152) of Reference 2 that, for simply-supported ends,

$$M_o\left[1 + (\xi_s\ell_d) + \frac{1}{6}(\xi_s\ell_d)^2\right] = \frac{Pt_d}{2}\left[\frac{1 + \frac{t_s}{t_d} + \frac{2\eta}{t_d}}{1 + \frac{E_s t_s}{E_d t_d}}\right] \tag{29}$$

$$\simeq \frac{Pt_d}{2} \quad . \tag{30}$$

In these equations, the subscripts d and s refer, respectively, to the doubler and skin, being equivalent to the subscripts 1 and 4. The bending stiffness parameter ξ_s for the skin is given above as

$$\xi_s^2 = \frac{P}{D_s} = \frac{12P(1 - \nu_s^2)}{(k_b)_s E_s t_s^3} \tag{31}$$

In this, the coefficient k_b serves to uncouple the bending and extensional stiffnesses so that the analysis covers filamentary composite materials as well

as the isotropic metals. (In the computer programs listed in the Appendix, the ratio E_s/E_d is set equal to unity. That is, the skin and doubler materials are the same. This restriction is in accord with common practice, but can easily be over-ridden in a specific case. Likewise, the assumption in equation (28) that the doubler is small in comparison with the extent of the skin can also be refined if desired.) The maximum stress in the skin, at the edge of the doubler, follows from equation (27) or (29) as

$$\sigma_{max} = \frac{P}{t_s} + \frac{6M_{max}}{t_s^2} = \sigma_{avg}(1 + 3k) \quad . \tag{32}$$

Equations (28), (30) and (32) are programmed to be solved by iteration in the digital computer program listed in the Appendix. Representative solutions, in non-dimensionalized form, are shown in Figures 2 and 3. It is apparent that, for all practical purposes, the point of inflexion in the built-in case is in the middle of the doubler since doubling the ℓ/t ratio with respect to the simply-supported case yields the same joint stresses when computed for the built-in case. It can be seen clearly that the effective length of the overlap should be as large as practical. Trying to save weight by skimping on the doubler has the effect of reducing significantly the allowable skin stress ($\sigma_{avg}/\sigma_{max} < 1$) so that a major weight penalty can be suffered for the entire panel. This is why fingered doublers are customarily applied with quite long overlaps rather than shallow scallops. The analysis above governs the fatigue failure mode illustrated in Figure 4. The cracks originate on the doubler side of the skin at the extremities of the fingers. Such cracks do not tend to occur on the (sloping) sides of the fingers because no clearly definable axis for bending of the skin exists there. The experimental evidence is strong that doublers should be either fingered or have feathered edges to prevent the formation of a long continuous crack in the skin adjacent to the edge of the doubler.

It will be noticed that nowhere in the analysis above is there any involvement of the adhesive properties. Consequently the solution can be applied also to integral doublers formed by chem-milling of a thick skin. In doing so, however, it must be recognized that there is an additional stress concentration due to the abrupt change in thickness which is not eliminated for the integral doubler as it is for the bonded doubler by the layer of adhesive.

EXAMPLE 1:

To illustrate the use of the analysis above, consider a 2024-T3 aluminum skin 0.025 inch thick with a doubler 0.015 inch thick. The required skin efficiency is 90 per cent, so the minimum overlap is read from Figure 2 as

$$\ell = 0.025 \times 14.85 \; / \; 0.22168 = 1.67 \text{ inch.}$$

(An increase to $\ell = 2.65$ inch overlap would be needed to raise the skin efficiency to 95 per cent.)

2.2 Adhesive Shear Stresses in Adhesive-Bonded Doublers

Consideration of adhesive stresses is not necessary in most bonded (edge) doubler applications because the analysis above for skin efficiency tends to over-ride such considerations. Nevertheless, the bonded doubler serves to illustrate simply the use of modified all-plastic design concepts for structural bonded joints.

The natural desire for high adherend efficiency is satisfied by minimizing the effect of any eccentricities in load paths. The accomplishment of this minimizes the differences between the actual adhesive stress distributions and those of a supported (double-lap) joint. Therefore, instead of adapting the more complex analysis of Reference 2 to the boundary conditions of bonded doublers, the simpler analysis techniques of Reference 1 are employed. The analysis presented here (see Reference 4) accounts for adhesive plasticity, while assuming that the skin and doubler remain elastic. An algebraic solution is derived which is sufficiently simple for design use. The solution describes the adhesive shear stress distribution between the skin and doubler, identifying the critical region (a narrow strip along the edge of the doubler) and those other regions in which small manufacturing defects can be tolerated without impairing the structural efficiency of the design. This analysis shows how to size minimum bond areas by estimating the extent of plastic adhesive zone necessary to transfer the load (and check that the adhesive is capable of generating such strengths for the given adherends) and adding to this the distance required to build up the elastic adhesive stresses from zero to the plastic level. This approach is more meaningful than that of sizing in terms of a uniform bond shear stress, no matter how the "allowable" was arrived at.

Peel stresses in the adhesive (or interlaminar tension stresses in an adjacent composite adherend) become a progressively more severe problem for either short overlaps or thick sections. Usually these conditions are not encountered in practical doubler design. In the event that they are, the single-lap joint analysis of Reference 2 can be modified easily in much the same manner as for the adherend analysis in Section 2.1 above.

Figure 5 depicts the geometry and nomenclature for the analysis of an arbitrary adhesive-bonded skin/doubler combination. A uniform tensile load P (per unit width) is applied to the skin and taken out at a row of close-spaced rivets adjacent to the outer edge of the skin/doubler combination. A compressive load would be equally well accounted for by this analysis, but it is necessary here to establish a sign convention. In order to define the problem sufficiently to permit a solution to be obtained it is assumed here that, at the row of rivets, both skin and doubler act is unison, each transferring load to the rivets in proportion to their extensional stiffness. It is also assumed that the doubler extends sufficiently beyond the row of rivets for the local stress variations around the rivets not to affect the analysis in the region of adhesive shear load transfer. The row of rivets are replaced mathematically by a thick extension beyond the end of the original skin and the doubler, as depicted in Figure 5.

The conditions for horizontal force-equilibrium for a differential element dx within the adhesive bonded area are

$$\frac{dT_d}{dx} + \tau = 0 \quad , \qquad \frac{dT_s}{dx} - \tau = 0 \quad , \tag{33}$$

in which the subscript s refers to the skin and d to the doubler. The stress-strain relations for the skin and doubler yield

$$\frac{d\delta_s}{dx} = \frac{T_s}{E_s t_s} \quad , \qquad \frac{d\delta_d}{dx} = \frac{T_d}{E_d t_d} \quad . \tag{34}$$

The adhesive shear strain γ is approximated by the relation

$$\gamma = \frac{(\delta_s - \delta_d)}{\eta} \tag{35}$$

and, within the elastic region (of unknown length s), the adhesive shear stress is assumed to be

$$\tau = G\gamma = \frac{G(\delta_s - \delta_d)}{\eta} = f(x) \tag{36}$$

while, throughout the remaining plastic region (of unknown length w), the adhesive shear stress is assumed to be constant, at the plastic adhesive shear

stress

$$\tau = \tau_p = \text{constant} \quad . \tag{37}$$

To solve the governing differential equations, one eliminates δ_s and δ_d between equations (34) and (35) and then uses equations (33) to eliminate T_s and T_d, yielding the differential equations

$$\frac{d\gamma}{dx} = \frac{1}{\eta}\left[\frac{T_s}{E_s t_s} - \frac{T_d}{E_d t_d}\right] \quad , \tag{38}$$

$$\frac{d^2\gamma}{dx^2} - \frac{1}{\eta}\left[\frac{1}{E_s t_s} + \frac{1}{E_d t_d}\right]\tau = 0 \quad . \tag{39}$$

Within the elastic region, which is assumed to extend to the rivet line because of the small relative displacement in that region, equation (39) becomes

$$\frac{d^2\gamma}{dx^2} - \lambda^2\gamma = 0 \quad . \qquad \left[\lambda^2 = \frac{G}{\eta}\left(\frac{1}{E_s t_s} + \frac{1}{E_d t_d}\right)\right] \tag{40}$$

In the elastic solution,

$$\gamma = A \sinh(\lambda x) + B \cosh(\lambda x) \quad , \tag{41}$$

the constant B can be set identically equal to zero because of the assumed absence of relative displacement across the bond line at the row of rivets. Equation (38) then predicts that the loads in the skin and doubler are not proportional to their respective stiffnesses at the row of rivets. In other words, the shear deformation in the adhesive prevents the doubler from fully developing a load in proportion to the relative stiffness of the skin and doubler. Provided that the doubler is not excessively narrow, this effect is inconsequential, as is confirmed by the analysis below.

In the plastic region, of assumed length w at the inner end of the doubler, the solution of equation (39) is

$$\gamma = \frac{\lambda^2}{2G}\tau_p\xi^3 + C\xi + F \tag{42}$$

in which $dx = d\xi$, the origin for ξ being at $x = +s$.

The constants B, C and F and the unknown s or w are found by satisfying the

boundary conditions

$$\gamma = \gamma_e \quad \text{at} \quad x = s,\ \xi = 0, \tag{43}$$

$$\gamma = \gamma_e + \gamma_p \quad \text{at} \quad \xi = w, \tag{44}$$

$$\frac{d\gamma}{dx} = \frac{d\gamma}{d\xi} \quad \text{at} \quad x = s,\ \xi = 0, \tag{45}$$

$$\frac{d\gamma}{d\xi} = \frac{P}{E_s t_s \eta} \quad \text{at} \quad \xi = w, \tag{46}$$

of which equation (45) ensures continuity in the adherend stresses. Hence

$$F = \gamma_e = \tau_p/G \quad , \tag{47}$$

$$A = \gamma_e/\sinh(\lambda s) = \tau_p/[G \sinh(\lambda s)] \quad , \tag{48}$$

$$C = \frac{\lambda \tau_p}{G \tanh(\lambda s)} \quad . \tag{49}$$

From equation (45) it now follows that

$$\left[\lambda w + \frac{1}{\tanh(\lambda s)}\right]^2 = \frac{1}{\tanh^2(\lambda s)} + 2\frac{\gamma_p}{\gamma_e} \tag{50}$$

so that, from equation (46)

$$P = \frac{\tau_p}{\lambda}\left(\lambda w + \frac{1}{\tanh(\lambda s)}\right)\left(1 + \frac{E_s t_s}{E_d t_d}\right) \quad , \tag{51}$$

whence

$$\frac{1}{\tanh^2(\lambda s)} + 2\frac{\gamma_p}{\gamma_e} = \left[\frac{\lambda P}{\tau_p\left(1 + \frac{E_s t_s}{E_d t_d}\right)}\right]^2 \quad . \tag{52}$$

Precise evaluation of these equations requires a digital computer program but, for sufficiently long overlaps, $\tanh(\lambda s) \to 1$, whence

$$(\lambda w + 1)^2 \to 1 + 2\frac{\gamma_p}{\gamma_e} \to \left[\frac{\lambda P}{\tau_p\left(1 + \frac{E_s t_s}{E_d t_d}\right)}\right]^2 \quad . \tag{53}$$

The failure criterion for the adhesive is taken to be the exceeding of its total shear strain capacity $(\gamma_e + \gamma_p)$, which has been shown to be a realistic approach in Reference 1.

Just as in the analysis of bonded lap joints (References 1 and 2), the extent of the plastic adhesive zone is limited by the adhesive and adherend properties and does not increase indefinitely with increasing applied load. Most of the load transferred by the adhesive bond between the skin and the doubler passes through a single narrow band at the edge of the doubler. This same narrow band follows the contour of finger doublers, as shown in Figure 6. Manufacturing defects in the bond away from the edges do not impair the load transfer capability of the bond.

Attention is now focused on the not quite ideal sharing of the load between the skin and doubler, as indicated above. The integral of the adhesive shear stress over the extent of both the elastic and plastic regions is

$$\int_0^s \tau \, dx + \int_0^w \tau \, d\xi = \frac{\tau_p}{\lambda \sinh(\lambda s)} [\cosh(\lambda s) - 1] + \tau_p w \quad . \tag{54}$$

If the skin and doubler were to share the load, at the row of rivets, in proportion to their respective stiffnesses, the load per unit width in the doubler (transferred through the adhesive bond) would have to be

$$P \Big/ \left(1 + \frac{E_s t_s}{E_d t_d} \right) \tag{55}$$

which, from equation (51), is precisely equal to

$$\frac{\tau_p}{\lambda \tanh(\lambda s)} + \tau_p w \quad . \tag{56}$$

A comparison with equation (54) indicates that it is realistic to use the approximation (55) whenever $\cosh(\lambda s) \gg 1$ which is practically always, because of the characteristically high values of λ.

The analysis above is now capable of re-interpretation in a form providing a meaningful comparison with the analysis of lap joints. Corresponding to equation (50), the equivalent analysis of the general double-lap joint yields equa-

tion (A.55) of Reference 1:

$$\left[\lambda b + \tanh\left(\frac{\lambda d}{2}\right)\right]^2 = \tanh^2\left(\frac{\lambda d}{2}\right) + 2\frac{\gamma_p}{\gamma_e} \quad . \tag{57}$$

In lap joints it is the extent of this plastic adhesive zone which limits the ultimate strength that can be attained by the joint. Likewise, for bonded doublers, it limits the load that can be transferred from the skin to the doubler without failing the bond. In the latter situation, however, the potential bond strength usually exceeds by far the strength of the adherends. At relatively low load intensities, the full plastic capability of the adhesive is not fully utilized. As the load is increased, a maximum load capacity is attained which fully extends the adhesive in shear. At this load level, no increase in the size of the doubler can increase the load transferred. Equations (54) to (56) and (50) indicate that the load transferred through any bond of realistic length is equal to

$$\frac{P}{1 + \frac{E_s t_s}{E_d t_d}} \simeq \frac{\tau_p}{\lambda}\left(\lambda w + \frac{\cosh(\lambda s) - 1}{\sinh(\lambda s)}\right) \to \frac{\tau_p}{\lambda}\sqrt{1 + 2\frac{\gamma_p}{\gamma_e}} \quad , \tag{58}$$

which is proportional to the square root of the strain energy of the adhesive in shear, just as for bonded lap joints. This explains why ductile adhesives are so much stronger than brittle ones despite the greater maximum shear stress of the latter.

For practical stressing of the adhesive in shear, equation (58) contains all the pertinent information. The design sequence is as follows:

(1) compute the bond load $P \Big/ \left(1 + \frac{E_s t_s}{E_d t_d}\right)$

(2) compare (1) with the maximum bond strength

$$\frac{\tau_p}{\lambda}\sqrt{1 + 2\frac{\gamma_p}{\gamma_e}}$$

which is limited by the adhesive shear strain capacity $(\gamma_e + \gamma_p)$ and

(3) if the comparison in (2) indicates that the adhesive is suitable, determine the minimum width of the doubler, from the row of rivets to the nearest edge of the fingers on the doubler as at least the sum of the widths of the plastic and elastic adhesive zones. For this purpose it would appear to be good design practice to base the load on the ultimate strength of the skin with an adequate margin of safety. A simple and generally not unduly conservative approach is to assume that $\tanh(\lambda s) \simeq 1$ for the elastic region, so that $s = 3/\lambda$, and that all the load is carried in the plastic region, so that

$$w = P \Big/ \left[\left(1 + \frac{E_s t_s}{E_d t_d}\right)\tau_p\right].$$

(4) Then, $\ell_{minimum} = s + w$.

EXAMPLE 2:

Consider a 0.030 inch 7075-T6 aluminum alloy skin with a 0.020 inch doubler of the same material, bonded together with Epon 951 adhesive, for which $\tau_p = 6000$ psi, $\gamma_p/\gamma_e = 20$, $G = 6.0 \times 10^4$ psi, and $\eta = 0.005$ inch. For these materials,

$$\lambda = \sqrt{\frac{6.0 \times 10^4}{5 \times 10^{-3}} \times \frac{1}{10^7}\left(\frac{10^3}{30} + \frac{10^3}{20}\right)} = 10.0 \quad .$$

Taking $\sigma_{ult} = 75$ ksi for the aluminum (for which also $E = 10^7$ psi), the maximum bond load per inch is $75 \times 10^3 \times 30 \times 10^{-3} / (1.0 + 1.5) = 900$ lb/in. The adhesive bond capability is $(6000 / 10) \times \sqrt{41} = 3842$ lb/in., so the adhesive has more than adequate strength.

The minimum width of the doubler (see Section A-A in Figure 6) then follows as

$$\ell = \frac{3}{10.0} + \frac{900}{6000} = 0.45 \quad \text{inch} \quad .$$

The fingers can then be proportioned according to current accepted design practice. The minimum width ℓ above is likely to be so small in general that manufacturing tolerances and the adherend efficiency considerations above may well dictate a much greater length.

3. SELECTIVE REINFORCEMENT BY BONDED-ON DOUBLERS

In the application of advanced composites to aerospace structures in the form of selective reinforcement, the objective is to minimize the total cost of the composite by restricting its application to those situations in which it is used most efficiently. These are the unidirectional reinforcement of beam caps, strut flanges, stringers and longerons. The key problem in such applications is any load transfer from the composite to a metal end fitting. The brittleness of the composite has led to the acceptance of the concept of using only adhesive bonding between the composite and the end fitting and employing mechanical fasteners between the end fitting and the adjacent structure. The direct bolting of composite to the structure would necessarily require cross-plies to develop adequate bearing strength and, with the associated stress concentrations around the holes, this does not represent a particularly efficient application of advanced composites if the bolt holes run along the entire length of the part. A related concept, which has not received the attention it merits, is that of a bonded-on unidirectional reinforcement with cross-plies interleaved at the ends which can then be bolted as well as bonded. The efficient use of interleaved metal reinforcement or boron film reinforcement is limited to fairly thin sections because of non-uniform load sharing problems associated with the many rows of bolts needed to transfer load in to and out of a thick section. Under such constraints, it becomes apparent that reliance on pure adhesive bonding will continue in such applications.

There are two mathematically distinct types of problems in this classification: the thin laminates with uniform thickness and the thicker ones with a scarfed (or stepped) end to effect the load transfer over a greater length. These are treated below in turn. Because of the interest in boron-infiltrated composite-reinforced structures (Reference 5), the solutions will be presented directly in terms of section areas per unit bond width rather than in terms of "equivalent adherend thicknesses".

3.1 Uniform Thickness Doublers

Starting with the uniform thickness adherends, the basic problem is that of how much composite can be bonded on before it splits off. This problem arises as the result of thermal stresses induced by the dissimilar coefficients of thermal expansion for metals and composites and the fact that the operating temperature is almost invariably much less than the bonding (curing) temperature required for good environmental resistance. Once this limit is set, one can proceed to compute how much mechanical load can be transferred and how best to do so. The pertinent variables are depicted in Figure 7, in which the link supports are meant to indicate the lack of eccentricities and of any deflections perpendicular to the x-axis. Precise elastic-plastic analysis will show that, to all intents and purposes, most of the adhesive load is developed in the end zones of the joint while the bulk of the structure is subjected to essentially uniform stresses. The distance d shown is independent of the total length for long overlaps but is characteristic of the cross section and the materials and the temperature differential ΔT. The governing equations, for the sign convention employed in Figure 7, are:

for equilibrium

$$\frac{dT_1}{dx} - w\tau_p = 0 \quad , \tag{59}$$

and

$$\frac{dT_2}{dx} + w\tau_p = 0 \quad , \tag{60}$$

for continuity

$$\gamma = (\delta_1 - \delta_2) / \eta \quad , \tag{61}$$

while, for the stress-strain relations for the adherend materials

$$\frac{d\delta_1}{dx} = \frac{T_1}{E_1 A_1} + \alpha_1 \Delta T \quad , \tag{62}$$

and

$$\frac{d\delta_2}{dx} = \frac{T_2}{E_2A_2} + \alpha_2\Delta T \quad . \tag{63}$$

The governing boundary conditions for the adhesive are that

$$\tau = \tau_p \quad \text{for} \quad 0 \leq x \leq d \quad , \tag{64}$$

$$\tau = 0 \quad \text{for} \quad x > d \quad , \tag{65}$$

$$\gamma = \gamma_p \quad \text{at} \quad x = 0 \quad , \tag{66}$$

and

$$\gamma = 0 \quad \text{at} \quad x = d \quad . \tag{67}$$

The joint is symmetrical with respect to the centerline at $x = L/2$.

In the range $d \leq x \leq L/2$, there is no differential displacement across the adhesive layer so that, from equations (62) and (63),

$$\frac{T_1}{E_1A_1} + \alpha_1\Delta T = \frac{T_2}{E_2A_2} + \alpha_2\Delta T \quad . \tag{68}$$

At the elastic-to-plastic transition at $x = d$, equilibrium requires that

$$T_1 = -T_2 \quad . \tag{69}$$

The simultaneous solution of equations (68) and (69) leads to the results

$$T_1 = (\alpha_2 - \alpha_1)\Delta T \Big/ \left(\frac{1}{E_1A_1} + \frac{1}{E_2A_2}\right) = -T_2 \quad . \tag{70}$$

This same result is deduced for the location $x = L/2$ by a perfectly elastic analysis, in association with an exponential increase in adhesive shear stresses towards the ends of the joint (see Reference 6).

Turning now to the adhesive stresses, equations (59) and (60) require that the forces T_1 and T_2 be reduced linearly to zero at the free edges of the specimen by a uniform shear stress over the distance d. It follows that the length of plastic adhesive zone at each end of the overlap is given by

$$d = \frac{|(\alpha_2 - \alpha_1)\Delta T|}{w\tau_p} \Big/ \left(\frac{1}{E_1A_1} + \frac{1}{E_2A_2}\right) \quad , \tag{71}$$

in which the modulus signs are necessary to ensure that the length d is positive without prior knowledge of the relative magnitudes of α_1 and α_2. It is now appropriate to relate this distance d to the shear strain capacity of the

adhesive, which serves as the failure criterion. In the end zone, from equations (59) through (63),

$$\gamma = \frac{1}{\eta}(\delta_1 - \delta_2) = C + \frac{1}{\eta}\left[(\alpha_1 - \alpha_2)\Delta T x + \left(\frac{1}{E_1A_1} + \frac{1}{E_2A_2}\right)w\tau_p\left(\frac{x^2}{2}\right)\right] \quad . \tag{72}$$

At $x = 0$,

$$\gamma = C = \gamma_e + \gamma_p \qquad (x = 0) \tag{73}$$

while, at $x = d$,

$$\gamma = 0 \qquad (x = d) \tag{74}$$

for the upper bound solution and

$$\gamma = \gamma_e \qquad (x = d) \tag{75}$$

for the lower bound solution.

While the condition (75) is obviously associated with some displacement incompatibility for $x > d$, equation (65) requires that there be no change from the forces in equation (70) for long and moderate overlaps. For the upper bound solution, then, equations (71) through (74) indicate that

$$(\gamma_e + \gamma_p) = \frac{d}{2\eta}[\,|(\alpha_2 - \alpha_1)\Delta T|\,] \quad , \tag{76}$$

whence the failure condition

$$2\tau_p w\eta(\gamma_e + \gamma_p)\left(\frac{1}{E_1A_1} + \frac{1}{E_2A_2}\right) = [(\alpha_2 - \alpha_1)\Delta T]^2 \quad . \tag{77}$$

Various dominant influences are apparent in this relation. The thermal stress terms appear to the second power, so their influence becomes progressively more severe. With all other variables held constant, the left-hand side indicates a definite limit in adherend stiffnesses that can be loaded up, without failure of the adhesive, by a given adhesive and width of bond. The greater is w in proportion to E_1A_1 and E_2A_2, the higher the temperature differential that can be withstood. The important role of adhesive ductility is again evident. The quantity $\eta\tau_p(\gamma_e + \gamma_p)$ represents the strain energy per unit bond area for the adhesive and this alone characterizes the influence of the adhesive. The same importance of the adhesive strain energy is evident in Reference 1 for double-lap joints. The lower-bound equivalent of equation (77) is

$$2\tau_p w \eta \gamma_p \left(\frac{1}{E_1 A_1} + \frac{1}{E_2 A_2}\right) = [(\alpha_2 - \alpha_1)\Delta T]^2 \quad . \tag{78}$$

Equations (77) and (78) are appropriate for the AVCO boron-infiltrated extrusion concept (Reference 5) because the circumferential symmetry prevents the development of peel stresses at the ends of the overlap. For the exposed type of reinforcement illustrated in Figure 7, it is probable that peel stresses or associated interlaminar tension stresses impose a more severe restriction than equations (77) or (78). This kind of problem is discussed in Section 6 of Reference 1 and imposes a definite limit on the thickness of doubler which can be bonded on without having a scarfed end. For a uniform thickness of reinforcement, designated by the subscript o, this thickness is

$$t_o = \frac{E_o \eta}{3E_c'(1 - \nu^2)} \left(\frac{\sigma_c}{\tau_p}\right)^4 \tag{79}$$

in which σ_c is the maximum allowable peel or interlaminar tension stress, E_c' is the effective modulus in peel, and the other quantities have been defined above. This constraint does not include any thermal effect terms because it derives from a purely plastic analysis and need not distinguish between how much of the adhesive strain was thermally induced and how much was developed by the applied mechanical loads. Were one to include the elastic stresses also, one could extend this thickness ever so slightly for very low thermal mismatches and/or very low temperature differentials.

EXAMPLE 3:

While this example should be regarded as only approximate because it deals with a very brittle resin system (and the theory above is precise only for reasonably ductile systems), it may be of interest to examine the permissible size of boron-epoxy infiltrated rods in aluminum extrusions. One uses equation (77) with an aluminum area equal to that of the boron-epoxy as a typical example. The resin has properties of the order of $\eta = 0.005$ inch, $\tau_p = 9000$ psi, $(\gamma_e + \gamma_p) = 0.1$, so that, if the hole in the extrusion be of diameter d and the temperature differential be 400 °F (from 350 °F to -50 °F),

$$2 \times 9000 \times \pi d \times 0.005 \times 0.1 \left(\frac{4}{30 \times 10^6 \times \pi d^2} + \frac{4}{10 \times 10^6 \times \pi d^2}\right) = [(13.0 - 2.7) \times 10^{-6} \times 400]^2$$

whence d = 0.283 inch.

It is evident that the 0.25 inch diameter selected by AVCO is close to optimum for the 350 °F cure-in-situ resin system which has been used to date. To increase this diameter significantly requires either a decrease in the cure temperature or a layer of ductile adhesive between the boron-epoxy and the aluminum. AVCO is currently increasing the diameter of the reinforcing rods by use of a room-temperature-curing resin system which is subsequently post-cured to improve the strength and environmental resistance. This scheme is effective for two reasons. First, the thermal stresses are less severe in going from room temperature to either -67 °F or to the typically 250 °F post-curing temperature than is the case in going from 350 °F to -67 °F. Second, in the room-temperature-curing system, the stress-free state is at room temperature rather than at 350 °F. Therefore the residual stresses induced in the aluminum are far less severe and the fatigue life of the structure is improved. The major thermal stresses with this scheme occur at 250 °F and, as far as the bond is concerned, these are not subject to creep because there is no driving force at room temperature.

The analysis above concludes, in equation (77), with an estimate of the maximum possible size of composite reinforcement which can be bonded to the basic metal structure. If mechanical loads T_1 and/or T_2 are applied at the end of the composite, where the maximum induced shear transfer stresses are located, this size will necessarily be reduced in order to accomodate both components of load. The understanding of this phenomenon permits of simple design modifications to alleviate this difficulty. This is illustrated in Figure 8 in which, in the upper configuration, both mechanical and thermal loads combine at the same location. In the lower configuration, on the other hand, the extension of the reinforcement beyond the last fastener and beyond the softening cutout serves to separate the peaks of the two transfer stress components. As explained in Section 4, the peak mechanically-induced stresses are located at the last attachment and decay towards zero at the end of the member. The peak thermally-induced stresses necessarily occur at the extremity of the reinforcement. Therefore, the stress-concentration relief shown in the lower part of Figure 8 enables the resin matrix to react only one peak load condition at any one location, permitting the application of higher mechanical stresses to the reinforcement.

3.2 Feathered-Edge Doublers

For applications in which thick reinforcement sections are required, the abrupt cut-off at the end of the reinforcement is intolerable and the appropriate procedure is to feather the end, as illustrated in Figure 9. In this event, quite a different mathematical solution governs and peel stresses (or interlaminar tension stresses in the composite reinforcement) cease to be a problem. The design of this latter class of joints is dominated by two or three prime considerations. First, the net extensional stiffness of the metal plus filamentary composite parts should be constant throughout the joint, if at all possible, to promote maximum joint efficiency. Second, the net strengths at each end of the joint should not be so adversely unbalanced as to leave a long piece of reinforcement unable to accept any load because the end attachment area is too weak to load up the middle. Third, because the coefficiencts of thermal expansion of metals are distinctly higher than those of filamentary composites and because the stress-free temperature (just less than the cure temperature) is almost invariably higher than the operating temperature, a compressive load is usually more severe on the bond at each end than is a tensile load.

The notation and sign convention for this type of joint are defined in Figure 9. Again, deflections perpendicular to the axis of the filamentary reinforcement are excluded. Using classical mechanics of continuous structures, the equilibrium of the differential elements is given by

$$\frac{dT_c}{dx} - w\tau_p = 0 \tag{80}$$

and

$$\frac{dT_m}{dx} + w\tau_p = 0 \tag{81}$$

while the stress-strain relationships for the materials prescribe that

$$\frac{d\delta_c}{dx} = \frac{T_c}{(EA)_c} + \alpha_c \Delta T \tag{82}$$

and

$$\frac{d\delta_m}{dx} = \frac{T_m}{(EA)_m} + \alpha_m \Delta T \quad , \tag{83}$$

in which

$$(EA)_c = E_c A_c (x/\ell) \tag{84}$$

and

$$\left.\begin{aligned} (EA)_m &= (E_m A_m)_1 - [(E_m A_m)_1 - (E_m A_m)_2](x/\ell) \\ &= (E_m A_m)_1 - \Delta(E_m A_m)(x/\ell) \end{aligned}\right\} \tag{85}$$

while displacement continuity requires that, for the adhesive,

$$\gamma = (\delta_c - \delta_m) \; / \; \eta \quad . \tag{86}$$

The design problem may be expressed in its simplest form as the determination of the elngth, ℓ, of scarf necessary for a uniform bond stress τ_p to transfer the load. Usually a compressive load is more critical than a tensile load because the thermally-induced residual bond stresses tend to relieve applied tensile loads and to aggravate compressive loads. In the process of solving the equations, it is necessary to check on the maximum adhesive shear strain induced since this serves as the failure criterion. The adhesive shear strain is assumed to be zero at the inboard end of the scarf. Even if it is not precisely so there, it is zero close nearby. The numerically greatest adhesive shear strain will develop at the outer (feathered) end of the composite, regardless of whether the applied load be tensile or compressive. Thus, the solution proceeds as

$$\frac{d\gamma}{dx} = \frac{1}{\eta}\left\{(\alpha_c - \alpha_m)\Delta T + \frac{\tau_p w \ell}{E_c A_c} - \frac{(P - \tau_p w x)}{(E_m A_m)_1 - [(E_m A_m)_1 - (E_m A_m)_2](x/\ell)}\right\} \quad , \tag{87}$$

in which P is the total (tensile) load applied, whence

$$\gamma = \text{const.} + \frac{1}{\eta}\left\{(\alpha_c - \alpha_m)\Delta T x + \frac{\tau_p w \ell}{E_c A_c} x + \frac{P\ell}{\Delta(E_m A_m)} \ell n[(E_m A_m)_1 - \Delta(E_m A_m)(x/\ell)]\right.$$

$$\left. + \frac{\tau_p w \ell^2}{[\Delta(E_m A_m)]^2}\left[(E_m A_m)_1 - \Delta(E_m A_m)\left(\frac{x}{\ell}\right) - (E_m A_m)_1 \ell n[(E_m A_m)_1 - \Delta(E_m A_m)\left(\frac{x}{\ell}\right)]\right]\right\} \quad . \tag{88}$$

The substitution of the conditions $\gamma = 0$ at $x = \ell$ and $\gamma = \gamma_e + \gamma_p$ at $x = 0$ serves to evaluate the integration constant. A further equation follows from

the assumed zero differential displacement across the adhesive layer in the (uniform) central region of the overlap. From equations (82) and (83), with $\delta_m = \delta_c$,

$$\frac{(T_m)_2}{(E_m A_m)_2} - \frac{(T_c)_2}{E_c A_c} = (\alpha_c - \alpha_m)\Delta T \tag{89}$$

and, since,

$$(T_c)_2 = \tau_p w \ell \quad \text{and} \quad (T_m)_2 = P - \tau_p w \ell \quad , \tag{90}$$

$$\frac{P}{(E_m A_m)_2} = \tau_p w \ell \left[\frac{1}{E_c A_c} + \frac{1}{(E_m A_m)_2}\right] + (\alpha_c - \alpha_m)\Delta T \quad . \tag{91}$$

Equation (91) permits the load P to be eliminated from the failure criterion formed with equation (88) applied at each end of the scarf. This process leads to an expression for ℓ which may in turn be substituted into equation (91) to evaluate the maximum load capacity of the composite-reinforced structure. The equation for ℓ becomes

$$A\ell^2 + B\ell + C = 0 \quad , \tag{92}$$

where

$$A = \tau_p w \left(\frac{1}{E_c A_c} - \frac{1}{(E_m A_m)_1 - (E_m A_m)_2}\right)\left(1 + \frac{(E_m A_m)_2 \ell n[(E_m A_m)_2/(E_m A_m)_1]}{(E_m A_m)_1 - (E_m A_m)_2}\right) \quad , \tag{93}$$

$$B = (\alpha_c - \alpha_m)\Delta T\left(1 + \frac{(E_m A_m)_2 \ell n[(E_m A_m)_2/(E_m A_m)_1]}{(E_m A_m)_1 - (E_m A_m)_2}\right) \quad , \tag{94}$$

and

$$\left.\begin{aligned} C = \eta[\gamma_{(x=0)} - \gamma_{(x=\ell)}] &= \pm\eta(\gamma_e + \gamma_p) \quad \text{for the upper bound} \\ &= \pm\eta\gamma_p \quad \text{for the lower bound} \end{aligned}\right\} . \tag{95}$$

The apparent problem of evaluating $\ell n(0)$ for the case $(E_m A_m)_2 = 0$ does not in fact arise because

$$0\ell n(0) = \ell n(0^0) = \ell n(1) = 0 \quad . \tag{96}$$

Strictly this limiting case of a pure scarf joint is not covered by the present analysis because the thermal stress picture can change to the extent that $\gamma \neq 0$ at $x = \ell$.

The reason for the ± sign in equation (95) is explained in Figure 10. The mathematical confirmation of the precise adhesive shear behavior depicted in Figure 10 can be established by the following reasoning. Equation (87) may be re-arranged by means of equation (89) to read

$$\frac{d\gamma}{dx} = \frac{1}{\eta}\left\{\frac{\{P[(E_mA_m)_1 - (E_mA_m)_2] - \tau_p w\ell(E_mA_m)_1\}\left(1-\frac{x}{\ell}\right)}{(E_mA_m)_2\{[(E_mA_m)_1 - (E_mA_m)_2]\left(1-\frac{x}{\ell}\right) + (E_mA_m)_2\}}\right\} \quad . \tag{97}$$

It is clearly evident that $d\gamma/dx = 0$ only at and beyond $x = \ell$, except for the particular positive value of P, for each joint, for which $d\gamma/dx = 0$ at all values of x. At $x = 0$,

$$\left.\frac{d\gamma}{dx}\right|_0 = \frac{1}{\eta}\left[\frac{P[(E_mA_m)_1 - (E_mA_m)_2] - \tau_p w\ell(E_mA_m)_1}{(E_mA_m)_1(E_mA_m)_2}\right] \tag{98}$$

$$= \frac{1}{\eta}\left[(\alpha_c - \alpha_m)\Delta T + \frac{\tau_p w\ell}{E_cA_c} - \frac{P}{(E_mA_m)_1}\right] \tag{99}$$

and $d\gamma/dx|_0$ will tend to be positive as the result of usual thermal mismatches and compressive loads, so that γ_0 will be negative while, for large tensile loads P, $d\gamma/dx|_0$ will tend to be negative and γ_0 positive.

Returning now to equations (82) through (85) it is evident that A = 0 for $E_cA_c = \Delta(E_mA_m)$ which promotes longer effective scarfs as the result of carefully matching extensional stiffnesses along the length of the joint. (It is established in Reference 3 that only the unbalanced varieties of scarf joints suffer from limitations in joint efficiency.) In other words, it is sound design practice to make

$$(E_mA_m)_1 = (E_mA_m)_2 + E_cA_c \quad . \tag{100}$$

The evaluation of the optimum length ℓ for a design governed by compressive loads is straightforward. The length ℓ is determined from equations (60) through (63) by reversing the sign of $(\alpha_c - \alpha_m)\Delta T$ and using the positive sign for γ in equation (95). Actually, all the other quantities change sign except for the thermal terms, but it is simpler to compensate in this manner. The load capacity then follows from equation (91), again with the sign of the thermal stress terms reversed. The case of tensile loading is a little more tricky. The blind use of equations (82) through (85) with positive values of P

could easily result in a joint design which will hold its load only if applied gradually during cooling down in the autoclave after bonding. Once the load were released, the thermally-induced stresses could cause failure of the structure. In other words, for tensile loads it is necessary to check also the no-load condition to ensure that it is not more severe on the adhesive than is the load condition itself. For tensile loads, the appropriate sign in equation (85) follows from equation (99). If $d\gamma/dx|_0$ is positive, γ_0 is negative, and vice versa. The shear stress γ_0 is usually negative for zero mechanical load.

In the design of composite-reinforced structures it is necessary to guard against discontinuity problems in the transverse direction also. It is pointless to carefully taper the ends in the primary load direction and leave a severe thickness discontinuity in the orthogonal direction. An interesting discussion of this problem and its solution is given in Reference 7.

The analyses above do not lend themselves to ready graphical representation because of the large number of variables involved. It is appropriate to demonstrate the conclusions and the use of the analysis by simple numerical examples. Consider, in turn, balanced and unbalanced joints to show the adverse effects of poor detailing and thin and thick sections to demonstrate how thick sections tend to exceed the predicted bond load capacity. Since the boron-epoxy to aluminum combination is receiving attention for selectively-reinforced structures the examples discussed will be so oriented.

EXAMPLE 4:

For a bonded composite-reinforced metal structure of the type illustrated in Figure 10, let $t_c = 0.100$ in., $(t_m)_2 = 0.060$ in., $(t_m)_1 = 0.360$ in., $w = 1.0$ in., $E_m = 10\times10^6$ psi, $E_c = 30\times10^6$ psi, $\alpha_m = 13.0\times10^{-6}$ /°F, $\alpha_c = 2.7\times10^{-6}$ /°F, $\Delta T = -50 - 350 = -400$ °F, $\tau_p = 6000$ psi, $\eta = 0.005$ in., and $(\gamma_e + \gamma_p) = 2.0$. Then, from equations (92) through (95),

$$A = 0,\ B = (2.7 - 13.0)\times10^{-6}\times(-400)\left[1 + \frac{1}{5}\ell n\left(\frac{1}{6}\right)\right] = 0.002645,\ C = 0.005\times2.0 = 0.01$$

whence, for compressive loading, $\ell = -C/(-B) = 3.780$ in.. From equation (91),

$$P = 10\times10^6\times0.06\left[6000\times3.780\times\left(\frac{1}{30\times10^6\times0.1}+\frac{1}{10\times10^6\times0.06}\right)-(2.7-13.0)\times10^{-6}\times(-400)\right]$$

$= 27,218 - 2,472 = 24,747$ lb/inch width in compression and $P = 27,218 + 2,472 = 29,691$ lb/inch width in tension.

These loads correspond to composite stresses of 226,800 psi in both load senses.

As the maximum allowable adhesive shear strain is reduced, the theory above predicts a progressive decrease in joint load capacity. The theory is conservative with respect to brittle adhesives because of the somewhat surprising behavior of perfectly elastic scarf joints subject to thermal mismatch between the adherends. It is established in Reference 3 that, for both very short and very long overlaps (but not those in between) adherend thermal mismatch does not prevent the design of a scarf joint to transfer a required load between specified adherends. The dominant adverse effect is any stiffness mismatch which may exist between the adherends at each end of the joint. In the present context this scarf joint behavior translates into a statement that, provided the total extensional stiffness remains uniform throughout the joint region, a sufficiently small scarf angle can always be found to enable any adhesive, no matter how weak or brittle, to effect an adequate load transfer. The prime drawbacks to reliance on this idea are that, in the first place, the scarf may need to be so long that there is no room in the structure for a constant section between the joints at each end and that, secondly, the elastic analysis to determine such a scarf length is necessarily extremely difficult, being even more complicated than for a scarf joint (Reference 3).

Example 5:

Suppose that all data are the same as for Example 4 with the single exception of the presence of adherend stiffness imbalance with $(t_m)_1 = 0.160$ in., so that there is no bend in the reinforcement. The metal end of the joint is not built up adequately to carry the load which the filamentary composite reinforcement could otherwise develop.

From equations(92) through(95) now

$$A = 6000\left(\frac{1}{30\times10^6\times0.1}-\frac{1}{10\times10^6\times0.1}\right)\left[1+0.6\ell n\left(\frac{0.6}{1.6}\right)\right] = -0.001646$$

$$B = (2.7 - 13.0)\times10^{-6}\times(-400)\times 1 + 0.6\ell n\left(\frac{0.6}{1.6}\right) = 0.001695$$

$$C = 0.005\ 2.0 = 0.01$$

Then, for compression

$$\ell = \frac{0.001695 - \sqrt{(0.001695)^2 + 4(0.001646)(0.01)}}{-2\times(0.001646)} = 2.003 \text{ in..}$$

The associated load capacity then follows from equation (59) as

$$P = 10\times10^6\times0.06\times\left[6000\times2.003\left(\frac{1}{30\times10^6\times0.1} + \frac{1}{10\times10^6\times0.06}\right) - (2.7-13.0)\times10^{-6}\times(-400)\right],$$

$$= 14{,}421 - 2{,}472 = 11{,}950 \text{ lb/in. for compression,}$$

$$= 14{,}421 + 2{,}472 = 16{,}894 \text{ lb/in. for tension.}$$

These values are only about half those predicted for the stiffness-balanced joint examined in Example 4. This comparison serves to emphasize the importance of careful design detailing to ensure maximum joint efficiency by minimizing any imbalances which may be necessary.

EXAMPLE 6:

Consider a joint of the same materials as in Example 4 but with the adherends four times as thick. The plastic scarf length remains unaltered at 3.780 inches and the composite stress consequently drops to 56,700 psi. The load capacity increases to

$$P = 10\times10^6\times0.24\left[6000\times3.780\left(\frac{1}{30\times10^6\times0.4} + \frac{1}{10\times10^6\times0.24}\right) - (2.7-13.0)\times10^{-6}\times(-400)\right],$$

$$= 68{,}040 - 9{,}888 = 58{,}152 \text{ lb/in. for compression,}$$

$$= 68{,}040 + 9{,}888 = 77{,}928 \text{ lb/in. for tension,}$$

but the adherend materials are being used much less efficiently. (Actually, as discussed in Example 4, greater reliance should be placed upon the elastic capacity of the bond in a scarf joint, so this inefficiency prediction for thick sections is somewhat conservative.)

4. BONDED METAL REINFORCEMENT AROUND BOLT HOLES IN COMPOSITES

The application of bolted joints in advanced composite structures depends upon several factors. On an individual basis, load transfer by bolts in plain holes in isotropic pattern filamentary composites (0°/45°/90°/-45°) can be quite efficient. On a specific weight basis there is a strong case for not reinforcing the laminate with metal but for building up the laminate thickness as necessary instead. However, while this usually gives the lightest (and frequently the least expensive) bolted joint, it may be excessively bulky. There remains a case for analyzing bonded metal reinforcements around the bolt hole(s) for applications in which space does not permit a thicker laminate to be used.

There are two possible locations for such doublers: within the laminate or externally. The two schemes are depicted in Figure 11. The internal doubler has twice the effective bond area of the external doubler but, in practice, is found to be associated with joggled fibers and poor quality laminates. External doublers are generally to be preferred because of the higher quality laminates and superior fit over the area to be bonded. The feathered edge shown in Figure 11 is reserved for thick doublers. The thickness beyond which uniform doublers cannot be employed effectively is determined by peel-stress considerations explained in Reference 1 [see also Equation (79) here].

The analysis of external bonded doublers begins with a demonstration that, for uniform thickness doublers, the optimum location of the bolt hole is in the middle of the doubler. The nomenclature and mathematical model are defined in Figure 12. Equilibrium of differential elements in each of the four areas requires that, for one side of the joint,

$$\left.\begin{aligned} \frac{dT_1}{dx} + \tau_p = 0 \quad , \quad \frac{dT_2}{dx} - \tau_p = 0 \quad , \\ \frac{dT_3}{dx} + \tau_p = 0 \quad , \quad \text{and} \quad \frac{dT_4}{dx} - \tau_p = 0 \quad . \end{aligned}\right\} \tag{101}$$

The thermo-elastic material equations are

$$\frac{d\delta_k}{dx} = \frac{T_k}{E_k t_k} + \alpha_k \Delta T \qquad (k = 1,2,3,4) \quad , \tag{102}$$

while the adhesive shear strains are given by

$$\gamma_{12} = \frac{\delta_2 - \delta_1}{\eta} \quad \text{and} \quad \gamma_{34} = \frac{\delta_4 - \delta_3}{\eta} \quad . \tag{103}$$

The boundary conditions apply largely to $d\gamma/dx$. For the assumed fully-plastic adhesive stress state, with reference to Figure 12,

$$k = e/\ell \quad . \tag{104}$$

The critical strain developed in the adhesive occurs at the location $x = \ell$, while the adhesive is stress-free at $x = 0$. The solution proceeds along the path

$$\frac{d\gamma_{12}}{dx} = \frac{1}{\eta}\left[\frac{2\ T_2}{E_i t_i} - \frac{2\ T_1}{E_o t_o} + (\alpha_i - \alpha_o)\Delta T\right] \quad , \tag{105}$$

$$\frac{d^2\gamma_{12}}{dx^2} = \frac{2}{\eta}\left[\frac{1}{E_i t_i} + \frac{1}{E_o t_o}\right]\tau_p = \frac{\lambda^2}{G}\tau_p \quad , \tag{106}$$

$$\frac{d\gamma_{34}}{dx} = \frac{1}{\eta}\left[\frac{2\ T_4}{E_i t_i} - \frac{2\ T_3}{E_o t_o} + (\alpha_i - \alpha_o)\Delta T\right] \quad , \tag{107}$$

and

$$\frac{d^2\gamma_{34}}{dx^2} = \frac{2}{\eta}\left[\frac{1}{E_i t_i} + \frac{1}{E_o t_o}\right]\tau_p = \frac{\lambda^2}{G}\tau_p \quad . \tag{108}$$

The solutions of these differential equations are

$$\gamma_{12} = A_{12} + B_{12}x + \frac{\lambda^2\tau_p}{2G}x^2 \tag{109}$$

and

$$\gamma_{34} = A_{34} + B_{34}(x - e) + \frac{\lambda^2\tau_p}{2G}(x - e)^2 \quad . \tag{110}$$

The application of the boundary conditions to equations (105), (107), (109) and (110) needs the evaluation of the adherend stresses due to thermal mismatch.

It is assumed that the overlap is sufficient to induce the maximum stresses, given by equation (70).

$$T_o = -T_i = (\alpha_i - \alpha_o)\Delta T \Big/ \left(\frac{2}{E_o t_o} + \frac{2}{E_i t_i}\right) \qquad \text{at} \quad x = e \quad . \tag{111}$$

The adhesive shear strain at $x = 0$ will, by inspection, be zero for the maximum load case, being usually negative due to thermal stresses prior to application of load. The various boundary conditions are

$$A_{12} = 0 \qquad (\text{from } \gamma_{12} \text{ at } x = 0), \tag{112}$$

$$B_{12} = (\alpha_i - \alpha_o)\Delta T/\eta \qquad (\text{from } d\gamma_{12}/dx \text{ at } x = 0), \tag{113}$$

$$B_{12} + \frac{\lambda^2 \tau_p}{G} e = \frac{(\alpha_i - \alpha_o)\Delta T}{\eta}\left[1 + \left(\frac{2}{E_o t_o} - \frac{2}{E_i t_i}\right)\left(\frac{2}{E_o t_o} + \frac{2}{E_i t_i}\right)\right] + \frac{Pe}{\eta \ell}\left(\frac{2}{E_i t_i} + \frac{2}{E_o t_o}\right)$$

$$(\text{from } d\gamma_{12}/dx \text{ at } x = e), \tag{114}$$

$$A_{34} = A_{12} + B_{12}e + (\lambda^2 \tau_p/2G)e^2 \qquad (\text{from } \gamma_{12} = \gamma_{34} \text{ at } x = e), \tag{115}$$

$$B_{34} = \frac{(\alpha_i - \alpha_o)\Delta T}{\eta}\left[1 + \left(\frac{2}{E_o t_o} - \frac{2}{E_i t_i}\right)\left(\frac{2}{E_o t_o} + \frac{2}{E_i t_i}\right)\right] + \frac{Pe}{\eta \ell}\left(\frac{2}{E_i t_i} + \frac{2}{E_o t_o}\right) - \frac{2P}{\eta E_o t_o}$$

$$(\text{from } d\gamma_{34}/dx \text{ at } x = e), \tag{116}$$

$$B_{34} + \frac{\lambda^2 \tau_p}{G}(\ell - e) = \frac{(\alpha_i - \alpha_o)\Delta T}{\eta} + \frac{2P}{\eta E_i t_i} \qquad (\text{from } d\gamma_{34}/dx \text{ at } x = \ell), \tag{117}$$

and

$$(\gamma_e + \gamma_p) = A_{34} + B_{34}(\ell - e) + (\lambda^2 \tau_p/2G)(\ell - e)^2 \quad (\text{from } \gamma_{34} \text{ at } x = \ell). \tag{118}$$

Elimination of A_{34} and B_{34} by means of equations (111) through (117) leads to the following expression for the load carried:

$$P = \tau_p \ell = \frac{\eta(\gamma_e + \gamma_p) - (\alpha_i - \alpha_o)\Delta T \ell}{\frac{\ell}{2}\left(\frac{2}{E_i t_i}\right) - \left(\frac{\ell - 2e}{2}\right)\left(\frac{2}{E_o t_o}\right)} \quad . \tag{119}$$

The load is seen to be greatest when

$$e = \ell/2 \quad . \tag{120}$$

Therefore, for efficient design, the bolt (row) should be located in the middle of the doubler. The adhesive shear strain at the middle of the doubler then follows from equations (83) and (88) as

$$\gamma = A_{34} = \frac{(\alpha_i - \alpha_o)\Delta T}{\eta}\left(\frac{\ell}{2}\right) + \frac{\lambda^2 \tau_p}{2G}\left(\frac{\ell}{2}\right)^2$$

$$= \frac{(\gamma_e + \gamma_p)}{2} + \frac{\tau_p \ell^2}{8}\left(\frac{2}{E_o t_o} - \frac{2}{E_i t_i}\right) \quad , \tag{121}$$

which is precisely half that at the critical end ($x = \ell$) in the event that the doublers are balanced with respect to the basic adherend. That is $E_o t_o = E_i t_i$. While the stiffness ratio $(E_i t_i)/(E_o t_o)$ has no effect on the total load transferred, it can be shown that the adhesive shear strain gradients are minimized when $E_i t_i = E_o t_o$. In this event, and with the bolt in the middle of the doubler, $d\gamma_{12}/dx$ equals $d\gamma_{34}/dx$ at $x = \ell/2$. Equation (119) seems to suggest that P decreases as ℓ increases. Actually, however, ℓ is not really a variable since the length of overlap is determined by the conditions that, at P_{ult}, $\gamma_{34} = (\gamma_e + \gamma_p)$ at $x = \ell$ and $\gamma_{12} = 0$ at $x = 0$. Re-arrangement of equation (119) leads to the following expression for ℓ

$$\frac{\tau_p}{E_i t_i}\ell^2 + (\alpha_i - \alpha_o)\Delta T\, \ell - \eta(\gamma_e + \gamma_p) = 0 \quad , \tag{122}$$

whence

$$\ell = \frac{-(\alpha_i - \alpha_o)\Delta T + \sqrt{[(\alpha_i - \alpha_o)\Delta T]^2 + \dfrac{4\tau_p \eta(\gamma_e + \gamma_p)}{E_i t_i}}}{(2\tau_p / E_i t_i)} \tag{123}$$

and, for each side of the joint,

$$P_{ult} = \tau_p \ell = \frac{\sqrt{[(\alpha_i - \alpha_o)\Delta T]^2 + \dfrac{4\tau_p \eta(\gamma_e + \gamma_p)}{E_i t_i}} - (\alpha_i - \alpha_o)\Delta T}{2/E_i t_i} \quad . \tag{124}$$

Strictly, this same load $P_{ultimate}$ given by equation (124) applies for any overlap $\geq \ell$ given by equation (123). The reason is the negligible load transferred by the elastic adhesive in the additional parts of the overlap. In determining ℓ from equation (123), care must be taken to ensure that the maximum positive and negative loads are inserted in turn. If no reverse load is ever to be applied, the appropriate other limit is zero load to protect against a

possible design which would hold together as long as the load was maintained, but split apart as soon as it was unloaded.

EXAMPLE 7:

To illustrate the application of the formulas above, consider a graphite-epoxy composite laminate 1.0 inch wide and 16 plies thick of the (0°/45°/0°/-45°) pseudo-isotropic pattern. This is to be loaded up through bonded titanium doublers and a single bolt in double-shear. The composite adherend strength outside the joint area is $103{,}000 \times 1.0 \times 16 \times 0.0055 = 9{,}064$ lb. A suitable bolt to carry this load in double shear is a 5/16 inch diameter AN or NAS bolt heat-treated to 125 ksi. The net section strength of the laminate through the bolt hole is adequate for the half-load carried there. There is no need to consider the use of a smaller bolt of higher heat-treatment. Some of the bolt load will be transferred to the composite by direct bearing on the bolt but, because the modulus of the laminate is only about half that of the titanium, it is only slightly conservative to assume that all the bolt bearing takes place on the titanium. With a yield bearing stress of 216 ksi at e/d = 2 for annealed 6Aℓ-4V titanium, each doubler needs a minimum thickness of 0.067 inch for the 5/16 inch bolt. Then, with a ductile adhesive, for which $\tau_p = 6000$ psi, $n(\gamma_e + \gamma_p) = 0.010$ inch, $\alpha_i = 0$, $\alpha_o = 5.8 \times 10^{-6}/°F$, $E_i = 11.9 \times 10^6$ psi, $t_i = 0.088$ inch, $\Delta T = -50 - 350 = -400$ °F, the maximum load that can be carried is evaluated by means of equation (124) as $P_{ult} = 6{,}804$ lb which, when doubled to account for the duplicated bond area, is adequate for the load required. The design minimum overlap is evaluated by means of equation (123) as $\ell = 1.13$ inch and is 50 per cent more than the theoretical minimum for a perfect bond. This, then is a satisfactory design with a margin for environmental deterioration. A suitable actual overlap is 1.375 inch to allow adequate tolerances. Had the computed margin of potential bond strength to actual laminate strength (outside the joint) been less than 50 per cent, or even negative, it would have been necessary to increase the extensional stiffness of the composite locally by adding 0° plies. It should be noted that the bond strength increase goes up slightly less rapidly than $\sqrt{Et}$. Also, it can be seen from equation (124) that, for thick laminates and brittle adhesives, there is a distinct possibility that the doublers will split off. In this case, checking equation (83) of Reference 1 for peel stresses shows them not to be a problem. Assuming one bond-line

thickness of adherend affected by the peel stresses,

$$t_{o_{max}} = \left(\frac{8000}{6000}\right)^4 \frac{16 \times 10^6 \times 0.005}{3 \times (1 - 0.09)} \left(\frac{1}{0.5 \times 10^6} + \frac{1}{1.7 \times 10^6} + \frac{1}{16 \times 10^6}\right) = 0.245 \text{ inch}$$

while the actual value of t_o is 0.067 inch.

5. IN-PLANE SHEAR TRANSFER THROUGH BONDED JOINTS

The direct transfer of in-plane shear loads from one member to another is covered by the analyses in References 1 and 3. In essence, the governing equations are the same as for direct loads except that the adherend stiffnesses Et are replaced by the appropriate Gt. The thermal stress picture is more complicated, being a negligible problem except at the two diagonally opposite corners of the bond area because, elsewhere the thermally-induced adhesive shear strains are orthogonal with respect to those caused by mechanical loads. This situation is depicted in Figure 13. An effective simple technique for dealing with thermal stresses under in-plane shear loading is to use a modified form of equation (77) to compute the residual bond strain as

$$\gamma_r = [(\alpha_2 - \alpha_1)\Delta T]^2 \Big/ \left| 2\tau_p w n \left(\frac{1}{E_1 A_1} + \frac{1}{E_2 A_2} \right) \right| \qquad (125)$$

and subtracting this from the total adhesive shear strain otherwise available for reacting the mechanical loads.

The analysis of a single load path for in-plane shear is straightforward, but that for multiple load paths, as at the intersection of two cells of a multi-cell torsion box is more complicated. An illustrative example of such problems, below, serves to describe the technique to be employed in such cases. Thermal stress considerations have been omitted because, in practice, such structures are usually made of a single material throughout.

The mathematical model of the structure to be analyzed is defined in Figure 14. The governing equations, for the sign convention adopted, are as follows:

$$\frac{dS_1}{dx} + \tau = 0 \quad , \qquad \frac{d\delta_1}{dx} = \frac{S_1}{G_1 t_1} \quad , \qquad (126)$$

$$\frac{dS_2}{dx} - \tau = 0 \quad , \qquad \frac{d\delta_2}{dx} = \frac{S_2}{G_2 t_2} \quad , \qquad (127)$$

$$\frac{dS_3}{dy} + \tau = 0 \quad , \qquad \frac{d\delta_3}{dy} = \frac{S_3}{G_3 t_3} \quad , \qquad (128)$$

$$\frac{dS_4}{dy} - 2\tau = 0 \ , \qquad \frac{d\delta_4}{dy} = \frac{S_4}{G_4 t_4} \ , \tag{129}$$

$$\frac{dS_5}{dy} + \tau = 0 \ , \qquad \frac{d\delta_5}{dy} = \frac{S_5}{G_5 t_5} \ , \tag{130}$$

$$\frac{dS_6}{dx_1} - \tau = 0 \ , \qquad \frac{d\delta_6}{dx_1} = \frac{S_6}{G_6 t_6} \ , \tag{131}$$

$$\frac{dS_7}{dx_1} + \tau = 0 \ , \qquad \frac{d\delta_7}{dx_1} = \frac{S_7}{G_7 t_7} \ , \tag{132}$$

$$\gamma_{12} = \frac{\delta_2 - \delta_1}{\eta} \ , \quad \gamma_{34} = \frac{\delta_4 - \delta_3}{\eta} \ , \quad \gamma_{45} = \frac{\delta_4 - \delta_5}{\eta} \ , \quad \gamma_{67} = \frac{\delta_6 - \delta_7}{\eta} \ . \tag{133}$$

It follows that

$$\frac{d\gamma_{12}}{dx} = \frac{1}{\eta}\left(\frac{S_2}{G_2 t_2} - \frac{S_1}{G_1 t_1}\right) \ , \quad \frac{d^2\gamma_{12}}{dx^2} = \frac{\tau_p}{\eta}\left(\frac{1}{G_1 t_1} + \frac{1}{G_2 t_2}\right) = \frac{(\lambda_{12})^2}{G}\tau_p \ , \tag{134}$$

$$\frac{d\gamma_{34}}{dy} = \frac{1}{\eta}\left(\frac{S_4}{G_4 t_4} - \frac{S_3}{G_3 t_3}\right) \ , \quad \frac{d^2\gamma_{34}}{dy^2} = \frac{\tau_p}{\eta}\left(\frac{1}{G_3 t_3} + \frac{2}{G_4 t_4}\right) = \frac{(\lambda_{34})^2}{G}\tau_p \ , \tag{135}$$

$$\frac{d\gamma_{45}}{dy} = \frac{1}{\eta}\left(\frac{S_4}{G_4 t_4} - \frac{S_5}{G_5 t_5}\right) \ , \quad \frac{d^2\gamma_{45}}{dy^2} = \frac{\tau_p}{\eta}\left(\frac{2}{G_4 t_4} + \frac{1}{G_5 t_5}\right) = \frac{(\lambda_{45})^2}{G}\tau_p \ , \tag{136}$$

$$\frac{d\gamma_{67}}{dx_1} = \frac{1}{\eta}\left(\frac{S_6}{G_6 t_6} - \frac{S_7}{G_7 t_7}\right) \ , \quad \frac{d^2\gamma_{67}}{dx_1^2} = \frac{\tau_p}{\eta}\left(\frac{1}{G_6 t_6} + \frac{1}{G_7 t_7}\right) = \frac{(\lambda_{67})^2}{G}\tau_p \ , \tag{137}$$

The solutions of these differential equations are

$$\gamma_{12} = A_{12} + B_{12}x + \frac{(\lambda_{12})^2\tau_p}{2G}x^2 \ , \tag{138}$$

$$\gamma_{34} = A_{34} + B_{34}y + \frac{(\lambda_{34})^2\tau_p}{2G}y^2 \ , \tag{139}$$

$$\gamma_{45} = A_{45} + B_{45}y + \frac{(\lambda_{45})^2\tau_p}{2G}y^2 \ , \tag{140}$$

$$\gamma_{67} = A_{67} + B_{67}x_1 + \frac{(\lambda_{67})^2\tau_p}{2G}x_1^2 \quad , \tag{141}$$

in which x and x_1 differ only in origin. Most of the boundary conditions are applied by means of the first of each of the equation sets (134) through (137). Thus

$$B_{12} = -\frac{S_1}{\eta G_1 t_1} \quad , \qquad \text{at} \quad x = 0 \quad , \tag{142}$$

$$B_{12} + \frac{(\lambda_{12})^2\tau_p}{G}\ell_{12} = \frac{1}{\eta}\left[\frac{\tau_p\ell_{12}}{G_2t_2} - \frac{(S_1 - \tau_p\ell_{12})}{G_1t_1}\right] \quad , \qquad \text{at} \quad x = \ell_{12} \quad , \tag{143}$$

$$B_{34} = -\frac{\tau_p\ell_{12}}{\eta G_3 t_3} = -\frac{\tau_p\ell_{34}}{\eta G_3 t_3} \quad , \qquad \text{at} \quad y = 0 \quad , \tag{144}$$

$$B_{34} + \frac{(\lambda_{34})^2\tau_p}{G}\ell_{34} = \frac{S_4}{\eta G_4 t_4} \quad , \qquad \text{at} \quad y = \ell_{34} \quad , \tag{145}$$

$$B_{45} = -\frac{\tau_p\ell_{45}}{\eta G_5 t_5} = -\frac{\tau_p\ell_{67}}{\eta G_5 t_5} \quad , \qquad \text{at} \quad y = 0 \quad , \tag{146}$$

$$B_{45} + \frac{(\lambda_{45})^2\tau_p}{G}\ell_{45} = \frac{S_4}{\eta G_4 t_4} \quad , \qquad \text{at} \quad y = \ell_{45} \quad , \tag{147}$$

$$B_{67} = -\frac{1}{\eta}\left[\frac{(S_1 - \tau_p\ell_{12})}{G_7t_7} - \frac{\tau_p\ell_{67}}{G_6t_6}\right] \tag{148}$$

$$= -\frac{1}{\eta}\left[\frac{(S_7 + \tau_p\ell_{67})}{G_7t_7} - \frac{\tau_p\ell_{45}}{G_6t_6}\right] \quad , \qquad \text{at} \quad x_1 = 0 \quad , \quad (x = \ell_{12}) \tag{149}$$

$$B_{67} + \frac{(\lambda_{67})^2\tau_p}{G}\ell_{67} = -\frac{S_7}{\eta G_7 t_7} \qquad \text{at} \quad x_1 = \ell_{67} \quad , \quad (x = \ell_{12} + \ell_{67}) \quad . \tag{150}$$

In these equations, ℓ_{12}, ℓ_{34}, ℓ_{45} and ℓ_{67} refer to the effective fully-plastic zones out of the total overlaps, which may be greater but do not contribute to extra load transfer. Since the angles tying the skin and web together may also serve as concentrated spar caps, none of the frequently possible reductions in variables is effected here. Nevertheless, since the outer legs of the angles are stress free, it follows quite generally that

$$\ell_{12} = \ell_{34} \qquad \text{and} \qquad \ell_{45} = \ell_{67} \quad . \tag{151}$$

Gross equilibrium also requires that

$$(\ell_{12} + \ell_{67}) = (S_1 - S_7)/\tau_p = S_4/\tau_p \tag{152}$$

while, also,

$$(\ell_{34} + \ell_{45}) = S_4/\tau_p \quad . \tag{153}$$

Now, from equations (144) through (147),

$$(\ell_{45} - \ell_{34})\frac{\tau_p}{\eta}\left[\frac{1}{G_4 t_4}\right] = 0 \tag{154}$$

so that, quite generally,

$$\ell_{12} = \ell_{34} = \ell_{45} = \ell_{67} = \ell_{\text{effective}} = \frac{S_1 - S_7}{2\tau_p} = \frac{S_4}{2\tau_p} \quad . \tag{155}$$

In other words, each bond transfers precisely the same load as the other three.

One of these four extents of overlaps becomes critical first, depending on the relative adherend stiffnesses. The maximum possible extent of plastic adhesive zone occurs when the shear strain is zero in the middle (strictly γ_e to identify between upper and lower bounds) and at its maximum value $(\gamma_e + \gamma_p)$ at each extreme of the overlap. However, this is likely to occur only for the central web if $G_3 t_3 = G_5 t_5 = G_4 t_4/2$. In general, one side of the overlap will be more critical than the other and the extent of effective overlap less. The derivation of the critical overlap follows from the scheme outlined in Figure 15. Quite generally, the effective overlap is

$$\ell = \left(1 - \frac{dy_\alpha/dx}{dy_\beta/dx}\right)\sqrt{\frac{y_\beta}{A}} \tag{156}$$

where

$$\left|\frac{dy_\alpha}{dx}\right| \leq \left|\frac{dy_\beta}{dx}\right| \tag{157}$$

and, here,

$$A = (\lambda_{\alpha\beta})^2 \tau_p/2G \qquad \text{and} \qquad y_\beta = (\gamma_e + \gamma_p) \quad . \tag{158}$$

Note that the minus sign in equation (156) automatically takes care of the possibilities that the gradients have the same or opposite signs.

For the load transfer from element 1 to element 2,

$$\frac{d\gamma_\alpha/dx}{d\gamma_\beta/dx} = \frac{\dfrac{\tau_p{}^{\ell}{}_{eff}}{G_2t_2} - \left[\dfrac{(S_1 - \tau_p{}^{\ell}{}_{eff})}{G_1t_1}\right]}{-\left(\dfrac{S_1}{G_1t_1}\right)} = -\left[1 - \frac{\tau_p{}^{\ell}{}_{eff}}{S_1}\left(1 + \frac{G_1t_1}{G_2t_2}\right)\right] \tag{159}$$

or, if this ratio is numerically greater than unity, its inverse. Likewise, between elements 3 and 4,

$$\frac{d\gamma_\alpha/dy}{d\gamma_\beta/dy} = -\left(\frac{G_3t_3}{G_4t_4}\right)\left(\frac{S_4}{\tau_p{}^{\ell}{}_{eff}}\right) \qquad \text{(or its inverse)} \tag{160}$$

and, from 4 to 5,

$$\frac{d\gamma_\alpha/dy}{d\gamma_\beta/dy} = -\left(\frac{G_5t_5}{G_4t_4}\right)\left(\frac{S_4}{\tau_p{}^{\ell}{}_{eff}}\right) \qquad \text{(or its inverse)} \tag{161}$$

while, from 6 to 7,

$$\frac{d\gamma_\alpha/dx}{d\gamma_\beta/dx} = \frac{-\left(\dfrac{S_7}{G_7t_7}\right)}{-\left(\dfrac{\tau_p{}^{\ell}{}_{eff}}{G_6t_6}\right) - \left(\dfrac{S + \tau_p{}^{\ell}}{G_7t_7}\right)} = \frac{1}{1 + \dfrac{\tau_p{}^{\ell}}{S_7}\left(1 + \dfrac{G_6t_6}{G_7t_7}\right)}, \tag{162}$$

or its inverse, depending upon magnitude. In applying equation (156), it must be remembered that A is different for each zone because of the different values of $(\lambda_{\alpha\beta})^2$. Thus, the identification of the minimum effective overlap reduces to the problem of evaluating the least value of

$$\ell_{12} = \sqrt{\frac{2n(\gamma_e + \gamma_p)}{\tau_p}}\left\{\frac{\left[2 - \dfrac{\left(1 - \dfrac{S_7}{S_1}\right)}{2}\left(1 + \dfrac{G_1t_1}{G_2t_2}\right)\right]}{\sqrt{\left(\dfrac{1}{G_1t_1} + \dfrac{1}{G_2t_2}\right)}}\right\}, \tag{163}$$

$$\ell_{34} = \sqrt{\frac{2n(\gamma_e + \gamma_p)}{\tau_p}} \left\{ \frac{1 + 2\left(\frac{G_3 t_3}{G_4 t_4}\right)}{\sqrt{\left(\frac{1}{G_3 t_3} + \frac{2}{G_4 t_4}\right)}} \right\} , \tag{164}$$

$$\ell_{45} = \sqrt{\frac{2n(\gamma_e + \gamma_p)}{\tau_p}} \left\{ \frac{1 + 2\left(\frac{G_5 t_5}{G_4 t_4}\right)}{\sqrt{\left(\frac{1}{G_5 t_5} + \frac{2}{G_4 t_4}\right)}} \right\} , \tag{165}$$

$$\ell_{67} = \sqrt{\frac{2n(\gamma_e + \gamma_p)}{\tau_p}} \left\{ \frac{1 - \left[\frac{1}{1 + \frac{1}{2}\left(\frac{S_1}{S_7} - 1\right)\left(1 + \frac{G_6 t_6}{G_7 t_7}\right)}\right]}{\sqrt{\left(\frac{1}{G_6 t_6} + \frac{1}{G_7 t_7}\right)}} \right\} , \tag{166}$$

since

$$\tau_p \ell_{eff} = \frac{S_4}{2} = \frac{(S_1 - S_7)}{2} . \tag{167}$$

Once the minimum value of $\ell_{effective}$ has been established in terms of the adherend properties and load ratios and the adhesive properties, the actual adhesive and adherend loads at failure are proportional to

$$S_4 = 2\tau_p (\ell_{effective})_{minimum} . \tag{168}$$

It can be shown easily that, to maximize the total load capacity of the bond, it is necessary that the overlapping adherends be as stiff as practical, even if this means a thicker member reduced in thickness away from the joint. This problem is too complex to lead to such specific recommendations that the adherend stiffnesses should be balanced, except for the 3-4-5 elements for which, if the bond limits the total load capacity, maximum efficiency requires that

$$G_3 t_3 = G_5 t_5 = G_4 t_4 / 2 . \tag{169}$$

The actual use of this analysis is illustrated in the following example.

The analysis above is based on a hypothetical perfectly-plastic adhesive. Effectively, for real adhesives also, the plastic portion of the stress-strain curve contributes to most of the load transfer and it is only slightly conservative to neglect the elastic load transfer in comparison. On the other hand,

it is important, in sizing the overlaps, to add to the computed plastic zones a sufficient distance for the elastic stress to build up from zero to the plastic value. Typically this distance is of the order of $3/\lambda$ so that, if $d\gamma/dx$ has the same sign at each end of an overlap, a distance equal to $6/\lambda$ should be added to the sum of the two plastic zones.

EXAMPLE 8:

Consider the structure and load ratios shown in Figure 16. Use the notation of Figure 14, with adhesive properties $\tau_p = 6000$ psi, $\gamma_e = 0.1$, $\gamma_p = 2.0$, and $\eta = 0.005$ inch. Assume a 2024-T3 aluminum structure for the skins, web and angles, so that $G = 4.0 \times 10^6$ psi and $F_{su} = 40$ ksi. Then the maximum effective overlap is the least of

$$\ell_{12} = \sqrt{\frac{2 \times 0.005 \times 2.1}{6000}} \left\{ \frac{\left| 2 - \frac{(1-0.5)}{2}\left(1 + \frac{0.125}{0.063}\right)\right|}{\sqrt{\left(\frac{1}{4 \times 10^6 \times 0.125} + \frac{1}{4 \times 10^6 \times 0.25}\right)}} \right\} = 1.350 \text{ inch} \quad ,$$

$$\ell_{34} = \ell_{45} = 3.742 \times \left\{ \frac{1 + 2 \times \frac{0.063}{0.125}}{\sqrt{\left(\frac{2}{0.125} + \frac{1}{0.063}\right)}} \right\} = 1.331 \text{ inch} \quad ,$$

$$\ell_{67} = 3.742 \times \left\{ \frac{1 - \left[\frac{1}{1 + \left(\frac{1}{2}\,1 + \frac{0.25}{0.063}\right)}\right]}{\sqrt{\left(\frac{1}{0.25} + \frac{1}{0.063}\right)}} \right\} = 0.598 \text{ inch} \quad .$$

Thus the skin-to-angle bond governs the load capacity and $(\ell_{effective})_{minimum}$ is equal to 0.598 inch. In turn, it follows that

$$S_4 = 2 \times 0.598 \times 6000 = 7{,}176 \text{ lb/inch} \quad ,$$

$$S_1 = 2 \times S_4 = 14{,}352 \text{ lb/inch} \quad ,$$

$$S_7 = S_4 = 7{,}176 \text{ lb/inch} \quad .$$

The corresponding shear stresses in the skin and web are at a uniform value of

$$\tau = 7{,}176 \times 16 = 114{,}816 \text{ psi}$$

which is beyond the allowable F_{su}, so the adherend strengths govern. The recommended value of ℓ then becomes

$$\ell_{67} = \frac{40{,}000 \times 0.063}{2 \times 6000} \times 1.5 + \frac{3}{\lambda_{67}} + 0.25 = 0.315 + 0.671 + 0.25 = 1.236 \text{ inch}$$

for the 6 to 7 overlap, with the 1.5 factor being the design margin of potential bond strength over adherend strength, $3/\lambda$ the single elastic shear stress build-up zone, and the 0.25 the manufacturing tolerance. In the 1 to 2 and 3 to 4 (or 4 to 5) zones, the recommended overlaps are, respectively,

$$\ell_{12} = 0.315 + 6/\lambda_{12} + 0.25 = 0.315 + 1.732 + 0.25 = 2.297 \text{ inch} ,$$

$$\ell_{34} = \ell_{45} = 0.315 + 6/\lambda_{34} + 0.25 = 0.315 + 1.225 + 0.25 = 1.790 \text{ inch} .$$

Note that, even though the low-stress elastic troughs make up a large portion of the total overlaps, they contribute but little to the static joint strength. Their major important role is to attain a long service life by providing an area of inevitably small adhesive strain to resist creep and to serve as the plastic zone late in the life of the joint when the outer edges of the original plastic zones have deteriorated through environmental exposure.

6. PEEL STRESS RELIEF FOR DOUBLE-LAP JOINTS (TAPERED-LAP JOINTS)

Reference 1 suggests certain simple design modifications to extend the thickness range over which double-lap joints can develop adequate efficiencies. Basically, the usual strength limit is due to excessive peel stresses which develop at the ends of the outer adherends at a load level which may be significantly less than either the potential shear strength of the bond or the adherend ultimate strength. Beyond a certain adherend thickness, for a given combination of materials, the joint efficiency drops to intolerably low levels. The object of this section is to explain how to effect a major relief of the peel stress problem, thereby extending the economy in fabrication of uniform lap joints to a greater usable range of thicknesses. The design technique employed is that of tapering the ends of the outer adherends, as shown in Figure 17. Actually, the joint is slightly stronger if the thickness at the end is not quite reduced to zero. A tip approximately 0.010 inch thick is both easier to fabricate and handle without damage. This tip must be minimized to prevent the build up of peel stresses. The analysis below, for a completely feathered end of the overlap, is slightly conservative with regard to the ultimate bond strength but is only slightly so and effectively eliminates one variable from the analysis/design process.

A general analysis prepared for this problem proved to be so complicated as to be beyond algebraic manipulation without assistance from a digital computer. Therefore, what follows is a simpler procedure governing the approximate design of optimum proportions for static ultimate load only. Partial load conditions are not covered by this simplified design procedure but this is considered to be acceptable because such load conditions do not govern the geometry of the design. A slightly conservative analysis for the tapered-lap joints at any load level can be provided by ignoring the taper and using adhesive shear analysis for uniform lap joints. This particular analysis had been approached with a willingness to sacrifice some of the unrealized bond shear strength potential in order to develop the remainder. It transpired that it was quite simple to attain the entire potential bond shear strength while eliminating the

peel-stress problem completely. Indeed, by skillful design, it is possible to exceed by 24 per cent the shear strength potential of uniform double-lap joints by making each of the tapered outer adherends 33 per cent stiffer than one half of the uniform inner adherend.

The mathematical model for the analysis is illustrated in Figure 17 along with the element forces and displacements. Thermal mismatch effects are excluded to elucidate the dominant influences. The small load transfer throughout the elastic trough is ignored and an analysis for a perfectly-plastic adhesive is conducted. At ultimate load the optimum design will maximize the sum of ℓ_u and ℓ_t, the extents of the adhesive plastic zones in the uniform and tapered zones, respectively. The analyses of the zones A-B, B-C and C-D in Figure 17 must be performed separately and the solutions joined by matching boundary conditions. The location of C is defined to occur at the start of the taper on the outer adherends and the length ℓ_t is treated as an unknown to satisfy this condition. (This considerable simplification in analysis eliminates the matching of conditions at one more transition in behavior and is one reason why the analysis is inapplicable to partial load levels. Once designed for ultimate load, the start of the taper remains fixed but the width of the plastic adhesive zone varies with load level. A further reason is that the length ℓ_t would change with load direction in the presence of any adherend thermal mismatch.) Throughout the region A-B, the adhesive shear stress is constant at τ_p while the adhesive shear strain γ varies, reducing to zero at B because the adherend strains are identical throughout the region B-C. (The same is true in the presence of any adherend thermal mismatch and ensures that $d\gamma/dx \equiv 0$ at each end of the zone B-C). Because of the identical uniform adherend strain assumed in the zone B-C for all adherends, it is necessary that

$$\frac{2\tau_p \ell_t}{E_o t_o} = \frac{2\tau_p \ell_u}{E_i t_i} \quad , \tag{170}$$

whence

$$\frac{E_i t_i}{E_o t_o} = \frac{\ell_u}{\ell_t} \tag{171}$$

(Were precise allowance to be made for the elastic adhesive shear transfer in the region B-C, equation (171) would still apply at that single location for

which $d\gamma/dx = 0$). Throughout the zone A-B,

$$\frac{dT_o}{dx} + 2\tau_p = 0 \quad , \qquad \frac{dT_i}{dx} - 2\tau_p = 0 \quad , \tag{172}$$

where T_o represents the force per unit width in both of the outer adherends. The adherend displacements are given by

$$\frac{d\delta_o}{dx} = \frac{T_o}{E_o t_o} \quad , \qquad \frac{d\delta_i}{dx} = \frac{T_i}{E_i t_i} \quad , \tag{173}$$

while the adhesive shear strain is defined by

$$\gamma = (\delta_i - \delta_o) / \eta \quad . \tag{174}$$

It follows that

$$T_o = P - 2\tau_p x \quad , \qquad T_i = 2\tau_p x \quad , \tag{175}$$

where P is the applied load, so that

$$\frac{d\gamma}{dx} = \frac{1}{\eta}\left(\frac{T_i}{E_i t_i} - \frac{T_o}{E_o t_o}\right) \quad , \tag{176}$$

whence

$$\gamma = \gamma_o - \frac{P}{\eta E_o t_o} x + \frac{\tau_p}{\eta}\left(\frac{2}{E_i t_i} + \frac{2}{E_o t_o}\right)\left(\frac{x^2}{2}\right) \quad , \tag{177}$$

γ_o being the adhesive shear strain at $x = 0$. Since ℓ_u is defined to be such that $\gamma = 0$ (or $\gamma = \gamma_e$ for a lower-bound solution),

$$2\frac{\gamma_o}{\gamma_e} - \frac{4\tau_p(\ell_u + \ell_t)\ell_u}{\eta\gamma_e E_o t_o} + \frac{\tau_p}{\eta\gamma_e}\left(\frac{2}{E_i t_i} + \frac{2}{E_o t_o}\right)\ell_u^2 = 0 \quad . \tag{178}$$

At maximum possible load capacity, $\gamma_o = \gamma_e + \gamma_p$. In the zone C-D, equations (172) and (174) still hold, but equations (173) and (175) become

$$\frac{d\delta_o}{dx} = \frac{T_o}{E_o t_o} = \frac{T_o}{E_o t_o (\zeta/\ell_t)} \quad , \qquad \frac{d\delta_i}{dx} = \frac{T_i}{E_i t_i} \quad , \tag{179}$$

$$T_o = 2\tau_p \zeta \quad , \qquad T_i = P - 2\tau_p \zeta \quad . \tag{180}$$

Hence

$$\frac{d\gamma}{d\zeta} = -\frac{d\gamma}{dx} = \frac{1}{\eta}\left[\frac{2\tau_p \ell_t}{E_o t_o} + \frac{2\tau_p \zeta}{E_i t_i} - \frac{P}{E_i t_i}\right] \quad . \tag{181}$$

Using the condition $\gamma = \gamma_\ell$ at $\zeta = 0$, this equation may be integrated to read

$$\gamma = \gamma_\ell + \frac{1}{\eta}\left[\frac{2\tau_p \ell_t}{E_o t_o}\zeta - \frac{P\zeta}{E_i t_i} + \frac{2\tau_p}{E_i t_i}\left(\frac{\zeta^2}{2}\right)\right] \tag{182}$$

and, with the condition $\gamma = 0$ at $\zeta = \ell_t$, this becomes

$$2\frac{\gamma_\ell}{\gamma_e} + \frac{1}{\eta\gamma_e}\left[\frac{4\tau_p \ell_t \ell_t}{E_o t_o} - \frac{4\tau_p(\ell_u + \ell_t)\ell_t}{E_i t_i} + \frac{2\tau_p \ell_t \ell_t}{E_i t_i}\right] = 0 \quad . \tag{183}$$

For the most efficient design, γ_ℓ will reach $(\gamma_e + \gamma_p)$ at the same load level as that at which γ_o does the same at the other end of the joint. This ensures the maximumization of the sum $(\ell_u + \ell_t)$. The matching of γ_o and γ_ℓ requires that

$$\frac{4\ell_t \ell_t}{E_o t_o} - \frac{4(\ell_u + \ell_t)\ell_t}{E_i t_i} + \frac{2\ell_t \ell_t}{E_i t_i} = -\frac{4(\ell_u + \ell_t)\ell_u}{E_o t_o} + \left(\frac{2}{E_i t_i} + \frac{2}{E_o t_o}\right)\ell_u \ell_u \quad . \tag{184}$$

The inclusion of the constraint (171) reduces the number of variables so that

$$\left(\frac{\ell_t}{\ell_u}\right)^3 - \left(\frac{\ell_t}{\ell_u}\right) - 1 = 0 \quad . \tag{185}$$

It is easily shown that the solution of this cubic is

$$\frac{\ell_t}{\ell_u} = \frac{E_i t_i}{E_o t_o} = 1.3247 \quad . \tag{186}$$

That is, the net extensional stiffness of the outer adherends should exceed that of the inner adherend by 32.5 per cent in an optimally designed tapered-lap joint. It seems to be significant that current metal practice in bolted joints of similar configuration calls for each of the (tapered) outer adherends to be between 25 and 40 per cent thicker than half of the (uniform) inner adherend.

Because of this stiffness mismatch, the adhesive plastic zone A-B extends further than would be the case if $E_o t_o = E_i t_i$. For uniform thickness outer adherends with $E_o t_o > E_i t_i$, the end D would be critical, with reserve capacity at end A. Returning to equation (178), and incorporating equations (171) and

(186) for the optimized design, it can be shown that

$$2\left(\frac{\gamma_p}{\gamma_e}\right) = \frac{4\tau_p}{n\gamma_e E_i t_i}(\ell_u)^2\left(\frac{1 + 1.3247}{2 \times 1.3247}\right) \quad . \tag{187}$$

Hence

$$\ell_u = 1.0676\sqrt{\frac{2(\gamma_p/\gamma_e)}{(4\tau_p)/(n\gamma_e E_i t_i)}} \tag{188}$$

and is 1.07 times as great as would be the case if $E_o t_o = E_i t_i$ for a given inner adherend to be bonded. The effect of optimizing the design for peel-stress relief is, consequently, to increase the potential shear strength to

$$P_{optimum} = 1.0676 \times \left(\frac{1 + 1.3247}{2}\right)P_{balanced} \tag{189}$$

which is 24.09 per cent better than the best that could have been achieved with uniformly thick adherends.

It seems remarkable that this relatively inexpensive peel-stress relief modification should be associated with such a significant increase in potential bond shear strength. This simple design/fabrication modification permits the more economical lap joints to be employed effectively throughout a significant range of thicknesses which would otherwise have required the use of more expensive scarf or stepped-lap joints. The influence on joint strength of this concept is depicted in Figure 18 for HTS graphite-epoxy. The tapered-lap joints without the extra build-up on the outer adherends are found to have the same potential shear strength as for uniform outer adherends. The end A is more critical than the end D (Figure 17) because both the peel and shear stress concentrations are relieved by tapering. That tapering the outer adherends in accordance with Figure 17 has no effect on the shear transfer when $E_i t_i = E_o t_o$ follows from equation (171).

7. CONCLUSION

This report shows how to apply the simple concept of shear load transfer through definable fully-effective zones to adhesive-bonded joints of non-standard configuration which occur frequently in aerospace practice. The techniques have been illustrated through a variety of examples which are by no means the limit of applicability of the method. Actually, because the solution of the governing differential equations is far simpler for the all-plastic adhesive than for the perfectly-elastic adhesive, the use of upper and lower bound plastic solutions expands greatly the range of problems for which closed-form analytical solutions can be derived.

The adoption of this plastic zone approach offers a distinct advantage over the older method of computing bond strength as the product of a uniform allowable shear stress and the total bond area. The fact that most of the load is transferred through the plastic adhesive zones has been established by more precise elastic-plastic analyses (References 1 and 2). Likewise, it was shown that the extent of such plastic zones is independent of the total (long) overlap. Therefore, the use of the plastic zone analysis technique correctly relates the potential bond shear strength to the appropriate elastic and geometric parameters instead of to the total overlap area, of which precise analyses have shown the maximum bond strength between given adherends to be independent.

REFERENCES

1. Hart-Smith, L. J., "Adhesive-Bonded Double-Lap Joints," Douglas Aircraft Co., NASA Langley Contract Report CR-112235, January 1973.

2. Hart-Smith, L. J., "Adhesive-Bonded Single-Lap Joints," Douglas Aircraft Co., NASA Langley Contract Report CR-112236, January 1973.

3. Hart-Smith, L. J., "Adhesive-Bonded Scarf and Stepped-Lap Bonded Joints," Douglas Aircraft Co., NASA Langley Contract Report CR-112237, January 1973.

4. Hart-Smith, L. J., "The Bond Stresses in Adhesive-Bonded Doublers," Douglas Aircraft Co., IRAD Technical Report MDC-J0811, July 1970.

5. Henshaw, J., Roy, P. J. and Russell, M. D., "Fabricating Aero-Structures: A practical method of fabricating efficient aero-structures, utilizing unidirectional boron composite with metal," SAMPE Journal, April/May 1970, presented at 1969 National SAMPE Technical Conference, Seattle, Washington.

6. Jones, B. H. and Hart-Smith, L. J., "Reinforcing Conventional Materials with Filamentary Composite," Douglas Aircraft Co., IRAD Technical Report MDC-J0336, December 1969.

7. Dickerson, E. O. and Lackman, L. M., "Boron Reinforced Longerons," Los Angeles Division, North American Rockwell, Paper NA-72-728, presented at AFFDL/AFML Conference on Fibrous Composites in Flight Vehicle Design, Proceedings published as Technical Report AFFDL-TR-72-130, Dayton, Ohio, September 1972.

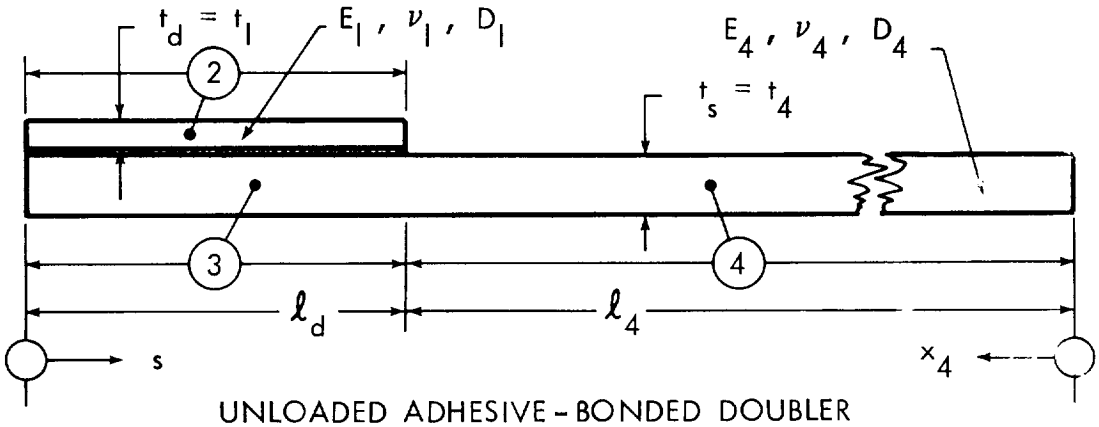

UNLOADED ADHESIVE-BONDED DOUBLER

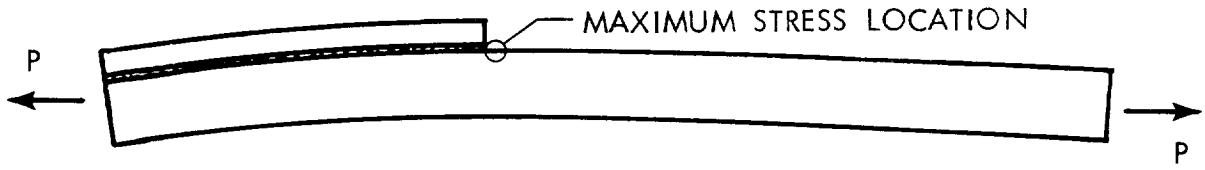

SKIN/DOUBLER DEFLECTION UNDER LOAD

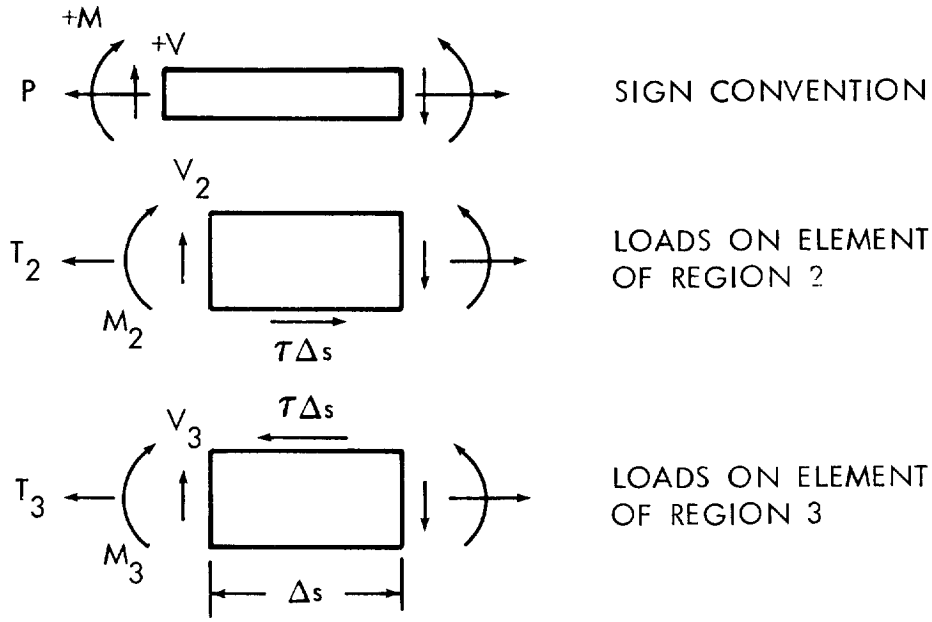

FIGURE 1. CO-ORDINATE SYSTEM AND DEFORMATIONS IN ADHESIVE-BONDED DOUBLERS

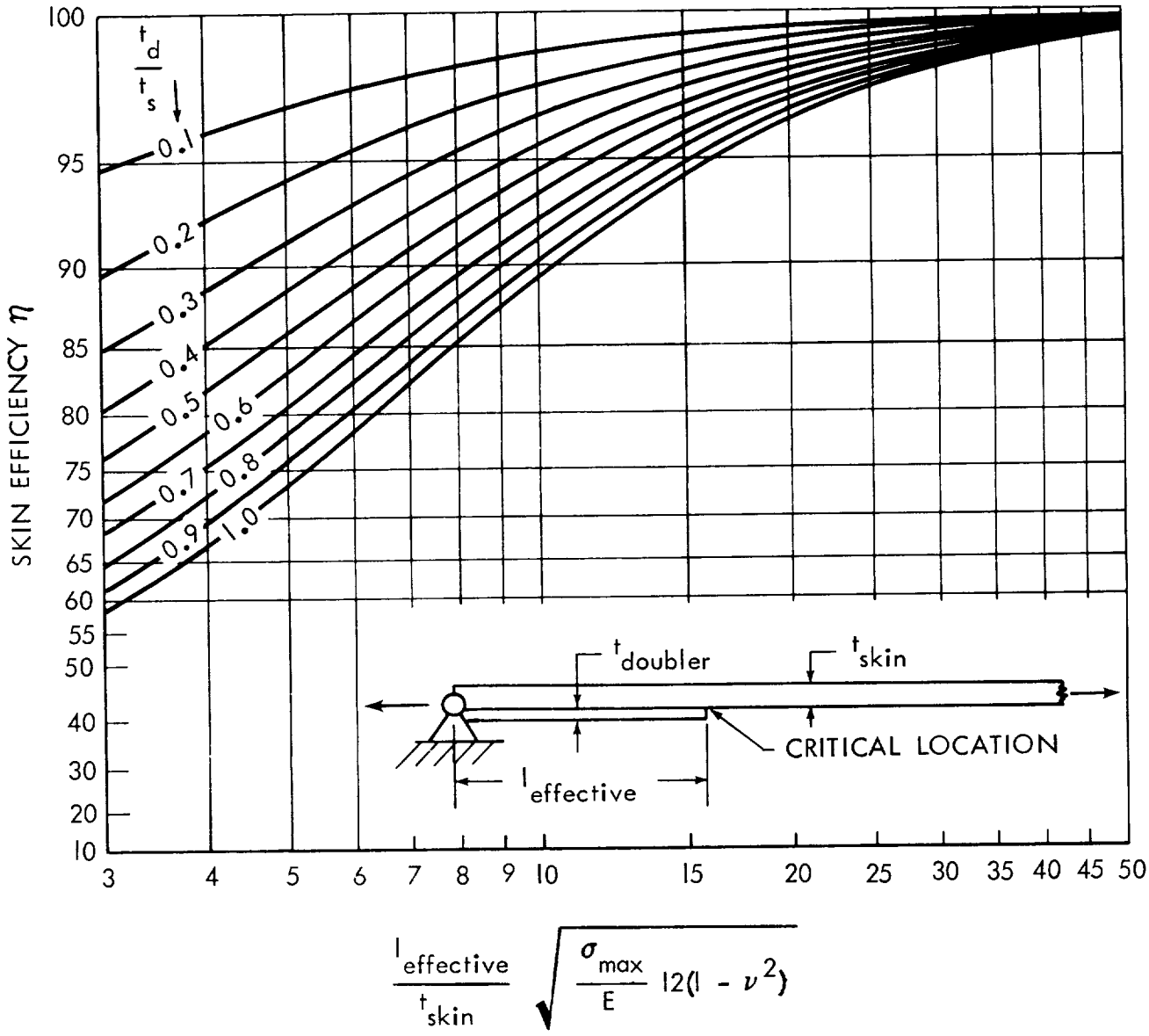

FIGURE 2. SKIN EFFICIENCY FOR BONDED DOUBLERS WITH SIMPLY-SUPPORTED EDGE CONDITIONS

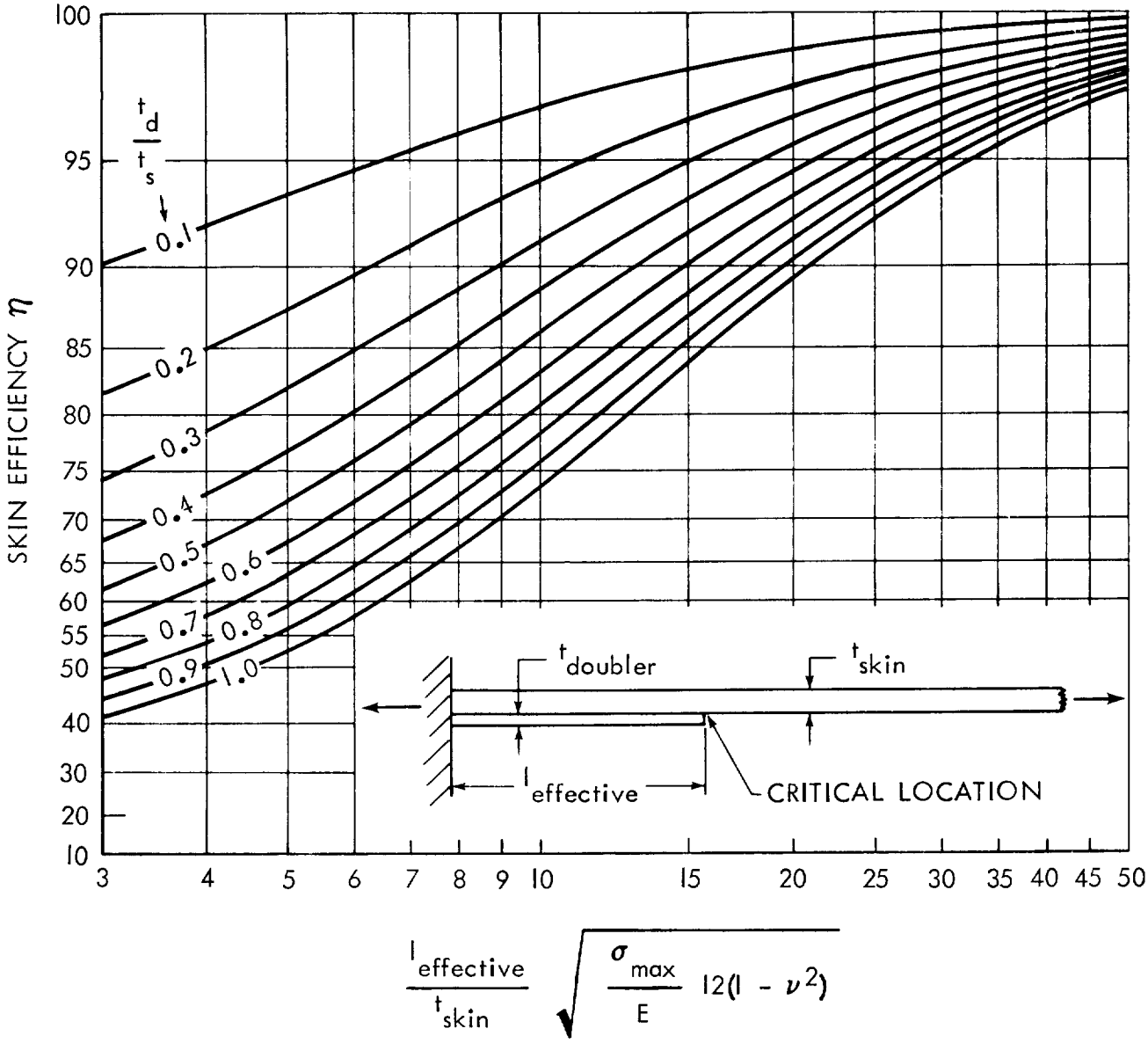

FIGURE 3. SKIN EFFICIENCY FOR BONDED DOUBLERS WITH BUILT-IN EDGE CONDITIONS

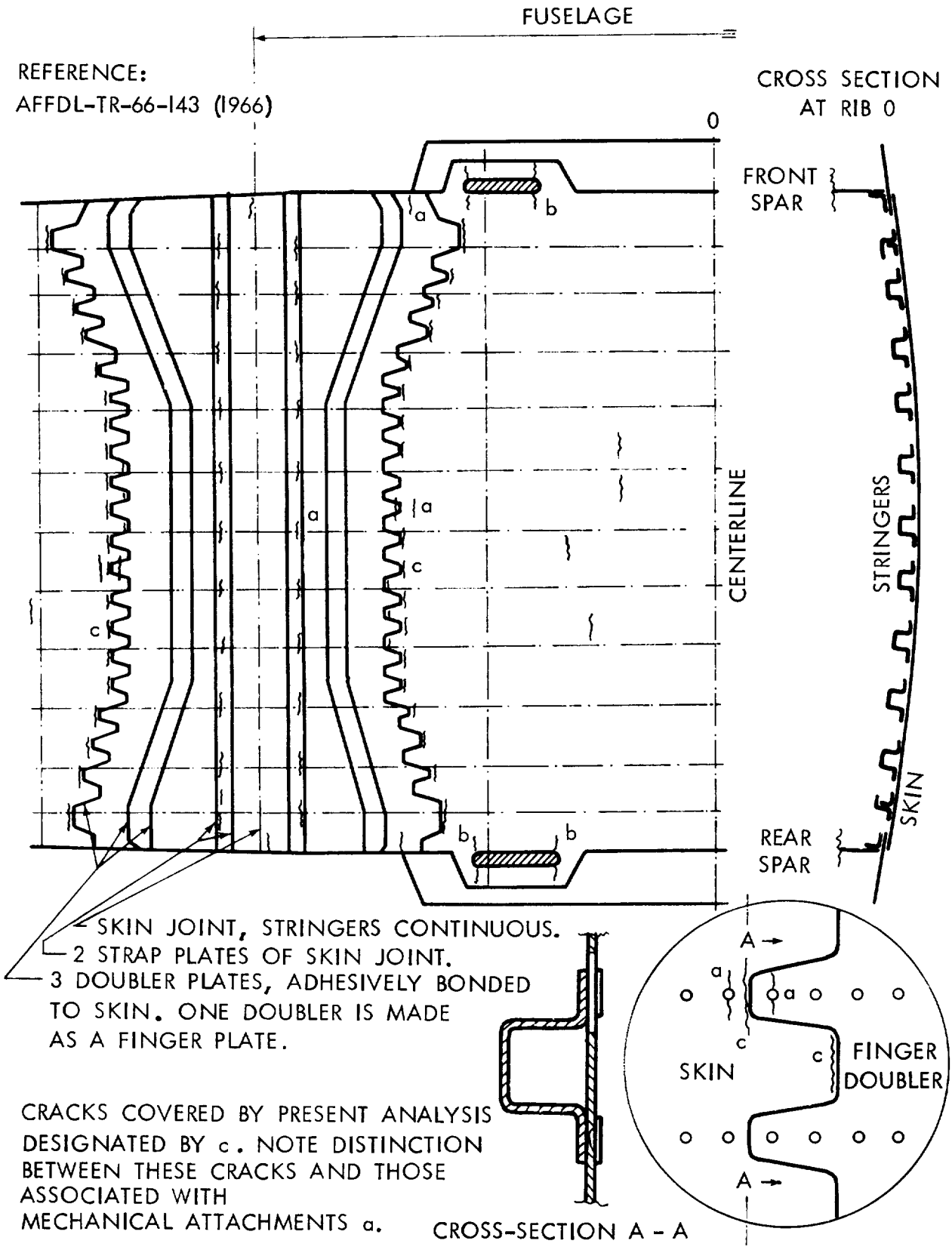

FIGURE 4. FATIGUE CRACKS DEVELOPED DURING TESTING OF AIRCRAFT STIFFENED PANELS WITH BONDED DOUBLERS

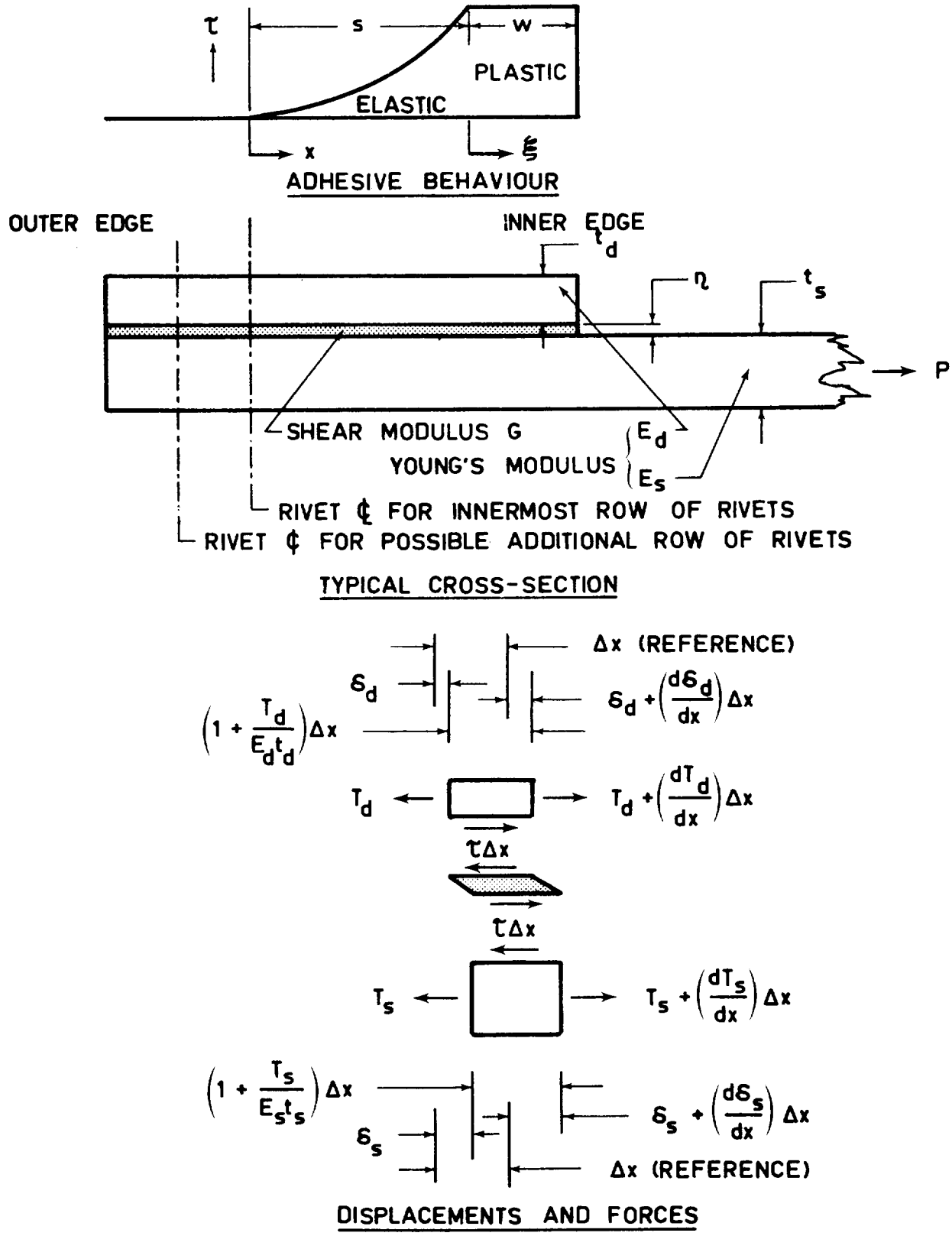

FIGURE 5. CO-ORDINATE SYSTEM AND DEFORMATIONS IN BONDED DOUBLERS

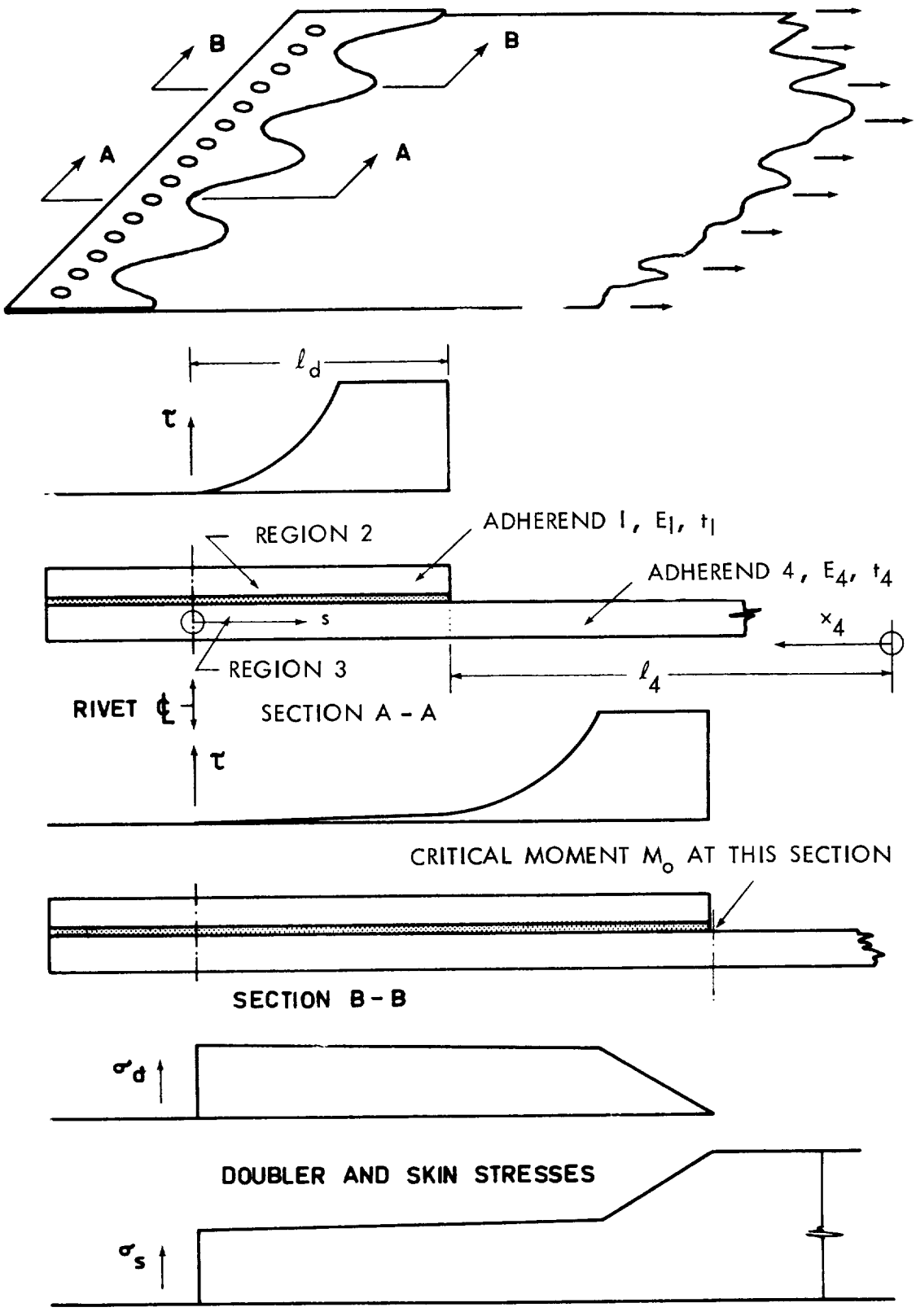

FIGURE 6. ADHESIVE SHEAR STRESS DISTRIBUTIONS FOR BONDED FINGER DOUBLERS

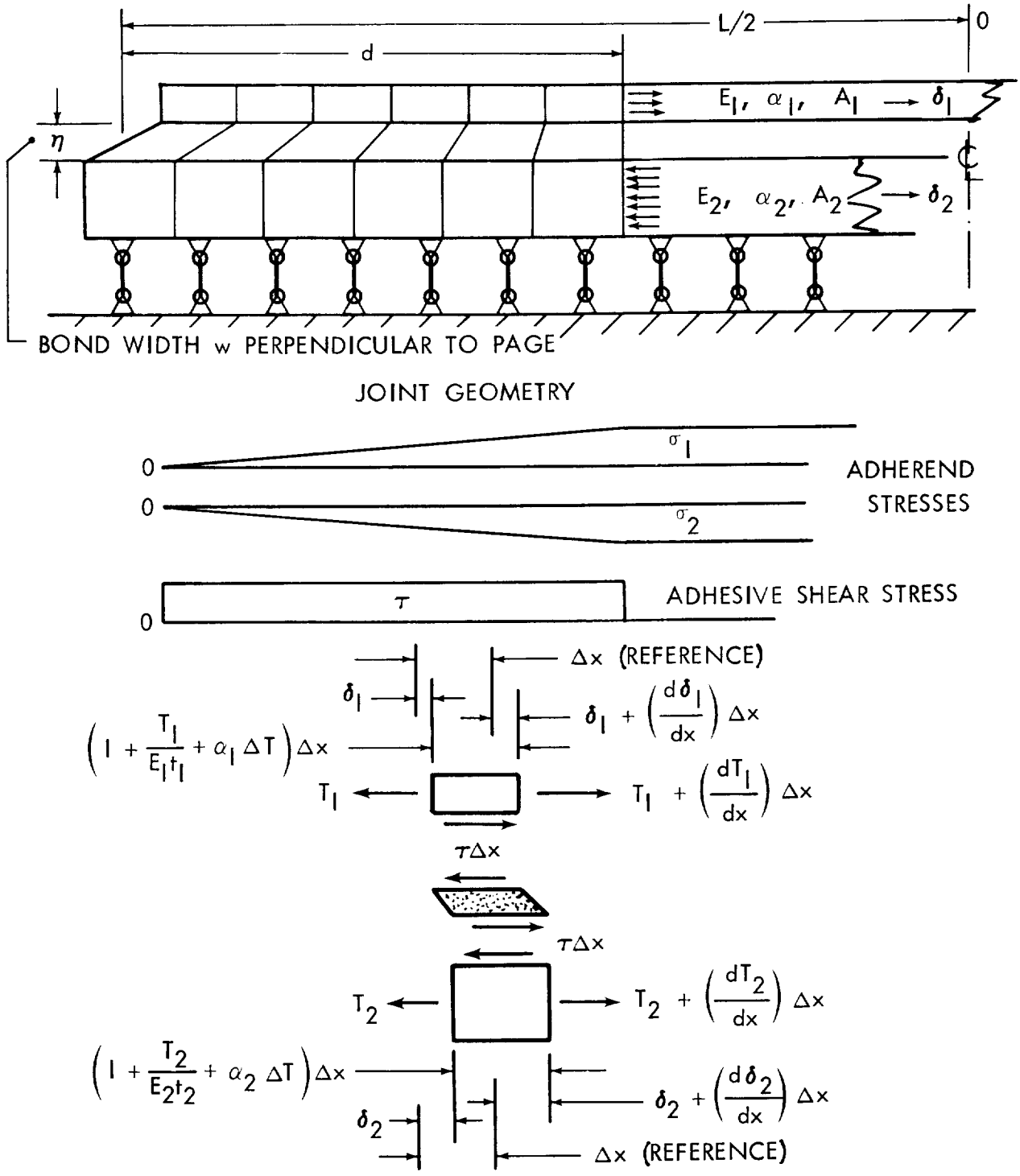

FIGURE 7. NOTATION AND MATHEMATICAL MODEL FOR ANALYSIS OF TRANSFER STRESSES WITH SELECTIVELY-REINFORCED STRUCTURES

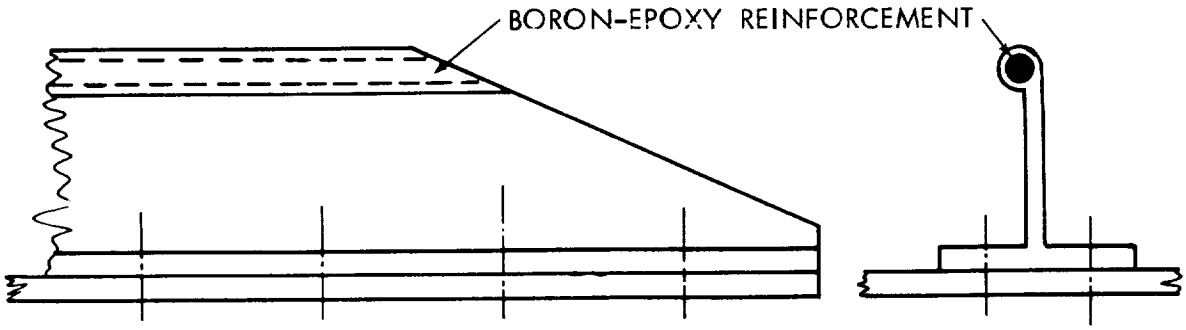

STRINGER RUNOUT CONFIGURATION TYPICAL OF METAL PRACTICE

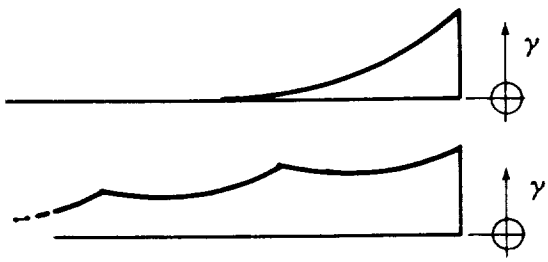

NOTE HOW PEAK SHEAR STRAINS COINCIDE ABOVE FOR EACH LOAD COMPONENT

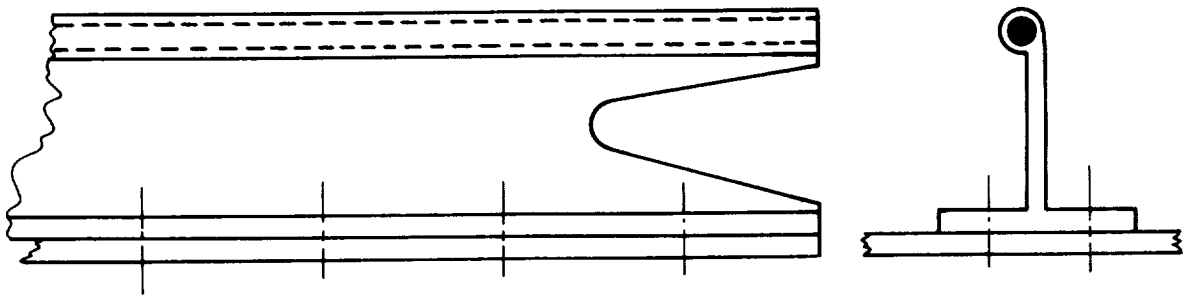

STRINGER RUNOUT CONFIGURATION SUITABLE FOR SELECTIVE REINFORCEMENT BY INFILTRATED EXTRUSIONS

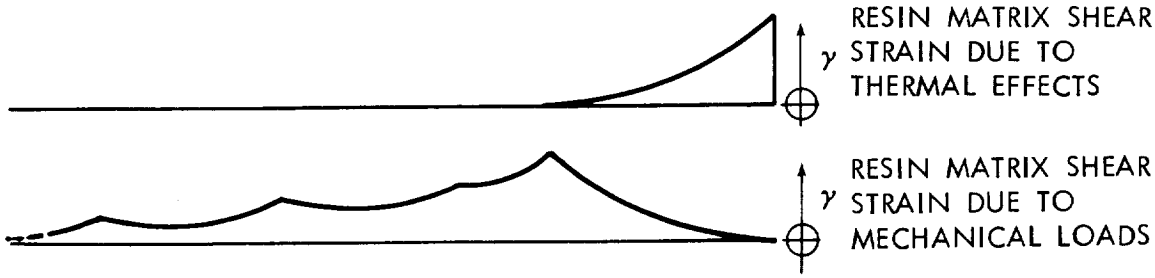

NOTE HOW PEAK SHEAR STRAINS FOR THE TWO LOAD COMPONENTS ARE SITUATED AT TWO DIFFERENT LOCATIONS

FIGURE 8. DESIGN DETAILING FOR SELECTIVE REINFORCEMENT OF METAL STRUCTURES BY BONDED COMPOSITES

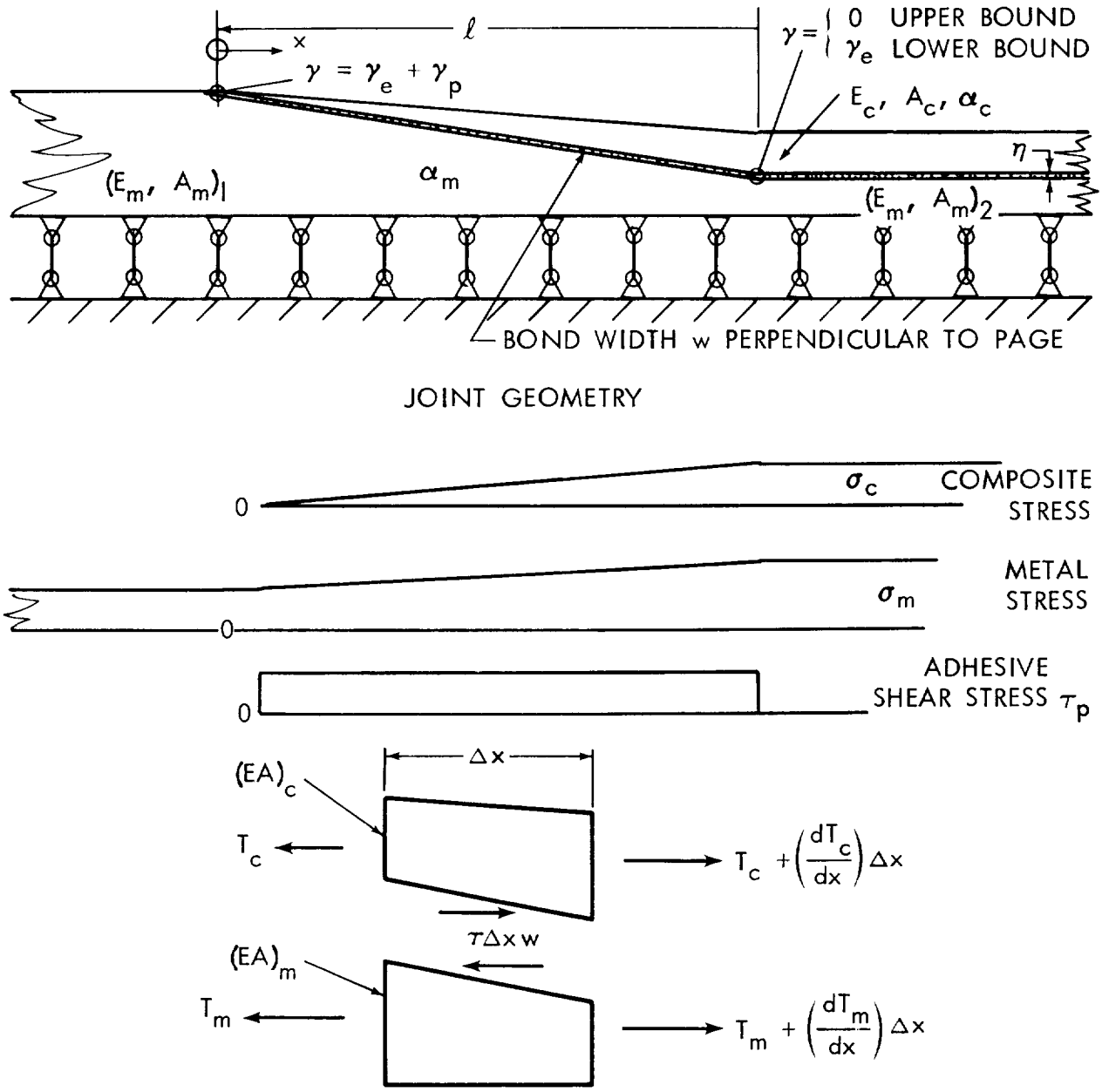

FIGURE 9. NOTATION AND MATHEMATICAL MODEL FOR ANALYSIS OF BONDED DOUBLERS WITH FEATHERED EDGES

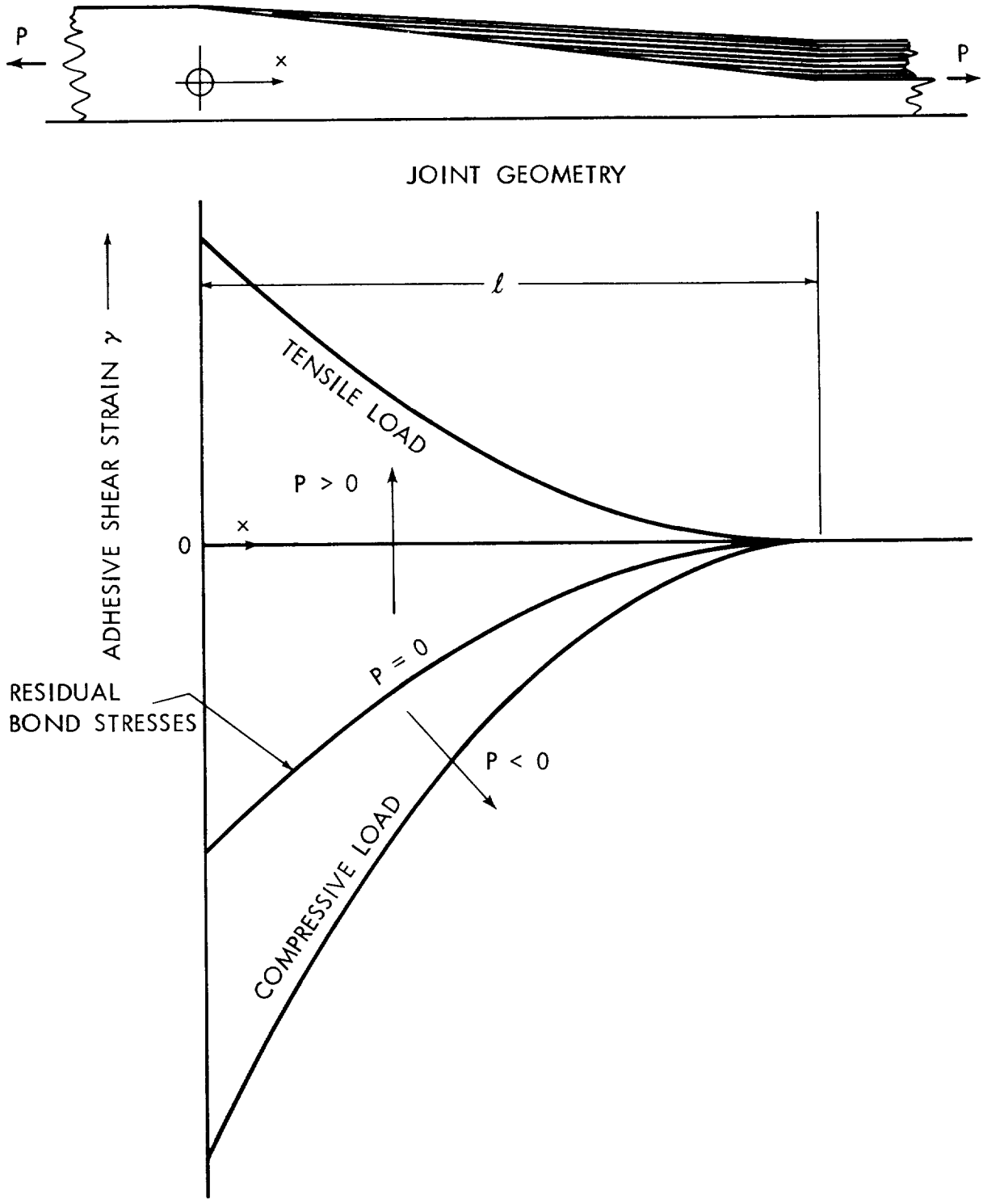

FIGURE 10. ADHESIVE SHEAR STRAIN DISTRIBUTION FOR BONDED TAPERED DOUBLERS

INTERNALLY-BONDED DOUBLERS (IDEAL)

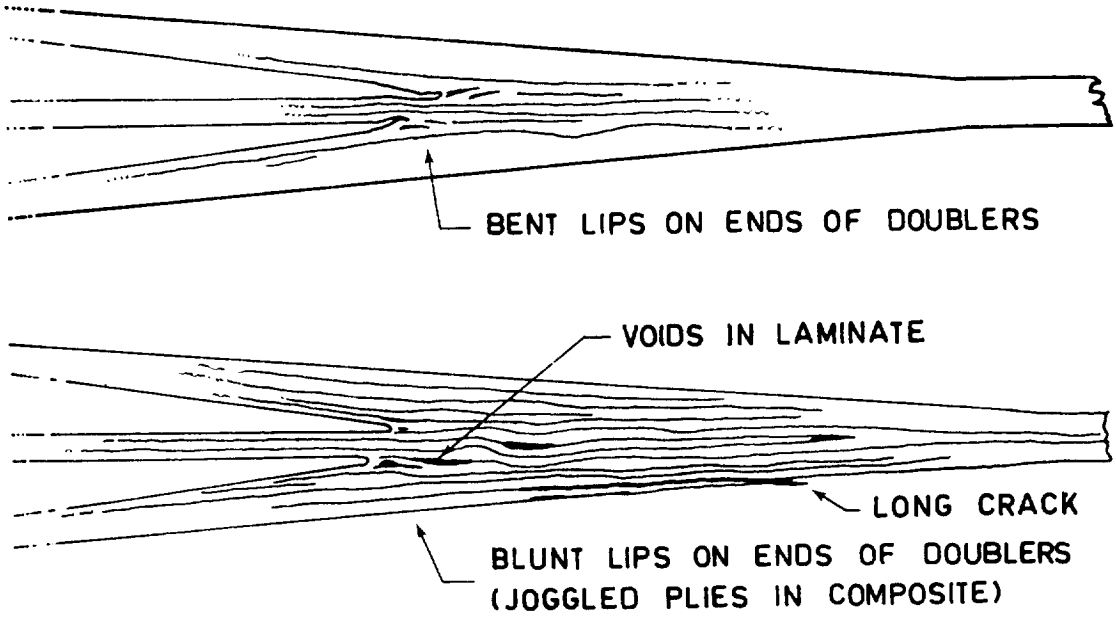

INTERNALLY-BONDED DOUBLERS
(REPRODUCED FROM ACTUAL PHOTOGRAPHS)

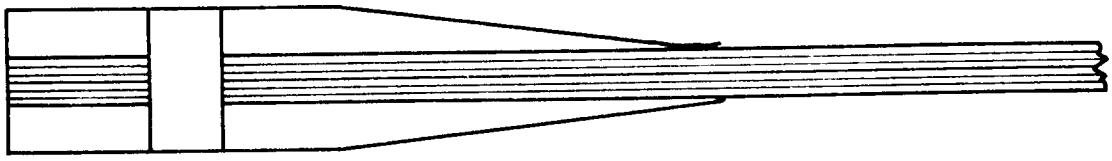

EXTERNALLY-BONDED DOUBLERS (ACTUAL)

FIGURE 11. INTERNAL AND EXTERNAL BONDED METAL DOUBLERS

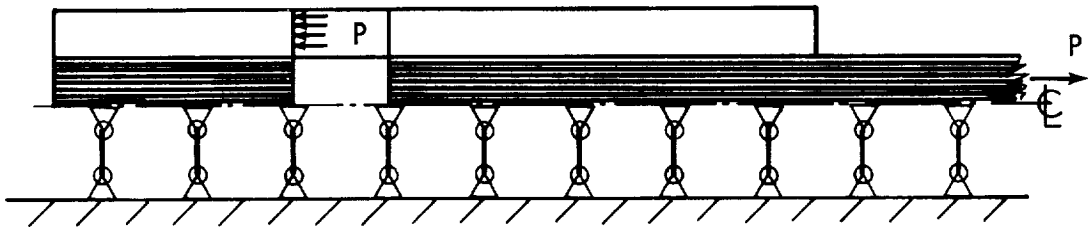

JOINT GEOMETRY

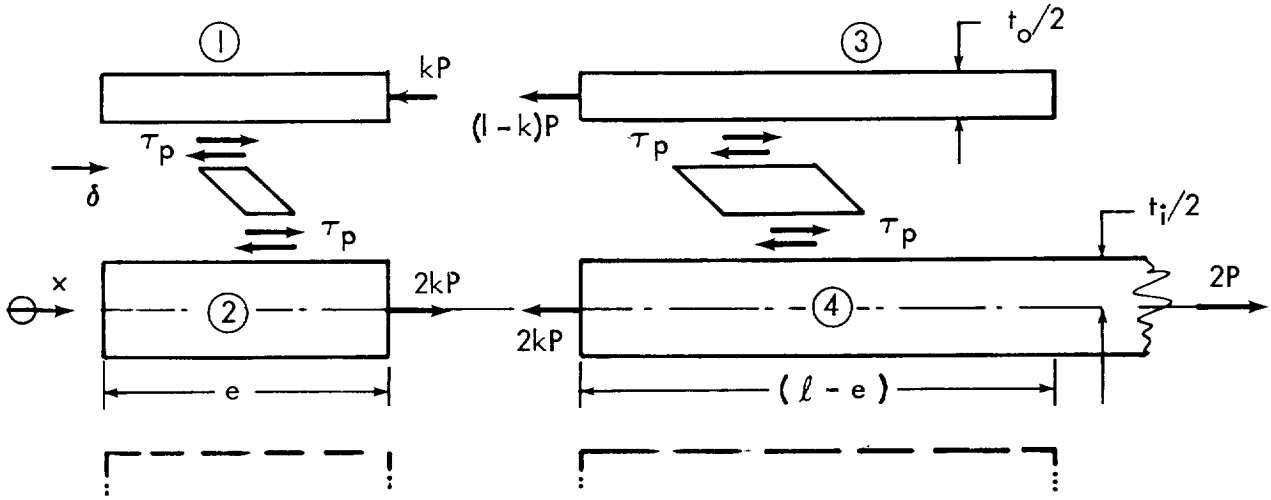

(NOTE THAT ENTIRE BEARING LOAD IS ASSUMED TO BE REACTED ON METAL DOUBLER(S) BECAUSE OF HIGHER MATERIAL STIFFNESS THAN FOR COMPOSITE).

LOAD DISTRIBUTION

FIGURE 12. NOTATION AND MATHEMATICAL MODEL FOR ANALYSIS OF BONDED METAL DOUBLERS AT BOLT HOLES IN COMPOSITE LAMINATES

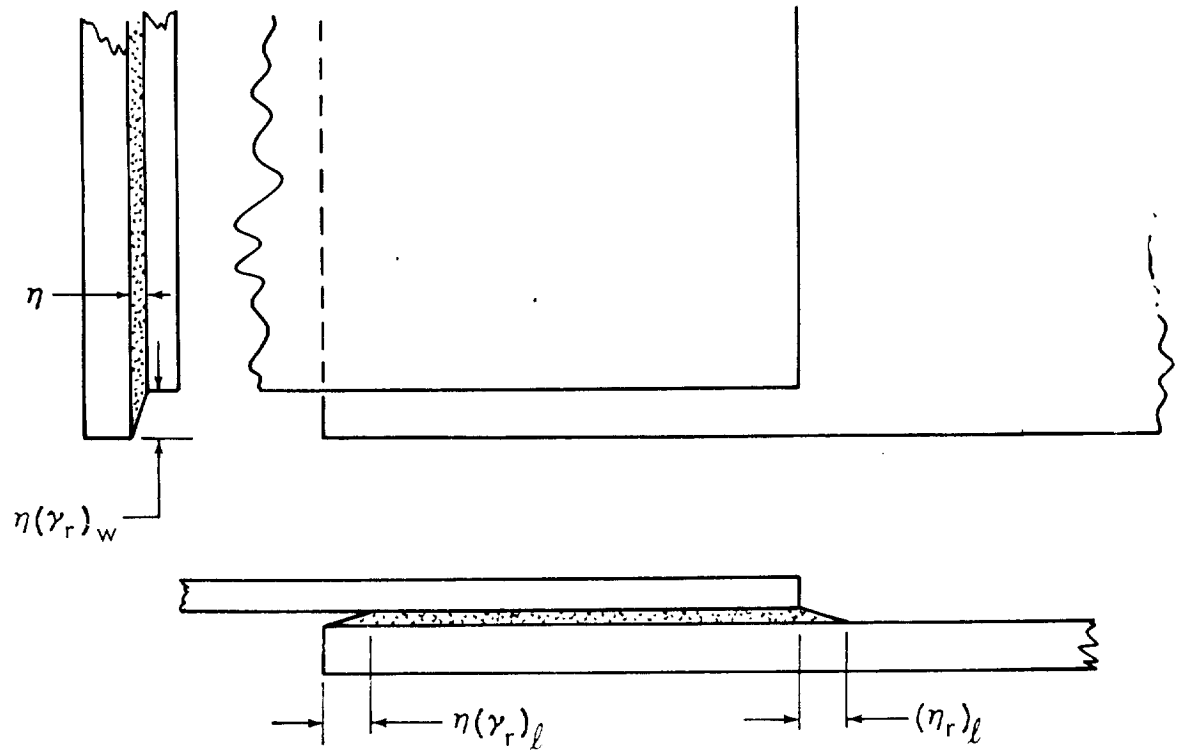

BOND-LINE DISPLACEMENTS DUE TO THERMAL MISMATCH

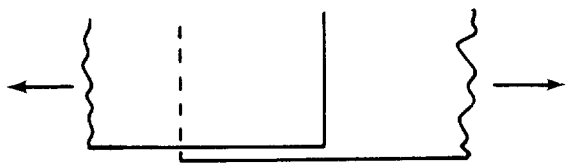

DIRECT LOADING

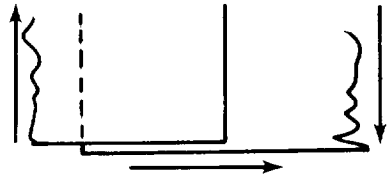

IN-PLANE SHEAR LOADING

$$(\gamma_e + \gamma_p)^2 = \left|(\gamma_r)_w\right|^2 + \left|\gamma_{mechanical} + (\gamma_r)_\ell\right|^2$$

$$(\gamma_e + \gamma_p)^2 = \left|(\gamma_r)_\ell\right|^2 + \left|\gamma_{mechanical} + (\gamma_r)_w\right|^2$$

$\gamma_{mechanical}$ = MAXIMUM ADHESIVE SHEAR STRAIN INDUCED BY MECHANICAL LOADS

γ_r = RESIDUAL ADHESIVE SHEAR STRAIN DUE TO THERMAL MISMATCH BETWEEN THE ADHERENDS

FIGURE 13. ADHESIVE SHEAR STRAIN MAXIMA UNDER MULTIPLE LOADS

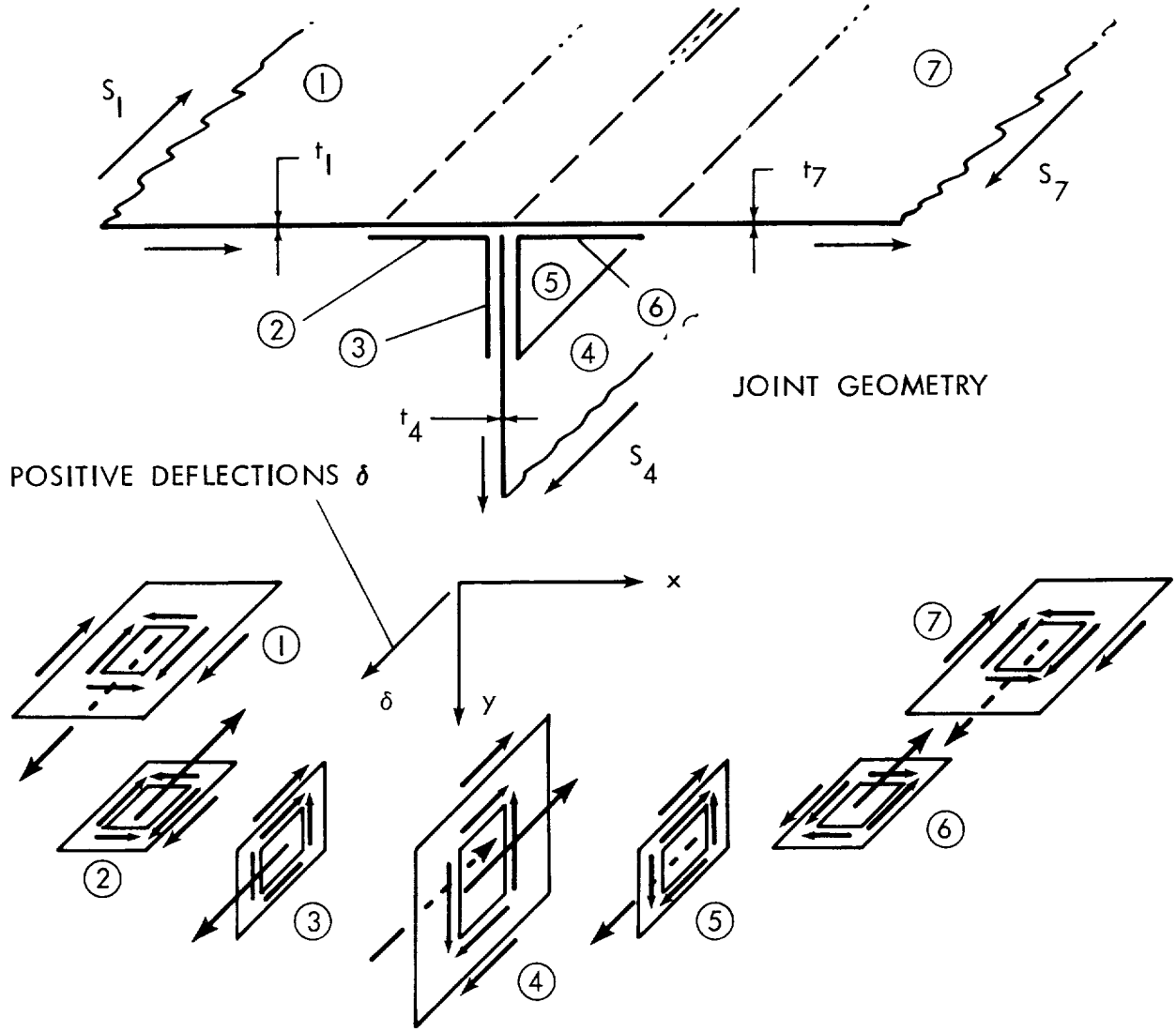

FIGURE 14. NOTATION FOR ANALYSIS OF SHEAR FLOWS IN MULTI-CELL TORSION BOXES

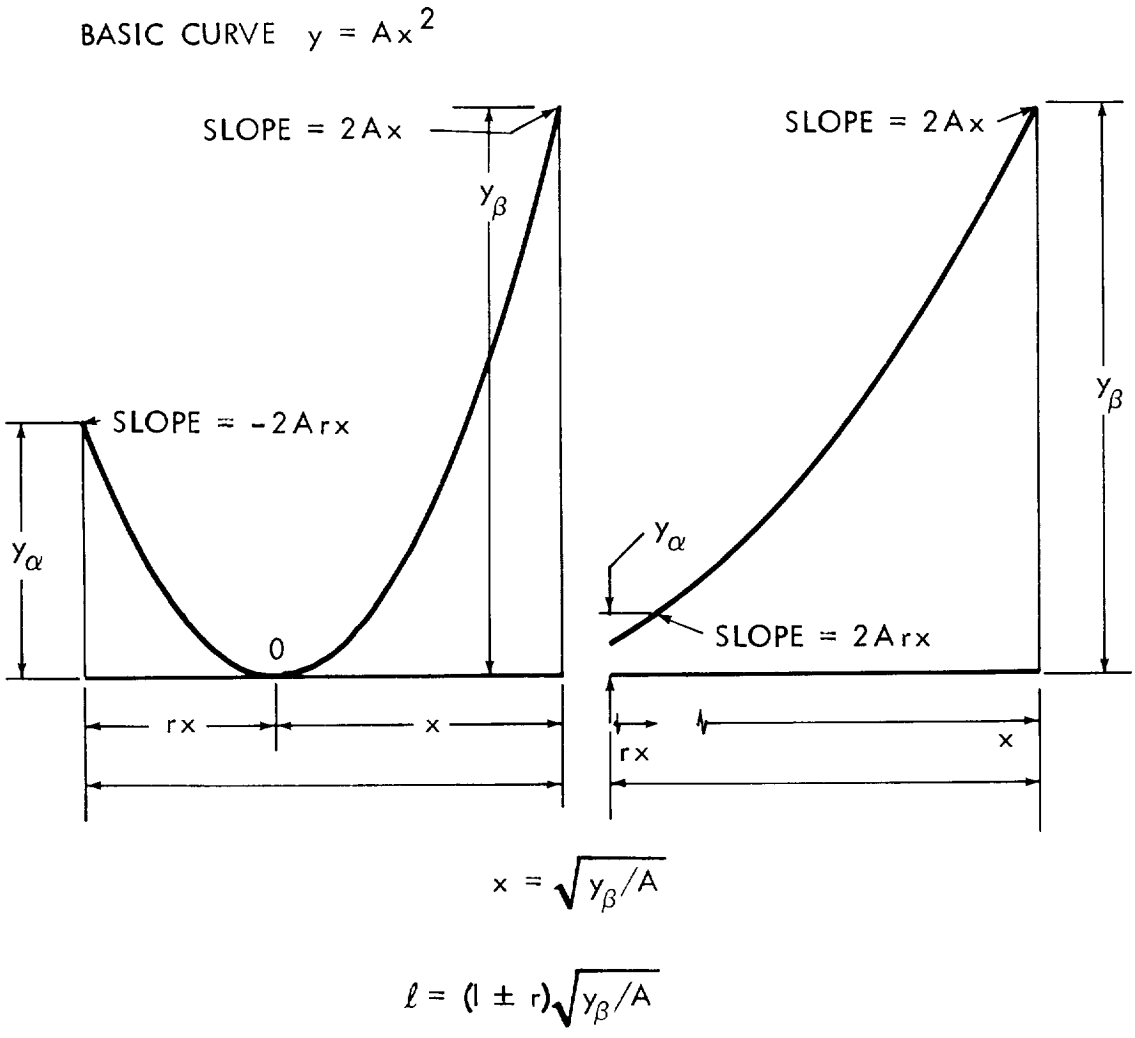

FIGURE 15. ADHESIVE SHEAR STRAIN DISTRIBUTIONS FOR SINGLE LEG OF MULTIPLE-PATH SHEAR FLOW

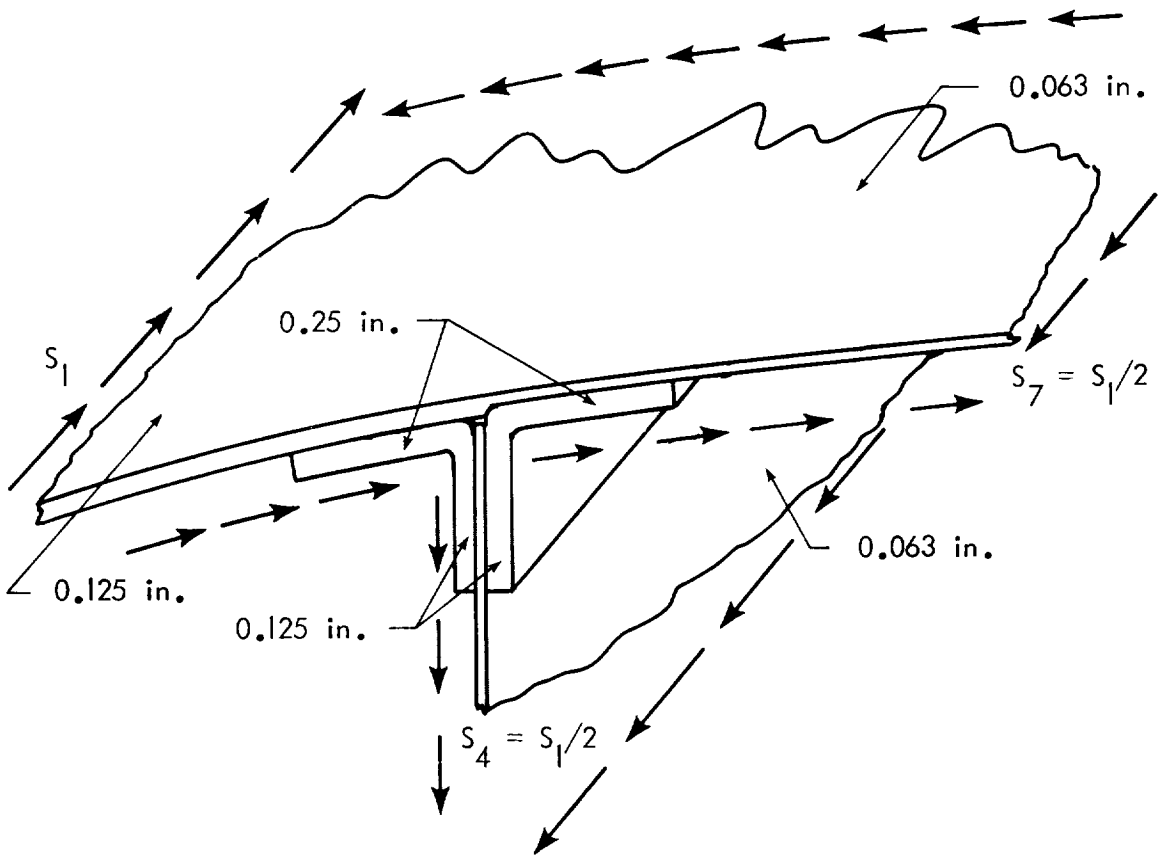

MATERIAL: ALUMINUM ALLOY

FIGURE 16. DETAIL OF MULTI-CELL BONDED TORSION BOX

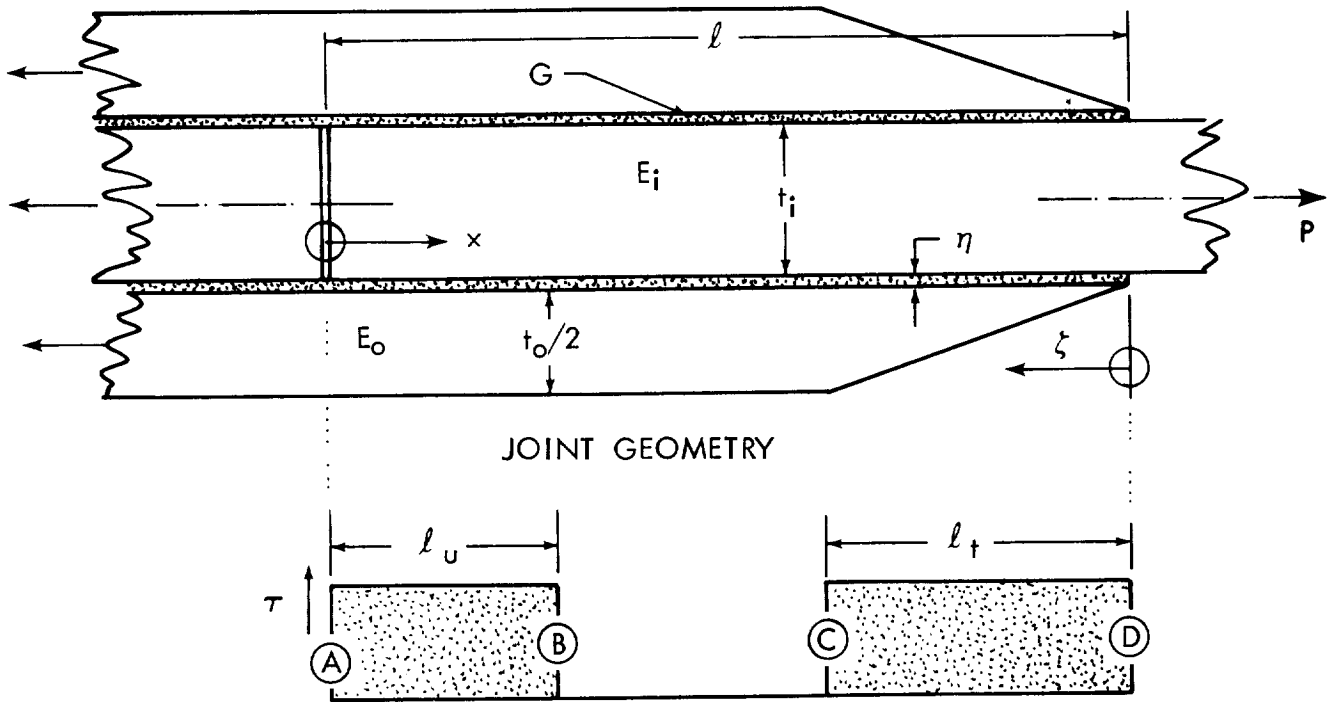

FIGURE 17. NOTATION AND MATHEMATICAL MODEL FOR ANALYSIS OF TAPERED-LAP BONDED JOINTS

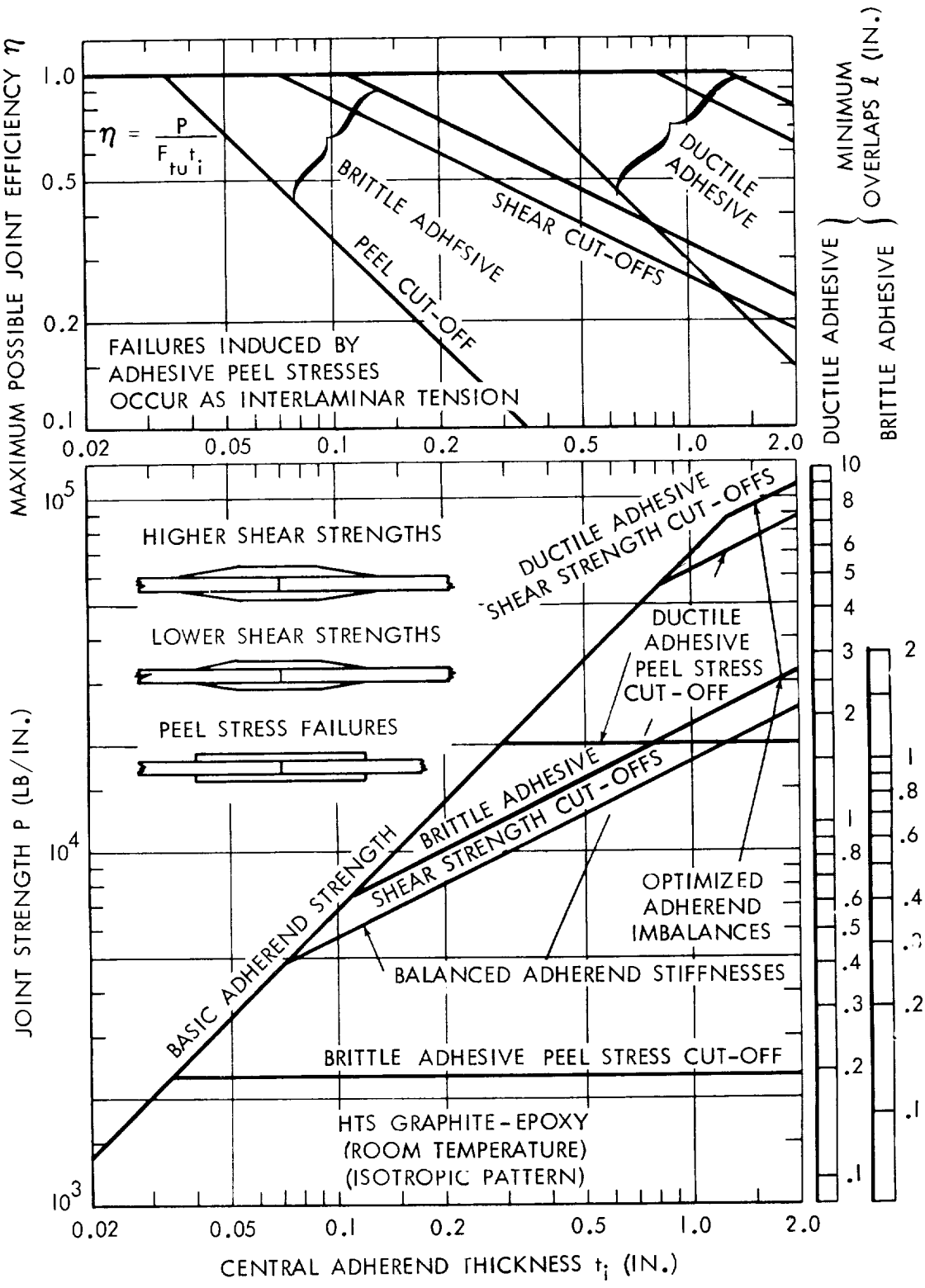

FIGURE 18. COMPARISON OF JOINT STRENGTHS FOR TAPERED AND UNIFORM DOUBLE-LAP JOINTS

TABLE OF MATERIAL PROPERTIES FOR FIGURE 18

HIGH-STRENGTH GRAPHITE-EPOXY:

$(0°/+45°/90°/-45°)_s$ pattern:

$E_L^t = 8.0 \times 10^6$ psi, $E_N^t = 1.7 \times 10^6$ psi,

$F_L^{tu} = 69$ ksi, $F_N^{tu} = 8$ ksi,

(in which the subscript N refers to properties in the thickness direction).

DUCTILE ADHESIVE:

$\tau_p = 6$ ksi, $\eta = 0.005$ in., $\gamma_p/\gamma_e = 20$,

$\eta(\frac{1}{2}\gamma_e + \gamma_p) = 0.0102$ in., $E_c \simeq 500$ ksi, $\sigma_{c_{max}} \simeq 10$ ksi.

BRITTLE ADHESIVE:

$\tau_p = 9$ ksi, $\eta = 0.005$ in., $\gamma_p/\gamma_e = 1.5$,

$\eta(\frac{1}{2}\gamma_e + \gamma_p) = 0.00042$ in., $E_c \simeq 1500$ ksi, $\sigma_{c_{max}} \simeq 17$ ksi.

APPENDIX

The following Fortran IV computer programs were developed in the preparation of Figures 2 and 3 for the efficiency of skin material when used in conjunction with bonded doublers around the edges on one side only. No data cards are required since the parameters are read in as part of the program. Illustrative sheets of output are included for each program. The first program applies for built-in edges at the outer periphery of the skin/doubler combination while the second one covers simply-supported edges. The doubler ℓ/t parameter is defined as

$$OL(J) = \frac{\ell_{doubler}}{t_{skin}} \left(\sqrt{\frac{\sigma_{max} 12(1-\nu^2)}{k_b E}} \right)_{skin}$$

and the bending stiffness parameter as

$$BENDK(M) = \left[\frac{D}{\left(\frac{Et^3}{12(1-\nu^2)} \right)} \right]_{skin}$$

```
C SINGLE-LAP ADHESIVE-BONDED DOUBLERS
C ADHEREND PLASTIC HINGE FORMATION (OR FRACTURE) - UNBALANCED STIFFNESS
C ADHEREND BENDING AND EXTENSIONAL STIFFNESSES UNCOUPLED FOR COMPOSITES
C NON-DIMENSIONALIZED FORMULATION
      DIMENSION OL(38), SIGAV(38,10), ESIGAV(10), BENDK(13)
C SET OVERLAP ARRAY
      OL(1) = 0.
      OL(2) = 0.1
      OL(3) = 0.15
      OL(4) = 0.2
      OL(5) = 0.25
      OL(6) = 0.3
      OL(7) = 0.35
      OL(8) = 0.4
      OL(9) = 0.5
      OL(10) = 0.6
      OL(11) = 0.7
      OL(12) = 0.8
      OL(13) = 0.9
      OL(14) = 1.
      OL(15) = 1.5
      OL(16) = 2.
      OL(17) = 2.5
      OL(18) = 3.
      OL(19) = 3.5
      OL(20) = 4.
      OL(21) = 5.
      OL(22) = 6.
      OL(23) = 7.
      OL(24) = 8.
      OL(25) = 9.
      OL(26) = 10.
      OL(27) = 15.
      OL(28) = 20.
      OL(29) = 25.
      OL(30) = 30.
      OL(31) = 35.
      OL(32) = 40.
      OL(33) = 50.
      OL(34) = 70.
      OL(35) = 100.
      OL(36) = 200.
      OL(37) = 500.
      OL(38) = 1000.
C SET BENDING STIFFNESS PARAMETER ARRAY
      BENDK(1) = 0.1
      BENDK(2) = 0.15
      BENDK(3) = 0.2
      BENDK(4) = 0.3
      BENDK(5) = 0.5
      BENDK(6) = 0.7
      BENDK(7) = 1.
      BENDK(8) = 1.5
      BENDK(9) = 2.
      BENDK(10) = 3.
      BENDK(11) = 5.
      BENDK(12) = 7.
      BENDK(13) = 10.
C SELECT BENDING STIFFNESS PARAMETER
      DO 50 M = 1, 13
C SET ADHEREND THICKNESS RATIO
      TR = 11.
      DO 30 K = 1, 10
      TR = TR - 1.
      T10VT4 = TR / 10.
      D10VD4 = T10VT4 ** 3
C SET INITIAL ESTIMATE ON AVERAGE ADHEREND STRESS
      V3 = 1. / (1. + (3. / BENDK(M)) * T10VT4)
      SIGAV(1,K) = V3
      DO 20 J = 2, 38
C SET NON-DIMENSIONALIZED OVERLAP
      V2 = OL(J) ** 2
      N = 0
    1 N = N + 1
      IF (N .GT. 500) GO TO 8
C PROGRAM USES L(DOUBLER) / T(SKIN) AS L/T RATIO
      V10 = V3 * V2 / BENDK(M)
C TO USE L/T RATIO FOR DOUBLER INSTEAD OF SKIN, USE
C     V10 = V3 * V2 * D10VD4 / BENDK(M)
C FOR SIMPLY-SUPPORTED ENDS OF SKIN-DOUBLER COMBINATION
C     V8 = 1. + SQRT(V10) + V10 / 6.
C FOR BUILT-IN ENDS OF SKIN-DOUBLER COMBINATION
      V8 = 1. + (SQRT(V10)) / 2. + V10 / 24.
C EVALUATE ECCENTRICITY PARAMETER
C     EK = 1. / V8
C RE-ESTIMATE AVERAGE SKIN STRESS
      V4 = 1. / (1. + (3. / BENDK(M)) * (T10VT4 / V8))
C CHECK CONVERGENCE OF AVERAGE STRESS
```

```
      R = V3 / V4
      IF ( (1.0001 .GT. R) .AND. (0.9999 .LT. R) ) GO TO 20
      V3 = V4
      GO TO 1
C EVALUATE AVERAGE SKIN STRESS AT LIMIT LOAD
C (YIELD STRENGTH FOR METALS - ULTIMATE STRENGTH FOR COMPOSITES)
   20 SIGAV (J,K) = V3
   30 CONTINUE
C PRINT OUT TABULATIONS
      WRITE (6,5) BENDK(M)
    5 FORMAT (1H1,  5(/), 30X, 35HSINGLE-LAP ADHESIVE-BONDED DOUBLERS//
     1 20X, 55HNON-DIMENSIONALIZED FORMULATION FOR STIFFNESS IMBALANCE//
     2 30X, 30HBENDING STIFFNESS PARAMETER =  , F5.1///
     3 3X, 7HDOUBLER, 18X, 49HAVERAGE ADHEREND STRESS / MAXIMUM ADHEREND
     4 STRESS/, 5X, 3HL/T/, 3X, 9HPARAMETER, 14X, 53HTHICKNESS RATIO  (D
     5OUBLER THICKNESS / SKIN THICKNESS)//
     6 15X, 75H1.0      0.9      0.8      0.7      0.6      0.5      0.4      0
     7.3      0.2      0.1/)
      DO 50 J = 1, 38
      DO 40 L = 1, 10
      RSIGAV(L) = SIGAV(J,L)
   40 CONTINUE
      WRITE (6,6) OL(J), RSIGAV
    6 FORMAT (1H , F8.2, F11.5, 9F8.5)
   50 CONTINUE
      WRITE (6,7)
    7 FORMAT (1H1, 17HPROGRAM COMPLETED)
      STOP
    8 WRITE (6,9)
    9 FORMAT  (1H1, 19HDIVERGENT ITERATION)
      STOP
      END
```

SINGLE-LAP ADHESIVE-BONDED DOUBLERS

NON-DIMENSIONALIZED FORMULATION FOR STIFFNESS IMBALANCE

BENDING STIFFNESS PARAMETER = 0.7

DOUBLER L/T PARAMETER	AVERAGE ADHEREND STRESS / MAXIMUM ADHEREND STRESS THICKNESS RATIO (DOUBLER THICKNESS / SKIN THICKNESS)									
	1.0	0.9	0.8	0.7	0.6	0.5	0.4	0.3	0.2	0.1
0.0	0.18919	0.20588	0.22581	0.25000	0.28000	0.31819	0.36842	0.43750	0.53846	0.70000
0.10	0.19322	0.21036	0.23082	0.25565	0.28642	0.32554	0.37689	0.44723	0.54929	0.71030
0.15	0.19526	0.21263	0.23336	0.25851	0.28967	0.32925	0.38115	0.45209	0.55465	0.71525
0.20	0.19732	0.21492	0.23592	0.26140	0.29294	0.33299	0.38543	0.45695	0.55997	0.72014
0.25	0.19941	0.21723	0.23850	0.26431	0.29624	0.33674	0.38971	0.46181	0.56525	0.72501
0.30	0.20151	0.21957	0.24111	0.26724	0.29956	0.34051	0.39401	0.46668	0.57048	0.72971
0.35	0.20363	0.22192	0.24374	0.27019	0.30290	0.34431	0.39832	0.47150	0.57563	0.73433
0.40	0.20577	0.22430	0.24639	0.27317	0.30626	0.34812	0.40264	0.47633	0.58082	0.73885
0.50	0.21011	0.22911	0.25176	0.27918	0.31304	0.35578	0.41129	0.48595	0.59097	0.74760
0.60	0.21454	0.23411	0.25741	0.28529	0.31990	0.36351	0.41997	0.49552	0.60093	0.75601
0.70	0.21904	0.23899	0.26275	0.29149	0.32684	0.37130	0.42866	0.50503	0.61069	0.76406
0.80	0.22365	0.24409	0.26841	0.29778	0.33389	0.37918	0.43741	0.51446	0.62025	0.77178
0.90	0.22831	0.24924	0.27413	0.30415	0.34103	0.38718	0.44611	0.52380	0.62959	0.77918
1.00	0.23306	0.25448	0.27992	0.31059	0.34814	0.39500	0.45490	0.53311	0.63872	0.78627
1.50	0.25795	0.28182	0.31013	0.34377	0.38465	0.43494	0.49777	0.57763	0.68112	0.81744
2.00	0.28465	0.31092	0.34174	0.37824	0.42190	0.47469	0.53922	0.61886	0.71811	0.84275
2.50	0.31232	0.34144	0.37458	0.41339	0.45915	0.51346	0.57933	0.65518	0.75009	0.86337
3.00	0.34252	0.37311	0.40809	0.44861	0.49564	0.55055	0.61468	0.68770	0.77762	0.88032
3.50	0.37207	0.40510	0.44165	0.48329	0.53098	0.58552	0.64802	0.71951	0.80128	0.89438
4.00	0.40383	0.43725	0.47476	0.51634	0.56451	0.61809	0.67830	0.74590	0.82166	0.90614
5.00	0.46535	0.49984	0.53794	0.57967	0.62537	0.67548	0.73020	0.79374	0.85448	0.92448
6.00	0.52389	0.55827	0.59521	0.63402	0.67751	0.72319	0.77192	0.82400	0.87933	0.93797
7.00	0.57775	0.61065	0.64551	0.68235	0.72133	0.76240	0.80556	0.85094	0.89840	0.94815
8.00	0.62572	0.65659	0.68835	0.72263	0.75787	0.79451	0.83271	0.87247	0.91343	0.95602
9.00	0.66771	0.69532	0.72534	0.75650	0.78824	0.82102	0.85481	0.89053	0.92539	0.96222
10.00	0.70424	0.73049	0.75748	0.78517	0.81370	0.84296	0.87295	0.90368	0.93506	0.96719
15.00	0.82485	0.84153	0.85459	0.87551	0.89281	0.91027	0.92749	0.94560	0.96360	0.98173
20.00	0.88604	0.89723	0.90643	0.91969	0.93100	0.94239	0.95375	0.96525	0.97678	0.98831
25.00	0.92042	0.92828	0.93606	0.94602	0.95196	0.95992	0.96790	0.97590	0.98392	0.99192
30.00	0.94133	0.94716	0.95306	0.95884	0.96476	0.97056	0.97643	0.98221	0.98815	0.99408
35.00	0.95504	0.95952	0.96400	0.96848	0.97297	0.97746	0.98198	0.98641	0.99095	0.99548
40.00	0.96446	0.96806	0.97155	0.97509	0.97864	0.98212	0.98576	0.98928	0.99286	0.99643
50.00	0.97620	0.97857	0.98095	0.98333	0.98562	0.98802	0.99043	0.99283	0.99522	0.99761
70.00	0.98723	0.98848	0.98967	0.99087	0.99227	0.99356	0.99486	0.99615	0.99743	0.99872
100.00	0.99343	0.99409	0.99475	0.99541	0.99607	0.99672	0.99738	0.99804	0.99869	0.99935
200.00	0.99823	0.99845	0.99862	0.99880	0.99897	0.99914	0.99931	0.99949	0.99966	0.99983
500.00	0.99972	0.99975	0.99977	0.99980	0.99983	0.99986	0.99989	0.99992	0.99994	0.99997
1000.00	0.99993	0.99994	0.99994	0.99995	0.99996	0.99996	0.99989	0.99992	0.99994	0.99997

SINGLE-LAP ADHESIVE-BONDED DOUBLERS

NON-DIMENSIONALIZED FORMULATION FOR STIFFNESS IMBALANCE

BENDING STIFFNESS PARAMETER = 1.0

DOUBLER L/T PARAMETER	AVERAGE ADHEREND STRESS / MAXIMUM ADHEREND STRESS THICKNESS RATIO (DOUBLER THICKNESS / SKIN THICKNESS)									
	1.0	0.9	0.8	0.7	0.6	0.5	0.4	0.3	0.2	0.1
0.0	0.25000	0.27027	0.29412	0.32258	0.35714	0.40000	0.45455	0.52632	0.62500	0.76923
0.10	0.25472	0.27543	0.29978	0.32882	0.36403	0.40765	0.46290	0.53532	0.63416	0.77681
0.15	0.25711	0.27804	0.30264	0.33196	0.36749	0.41142	0.46797	0.53978	0.63862	0.78051
0.20	0.25951	0.28066	0.30551	0.33512	0.37096	0.41523	0.47308	0.54423	0.64306	0.78412
0.25	0.26193	0.28330	0.30840	0.33829	0.37445	0.41906	0.47822	0.54865	0.64753	0.78765
0.30	0.26436	0.28595	0.31130	0.34147	0.37794	0.42293	0.47954	0.55304	0.65198	0.79110
0.35	0.26682	0.28863	0.31422	0.34467	0.38145	0.42671	0.48368	0.55741	0.65618	0.79448
0.40	0.26923	0.29131	0.31716	0.34788	0.38496	0.43054	0.48782	0.56175	0.66043	0.79779
0.50	0.27426	0.29673	0.32307	0.35433	0.39205	0.43820	0.49605	0.57034	0.66876	0.80425
0.60	0.27931	0.30221	0.32903	0.36084	0.39923	0.44586	0.50424	0.57882	0.67698	0.81039
0.70	0.28441	0.30775	0.33506	0.36738	0.40648	0.45352	0.51237	0.58717	0.68480	0.81627
0.80	0.28953	0.31335	0.34113	0.37396	0.41332	0.46117	0.52044	0.59540	0.69251	0.82191
0.90	0.29469	0.31900	0.34724	0.38058	0.42044	0.46879	0.52845	0.60349	0.70000	0.82731
1.00	0.30011	0.32474	0.35344	0.38727	0.42758	0.47639	0.53638	0.61145	0.70730	0.83248
1.50	0.32732	0.35397	0.38478	0.42081	0.46328	0.51387	0.57432	0.64912	0.74081	0.85531
2.00	0.35560	0.38403	0.41676	0.45453	0.49868	0.54994	0.61077	0.68312	0.76972	0.87395
2.50	0.38466	0.41467	0.44880	0.48730	0.53257	0.58420	0.64396	0.71351	0.79460	0.88929
3.00	0.41411	0.44534	0.48046	0.52025	0.56516	0.61622	0.67428	0.74050	0.81600	0.90204
3.50	0.44358	0.47568	0.51143	0.55134	0.59596	0.64583	0.70177	0.76439	0.83433	0.91272
4.00	0.47275	0.50534	0.54122	0.58096	0.62479	0.67312	0.72657	0.78551	0.85035	0.92176
5.00	0.52997	0.56156	0.59670	0.63497	0.67525	0.72064	0.76837	0.82068	0.87637	0.93607
6.00	0.58296	0.61235	0.64599	0.68178	0.71983	0.76016	0.80321	0.84836	0.89621	0.94679
7.00	0.62743	0.65730	0.68872	0.72172	0.75836	0.79761	0.83062	0.87035	0.91177	0.95502
8.00	0.66860	0.69544	0.72542	0.75557	0.78694	0.81937	0.85319	0.88794	0.92412	0.96147
9.00	0.70455	0.73025	0.75680	0.78414	0.81243	0.84156	0.87155	0.90234	0.93406	0.96661
10.00	0.73577	0.75937	0.78354	0.80843	0.83394	0.86007	0.88675	0.91417	0.94218	0.97071
15.00	0.83997	0.85525	0.87062	0.88625	0.90204	0.91799	0.93408	0.95028	0.96672	0.98329
20.00	0.89419	0.90453	0.91492	0.92537	0.93579	0.94638	0.95702	0.96769	0.97841	0.98913
25.00	0.92521	0.93251	0.93994	0.94738	0.95484	0.96232	0.96982	0.97733	0.98479	0.99240
30.00	0.94440	0.94992	0.95544	0.96098	0.96653	0.97208	0.97765	0.98314	0.98877	0.99439
35.00	0.95711	0.96138	0.96565	0.96993	0.97421	0.97849	0.98271	0.98704	0.99136	0.99568
40.00	0.96592	0.96932	0.97272	0.97612	0.97943	0.98286	0.98629	0.98972	0.99315	0.99658
50.00	0.97703	0.97930	0.98160	0.98389	0.98611	0.98843	0.99075	0.99307	0.99538	0.99769
70.00	0.98752	0.98867	0.98994	0.99120	0.99247	0.99373	0.99499	0.99624	0.99750	0.99875
100.00	0.99355	0.99420	0.99485	0.99549	0.99614	0.99678	0.99743	0.99807	0.99872	0.99936
200.00	0.99830	0.99847	0.99864	0.99881	0.99898	0.99915	0.99932	0.99949	0.99966	0.99983
500.00	0.99972	0.99975	0.99977	0.99980	0.99983	0.99986	0.99989	0.99992	0.99994	0.99997
1000.00	0.99993	0.99994	0.99994	0.99995	0.99996	0.99996	0.99989	0.99992	0.99994	0.99997

SINGLE-LAP ADHESIVE-BONDED DOUBLERS

NON-DIMENSIONALIZED FORMULATION FOR STIFFNESS IMBALANCE

BENDING STIFFNESS PARAMETER = 2.0

DOUBLER L/T PARAMETER	AVERAGE ADHEREND STRESS / MAXIMUM ADHEREND STRESS THICKNESS RATIO (DOUBLER THICKNESS / SKIN THICKNESS)									
	1.0	0.9	0.8	0.7	0.6	0.5	0.4	0.3	0.2	0.1
0.0	0.40000	0.42553	0.45455	0.48781	0.52632	0.57143	0.62500	0.68966	0.76923	0.86957
0.10	0.40534	0.43114	0.46041	0.49393	0.53265	0.57790	0.63147	0.69584	0.77463	0.87322
0.15	0.40934	0.43397	0.46338	0.49701	0.53583	0.58114	0.63469	0.69891	0.77729	0.87500
0.20	0.41073	0.43579	0.46632	0.50006	0.53898	0.58435	0.63787	0.70193	0.77990	0.87673
0.25	0.41365	0.43864	0.46925	0.50311	0.54212	0.58753	0.64102	0.70491	0.78246	0.87843
0.30	0.41616	0.44247	0.47224	0.50621	0.54525	0.59070	0.64415	0.70786	0.78499	0.88010
0.35	0.41886	0.44529	0.47518	0.50925	0.54843	0.59385	0.64726	0.71078	0.78748	0.88173
0.40	0.42157	0.44811	0.47812	0.51229	0.55154	0.59705	0.65034	0.71367	0.78993	0.88334
0.50	0.42693	0.45376	0.48398	0.51834	0.55772	0.60326	0.65648	0.71939	0.79469	0.88643
0.60	0.43243	0.45939	0.48982	0.52435	0.56385	0.60940	0.66247	0.72495	0.79934	0.88941
0.70	0.43792	0.46502	0.49564	0.53033	0.56992	0.61546	0.66835	0.73037	0.80393	0.89228
0.80	0.44324	0.47064	0.50144	0.53627	0.57593	0.62144	0.67412	0.73566	0.80831	0.89504
0.90	0.44864	0.47625	0.50721	0.54216	0.58189	0.62734	0.67979	0.74084	0.81256	0.89769
1.00	0.45407	0.48184	0.51295	0.54801	0.58777	0.63315	0.68536	0.74588	0.81669	0.90025
1.50	0.48122	0.50951	0.54119	0.57656	0.61623	0.66096	0.71157	0.76934	0.83550	0.91172
2.00	0.50754	0.53648	0.56840	0.60372	0.64293	0.68690	0.73541	0.79010	0.85173	0.92128
2.50	0.53341	0.56254	0.59442	0.62937	0.66779	0.71011	0.75683	0.80847	0.86576	0.92935
3.00	0.55844	0.58752	0.61910	0.65344	0.69083	0.73153	0.77611	0.82471	0.87796	0.93622
3.50	0.58249	0.61131	0.64237	0.67589	0.71207	0.75117	0.79336	0.83911	0.88869	0.94212
4.00	0.60545	0.63383	0.66421	0.69675	0.73161	0.76897	0.80895	0.85190	0.89793	0.94722
5.00	0.64791	0.67500	0.70360	0.73391	0.76507	0.79986	0.83567	0.87343	0.91341	0.95556
6.00	0.68555	0.71156	0.73767	0.76561	0.79485	0.82542	0.85730	0.89074	0.92564	0.96204
7.00	0.71953	0.74422	0.76697	0.79256	0.81912	0.84667	0.87516	0.90479	0.93546	0.96710
8.00	0.74751	0.76947	0.79213	0.81550	0.83969	0.86435	0.88996	0.91632	0.94345	0.97127
9.00	0.77273	0.79297	0.81375	0.83507	0.85695	0.87931	0.90233	0.92593	0.95003	0.97468
10.00	0.79479	0.81333	0.83238	0.85185	0.87166	0.89205	0.91276	0.93393	0.95553	0.97752
15.00	0.86978	0.88224	0.89482	0.90753	0.92036	0.93324	0.94636	0.95960	0.97295	0.98633
20.00	0.91091	0.91961	0.92826	0.93705	0.94594	0.95484	0.96379	0.97277	0.98180	0.99085
25.00	0.93537	0.94174	0.94814	0.95455	0.96099	0.96744	0.97391	0.98041	0.98697	0.99344
30.00	0.95168	0.95593	0.96079	0.96566	0.97053	0.97542	0.98032	0.98517	0.99011	0.99506
35.00	0.96170	0.96551	0.96932	0.97314	0.97696	0.98080	0.98456	0.98842	0.99228	0.99614
40.00	0.96921	0.97228	0.97535	0.97842	0.98149	0.98458	0.98762	0.99071	0.99381	0.99691
50.00	0.97986	0.98207	0.98308	0.98510	0.98724	0.98937	0.99150	0.99363	0.99576	0.99788
70.00	0.98818	0.98937	0.99056	0.99174	0.99293	0.99411	0.99529	0.99647	0.99765	0.99883
100.00	0.99394	0.99446	0.99508	0.99569	0.99631	0.99693	0.99754	0.99816	0.99877	0.99939
200.00	0.99834	0.99850	0.99867	0.99884	0.99900	0.99917	0.99934	0.99950	0.99967	0.99984
500.00	0.99972	0.99975	0.99978	0.99981	0.99983	0.99986	0.99989	0.99992	0.99994	0.99997
1000.00	0.99993	0.99994	0.99994	0.99995	0.99996	0.99996	0.99998	0.99998	0.99998	0.99999

```
C SINGLE-LAP ADHESIVE-BONDED DOUBLERS
C ADHEREND PLASTIC HINGE FORMATION (OR FRACTURE) - UNBALANCED STIFFNESS
C ADHEREND BENDING AND EXTENSIONAL STIFFNESSES UNCOUPLED FOR COMPOSITES
C NON-DIMENSIONALIZED FORMULATION
      DIMENSION OL(38), SIGAV(38,10), RSIGAV(10), BENDK(13)
C SET OVERLAP ARRAY
      OL(1) = 0.
      OL(2) = 0.1
      OL(3) = 0.15
      OL(4) = 0.2
      OL(5) = 0.25
      OL(6) = 0.3
      OL(7) = 0.35
      OL(8) = 0.4
      OL(9) = 0.5
      OL(10) = 0.6
      OL(11) = 0.7
      OL(12) = 0.8
      OL(13) = 0.9
      OL(14) = 1.
      OL(15) = 1.5
      OL(16) = 2.
      OL(17) = 2.5
      OL(18) = 3.
      OL(19) = 3.5
      OL(20) = 4.
      OL(21) = 5.
      OL(22) = 6.
      OL(23) = 7.
      OL(24) = 8.
      OL(25) = 9.
      OL(26) = 10.
      OL(27) = 15.
      OL(28) = 20.
      OL(29) = 25.
      OL(30) = 30.
      OL(31) = 35.
      OL(32) = 40.
      OL(33) = 50.
      OL(34) = 70.
      OL(35) = 100.
      OL(36) = 200.
      OL(37) = 500.
      OL(38) = 1000.
C SET BENDING STIFFNESS PARAMETER ARRAY
      BENDK(1) = 0.1
      BENDK(2) = 0.15
      BENDK(3) = 0.2
      BENDK(4) = 0.3
      BENDK(5) = 0.5
      BENDK(6) = 0.7
      BENDK(7) = 1.
      BENDK(8) = 1.5
      BENDK(9) = 2.
      BENDK(10) = 3.
      BENDK(11) = 5.
      BENDK(12) = 7.
      BENDK(13) = 10.
C SELECT BENDING STIFFNESS PARAMETER
      DO 50 M = 1, 13
C SET ADHEREND THICKNESS RATIO
      TR = 11.
      DO 30 K = 1, 10
      TR = TR - 1.
      T1OVT4 = TR / 10.
      D1OVD4 = T1OVT4 ** 3
C SET INITIAL ESTIMATE ON AVERAGE ADHEREND STRESS
      V3 = 1. / (1. + (3. / BENDK(M)) * T1OVT4)
      SIGAV(1,K) = V3
      DO 20 J = 2, 38
C SET NON-DIMENSIONALIZED OVERLAP
      V2 = OL(J) ** 2
      N = 0
    1 N = N + 1
      IF (N .GT. 500) GO TO 8
C PROGRAM USES L(DOUBLER) / T(SKIN) AS L/T RATIO
      V10 = V3 * V2 / BENDK(M)
C TO USE L/T RATIO FOR DOUBLER INSTEAD OF SKIN, USE
C     V10 = V3 * V2 * D1OVD4 / BENDK(M)
C FOR SIMPLY-SUPPORTED ENDS OF SKIN-DOUBLER COMBINATION
      V8 = 1. + SQRT(V10) + V10 / 6.
C FOR BUILT-IN ENDS OF SKIN-DOUBLER COMBINATION
C     V8 = 1. + (SQRT(V10)) / 2. + V10 / 24.
C EVALUATE ECCENTRICITY PARAMETER
C     EK = 1. / V8
C RE-ESTIMATE AVERAGE SKIN STRESS
      V4 = 1. / (1. + (3. / BENDK(M)) * (T1OVT4 / V8))
C CHECK CONVERGENCE OF AVERAGE STRESS
```

```
      R = V3 / V4
      IF ( (1.0001 .GT. R) .AND. (0.9999 .LT. R) ) GO TO 20
      V3 = V4
      GO TO 1
C EVALUATE AVERAGE SKIN STRESS AT LIMIT LOAD
C (YIELD STRENGTH FOR METALS - ULTIMATE STRENGTH FOR COMPOSITES)
   20 SIGAV (J,K) = V3
   30 CONTINUE
C PRINT OUT TABULATIONS
      WRITE (6,5) BENDK(M)
    5 FORMAT (1H1,  5(/), 30X, 35HSINGLE-LAP ADHESIVE-BONDED DOUBLERS//
     1 20X, 55HNON-DIMENSIONALIZED FORMULATION FOR STIFFNESS IMBALANCE//
     2 30X, 30HBENDING STIFFNESS PARAMETER =  , F5.1///
     3 3X, 7HDOUBLER, 18X, 49HAVERAGE ADHEREND STRESS / MAXIMUM ADHEREND
     4 STRESS/, 5X, 3HL/T/, 3X, 9HPARAMETER, 14X, 53HTHICKNESS RATIO  (D
     5OUBLER THICKNESS / SKIN THICKNESS)//
     6 15X, 75H1.0      0.9      0.8      0.7      0.6      0.5      0.4      0
     7.3      0.2      0.1/)
      DO 50 J = 1, 38
      DO 40 L = 1, 10
      RSIGAV(L) = SIGAV(J,L)
   40 CONTINUE
      WRITE (6,6) QL(J), RSIGAV
    6 FORMAT (1H , F8.2, F11.5, 9F8.5)
   50 CONTINUE
      WRITE (6,7)
    7 FORMAT (1H1, 17HPROGRAM COMPLETED)
      STOP
    8 WRITE (6,9)
    9 FORMAT  (1H1, 19HDIVERGENT ITERATION)
      STOP
      END
```

SINGLE-LAP ADHESIVE-BONDED DOUBLERS

NON-DIMENSIONALIZED FORMULATION FOR STIFFNESS IMBALANCE

BENDING STIFFNESS PARAMETER = 0.7

DOUBLER L/T PARAMETER	AVERAGE ADHEREND STRESS / MAXIMUM ADHEREND STRESS THICKNESS RATIO (DOUBLER THICKNESS / SKIN THICKNESS)								
	1.0	0.9	0.8	0.7	0.6	0.5	0.4	0.3	0.2	0.1
0.0	0.18919	0.20548	0.22541	0.25000	0.28000	0.31819	0.36842	0.43750	0.53846	0.70000
0.10	0.19732	0.21482	0.23631	0.26138	0.29294	0.33293	0.38542	0.45695	0.55996	0.72020
0.15	0.20151	0.21957	0.24111	0.26723	0.29955	0.34051	0.39401	0.46665	0.57048	0.72971
0.20	0.20577	0.22440	0.24639	0.27316	0.30625	0.34811	0.40263	0.47632	0.58082	0.73884
0.25	0.21011	0.22911	0.25176	0.27918	0.31304	0.35578	0.41129	0.48595	0.59097	0.74760
0.30	0.21454	0.23401	0.25721	0.28529	0.31992	0.36351	0.41997	0.49552	0.60093	0.75601
0.35	0.21904	0.23899	0.26275	0.29148	0.32688	0.37130	0.42866	0.50503	0.61069	0.76406
0.40	0.22365	0.24403	0.26841	0.29779	0.33395	0.37918	0.43741	0.51446	0.62025	0.77178
0.50	0.23309	0.25447	0.27992	0.31058	0.34813	0.39520	0.45480	0.53310	0.63876	0.78625
0.60	0.24278	0.26513	0.29174	0.32366	0.36260	0.41093	0.47211	0.55129	0.65637	0.79955
0.70	0.25281	0.27613	0.30395	0.33722	0.37725	0.42692	0.49026	0.56900	0.67310	0.81176
0.80	0.26313	0.28743	0.31624	0.35056	0.39255	0.44291	0.50619	0.58619	0.68836	0.82298
0.90	0.27377	0.29909	0.32940	0.36434	0.40794	0.45884	0.52235	0.60281	0.70396	0.83330
1.00	0.28466	0.31083	0.34175	0.37905	0.42432	0.47460	0.53918	0.61843	0.71813	0.84279
1.50	0.34251	0.37322	0.40858	0.44804	0.49571	0.55053	0.61466	0.68974	0.77759	0.88035
2.00	0.40385	0.43763	0.47475	0.51698	0.56453	0.61823	0.67329	0.74593	0.82165	0.90611
2.50	0.46535	0.49934	0.53704	0.57967	0.62237	0.67548	0.72220	0.78974	0.85448	0.92448
3.00	0.52399	0.55627	0.59521	0.63492	0.67751	0.72319	0.76192	0.82400	0.87933	0.93797
3.50	0.57775	0.60765	0.64655	0.68233	0.72132	0.76240	0.80556	0.85094	0.89840	0.94815
4.00	0.62572	0.65358	0.69096	0.72267	0.75767	0.79451	0.83271	0.87237	0.91343	0.95602
5.00	0.70427	0.73144	0.76746	0.78522	0.81373	0.84293	0.87293	0.90365	0.93503	0.96719
6.00	0.76806	0.79406	0.82028	0.83993	0.86334	0.87962	0.90655	0.92479	0.94951	0.97458
7.00	0.82709	0.84526	0.86341	0.88155	0.89375	0.92015	0.93378	0.95465	0.96165	0.97965
8.00	0.86037	0.87573	0.89122	0.90686	0.92263	0.93853	0.94453	0.95972	0.96702	0.98340
9.00	0.88604	0.89905	0.91215	0.92534	0.93855	0.94540	0.95193	0.96493	0.97254	0.98620
10.00	0.90511	0.91725	0.92836	0.93964	0.94987	0.95376	0.95526	0.96231	0.97671	0.98835
15.00	0.94137	0.94719	0.95295	0.95881	0.96463	0.97055	0.97642	0.98231	0.98820	0.99406
20.00	0.96444	0.96709	0.97154	0.97529	0.97964	0.98220	0.98575	0.98924	0.99284	0.99643
25.00	0.97620	0.97857	0.98095	0.98333	0.98662	0.98862	0.99043	0.99233	0.99522	0.99761
30.00	0.98206	0.98457	0.98629	0.98801	0.98973	0.99145	0.99316	0.99487	0.99658	0.99829
35.00	0.98715	0.98844	0.98972	0.99101	0.99230	0.99358	0.99487	0.99615	0.99744	0.99872
40.00	0.99001	0.99101	0.99201	0.99301	0.99401	0.99501	0.99601	0.99701	0.99801	0.99900
50.00	0.99345	0.99410	0.99476	0.99542	0.99607	0.99673	0.99738	0.99804	0.99869	0.99935
70.00	0.99657	0.99691	0.99725	0.99760	0.99794	0.99829	0.99863	0.99897	0.99931	0.99966
100.00	0.99828	0.99846	0.99863	0.99880	0.99897	0.99914	0.99931	0.99949	0.99966	0.99983
200.00	0.99956	0.99961	0.99965	0.99969	0.99974	0.99978	0.99982	0.99987	0.99991	0.99996
500.00	0.99983	0.99984	0.99984	0.99985	0.99986	0.99986	0.99987	0.99988	0.99991	0.99996
1000.00	0.99993	0.99994	0.99994	0.99995	0.99996	0.99996	0.99997	0.99998	0.99991	0.99996

SINGLE-LAP ADHESIVE-BONDED DOUBLERS

NON-DIMENSIONALIZED FORMULATION FOR STIFFNESS IMBALANCE

BENDING STIFFNESS PARAMETER = 1.0

DOUBLER L/T PARAMETER	AVERAGE ADHEREND STRESS / MAXIMUM ADHEREND STRESS THICKNESS RATIO (DOUBLER THICKNESS / SKIN THICKNESS)								
	1.0	0.9	0.8	0.7	0.6	0.5	0.4	0.3	0.2	0.1
0.0	0.25000	0.27027	0.29412	0.32258	0.35714	0.40000	0.45455	0.52632	0.62500	0.76923
0.10	0.25951	0.28060	0.30551	0.33611	0.37096	0.41523	0.47123	0.54422	0.64312	0.78415
0.15	0.26436	0.28595	0.31136	0.34147	0.37704	0.42208	0.47954	0.55364	0.65188	0.79114
0.20	0.26928	0.29131	0.31716	0.34747	0.38353	0.42930	0.48781	0.56175	0.66042	0.79784
0.25	0.27426	0.29674	0.32307	0.35433	0.39077	0.43820	0.49656	0.57034	0.66876	0.80425
0.30	0.27931	0.30221	0.32903	0.36093	0.39808	0.44586	0.50424	0.57892	0.67688	0.81039
0.35	0.28441	0.30775	0.33506	0.36738	0.40518	0.45352	0.51267	0.58717	0.68480	0.81627
0.40	0.28958	0.31335	0.34113	0.37396	0.41330	0.46117	0.52044	0.59546	0.69251	0.82191
0.50	0.30011	0.32473	0.35344	0.38726	0.42762	0.47643	0.53442	0.61142	0.70729	0.83248
0.60	0.31084	0.33629	0.36589	0.40064	0.44193	0.49154	0.55234	0.62697	0.72126	0.84219
0.70	0.32177	0.34803	0.37847	0.41409	0.45619	0.50649	0.56734	0.64189	0.73446	0.85113
0.80	0.33288	0.35992	0.39117	0.42754	0.47033	0.52124	0.58224	0.65623	0.74690	0.85936
0.90	0.34416	0.37194	0.40393	0.44106	0.48450	0.53574	0.59673	0.66997	0.75863	0.86695
1.00	0.35558	0.38406	0.41674	0.45451	0.49846	0.54997	0.61080	0.68313	0.76968	0.87397
1.50	0.41412	0.44535	0.48047	0.52018	0.56515	0.61621	0.67431	0.74047	0.81599	0.90201
2.00	0.47278	0.50536	0.54125	0.58094	0.62477	0.67317	0.72552	0.78549	0.85041	0.92174
2.50	0.52897	0.56156	0.59679	0.63497	0.67425	0.72084	0.76887	0.82068	0.87637	0.93607
3.00	0.58086	0.61235	0.64599	0.68174	0.71943	0.76016	0.80301	0.84836	0.89621	0.94679
3.50	0.62743	0.65736	0.68872	0.72172	0.75835	0.79261	0.83062	0.87035	0.91177	0.95502
4.00	0.66842	0.69644	0.72542	0.75557	0.79084	0.81937	0.85310	0.88794	0.92412	0.96147
5.00	0.73574	0.75935	0.78359	0.80845	0.83390	0.86005	0.88682	0.91412	0.94217	0.97079
6.00	0.78628	0.80677	0.82616	0.84669	0.86757	0.88879	0.91027	0.93222	0.95450	0.97709
7.00	0.82437	0.84102	0.85787	0.87493	0.89213	0.90958	0.92729	0.94519	0.96327	0.98148
8.00	0.85360	0.86767	0.88187	0.89620	0.91063	0.92519	0.93992	0.95477	0.96973	0.98477
9.00	0.87630	0.88830	0.90039	0.91249	0.92477	0.93712	0.94954	0.96204	0.97453	0.98725
10.00	0.89421	0.90446	0.91487	0.92534	0.93585	0.94642	0.95723	0.96776	0.97835	0.98917
15.00	0.94443	0.94986	0.95541	0.96096	0.96651	0.97208	0.97764	0.98322	0.98871	0.99437
20.00	0.96591	0.96931	0.97271	0.97611	0.97952	0.98292	0.98633	0.98969	0.99314	0.99657
25.00	0.97706	0.97930	0.98156	0.98389	0.98611	0.98843	0.99075	0.99307	0.99538	0.99769
30.00	0.98335	0.98502	0.98669	0.98836	0.99003	0.99169	0.99336	0.99502	0.99668	0.99834
35.00	0.98747	0.98873	0.98998	0.99124	0.99249	0.99375	0.99500	0.99626	0.99750	0.99875
40.00	0.99023	0.99121	0.99219	0.99317	0.99414	0.99512	0.99610	0.99707	0.99805	0.99903
50.00	0.99357	0.99421	0.99484	0.99550	0.99614	0.99679	0.99743	0.99807	0.99872	0.99936
70.00	0.99661	0.99695	0.99729	0.99763	0.99797	0.99831	0.99865	0.99899	0.99932	0.99966
100.00	0.99830	0.99847	0.99864	0.99881	0.99898	0.99915	0.99932	0.99949	0.99966	0.99983
200.00	0.99956	0.99961	0.99965	0.99969	0.99974	0.99978	0.99983	0.99987	0.99991	0.99996
500.00	0.99983	0.99984	0.99984	0.99985	0.99986	0.99986	0.99987	0.99988	0.99991	0.99996
1000.00	0.99993	0.99994	0.99994	0.99995	0.99996	0.99996	0.99997	0.99998	0.99991	0.99996

SINGLE-LAP ADHESIVE-BONDED DOUBLERS

NON-DIMENSIONALIZED FORMULATION FOR STIFFNESS IMBALANCE

BENDING STIFFNESS PARAMETER = 2.0

DOUBLER L/T PARAMETER	AVERAGE ADHEREND STRESS / MAXIMUM ADHEREND STRESS THICKNESS RATIO (DOUBLER THICKNESS / SKIN THICKNESS)								
	1.0	0.9	0.8	0.7	0.6	0.5	0.4	0.3	0.2	0.1
0.0	0.40000	0.42553	0.45455	0.48781	0.52632	0.57143	0.62500	0.68966	0.76923	0.86957
0.10	0.41075	0.43632	0.46535	0.50010	0.53962	0.58439	0.63790	0.70195	0.77934	0.87671
0.15	0.41616	0.44247	0.47224	0.50821	0.54930	0.59575	0.64920	0.70790	0.78497	0.88009
0.20	0.42157	0.44911	0.47812	0.51239	0.55154	0.59765	0.65039	0.71371	0.78990	0.88332
0.25	0.42693	0.45375	0.48398	0.51834	0.55772	0.60326	0.65644	0.71939	0.79469	0.88643
0.30	0.43245	0.45939	0.48982	0.52435	0.56555	0.60940	0.66247	0.72495	0.79934	0.88941
0.35	0.43782	0.46502	0.49564	0.53033	0.56992	0.61545	0.66835	0.73037	0.80393	0.89228
0.40	0.44324	0.47064	0.50144	0.53627	0.57593	0.62144	0.67415	0.73566	0.80831	0.89504
0.50	0.45406	0.48182	0.51294	0.54800	0.58775	0.63314	0.68535	0.74599	0.81644	0.90021
0.60	0.46486	0.49295	0.52432	0.55955	0.59933	0.64451	0.69616	0.75582	0.82456	0.90504
0.70	0.47567	0.50404	0.53557	0.57091	0.61064	0.65554	0.70657	0.76489	0.83197	0.90952
0.80	0.48638	0.51498	0.54673	0.58206	0.62167	0.66622	0.71656	0.77372	0.83835	0.91369
0.90	0.49701	0.52582	0.55766	0.59298	0.63242	0.67655	0.72617	0.78213	0.84553	0.91753
1.00	0.50755	0.53649	0.56841	0.60373	0.64289	0.68655	0.73538	0.79013	0.85174	0.92121
1.50	0.55847	0.58755	0.61907	0.65341	0.69081	0.73158	0.77613	0.82475	0.87794	0.93621
2.00	0.60549	0.63388	0.66418	0.69672	0.73159	0.76896	0.80931	0.85185	0.89791	0.94722
2.50	0.64701	0.67502	0.70360	0.73331	0.76547	0.79935	0.83780	0.88074	0.91554	0.95564
3.00	0.68555	0.71033	0.73967	0.76561	0.79485	0.82547	0.86516	0.90479	0.93545	0.96210
3.50	0.71859	0.74232	0.76897	0.79256	0.81912	0.84667	0.87496	0.91632	0.94345	0.96727
4.00	0.74751	0.76947	0.79213	0.81550	0.83959	0.86435	0.89096	0.92632	0.95053	0.97147
5.00	0.79466	0.81331	0.83236	0.85184	0.87173	0.89204	0.91273	0.93982	0.96153	0.97884
6.00	0.83054	0.84944	0.86249	0.87879	0.89535	0.91216	0.93019	0.95464	0.96910	0.98188
7.00	0.85835	0.87120	0.88541	0.89910	0.91306	0.92717	0.94149	0.95984	0.97041	0.98510
8.00	0.87997	0.89152	0.90309	0.91436	0.92673	0.93967	0.95276	0.96642	0.97862	0.98739
9.00	0.89724	0.90705	0.91711	0.92724	0.93743	0.94770	0.95802	0.96842	0.97859	0.98947
10.00	0.91047	0.91957	0.92883	0.93712	0.94597	0.95488	0.96378	0.97259	0.98177	0.99087
15.00	0.95104	0.95599	0.96077	0.96564	0.97052	0.97541	0.98031	0.98522	0.99007	0.99505
20.00	0.96921	0.97227	0.97534	0.97841	0.98149	0.98457	0.98757	0.99059	0.99362	0.99696
25.00	0.97886	0.98097	0.98308	0.98511	0.98724	0.98937	0.99150	0.99363	0.99576	0.99788
30.00	0.98452	0.98607	0.98762	0.98917	0.99072	0.99227	0.99382	0.99537	0.99691	0.99846
35.00	0.98824	0.98942	0.99060	0.99177	0.99295	0.99413	0.99531	0.99645	0.99765	0.99883
40.00	0.99076	0.99169	0.99261	0.99354	0.99446	0.99539	0.99631	0.99723	0.99816	0.99908
50.00	0.99346	0.99417	0.99509	0.99570	0.99632	0.99693	0.99755	0.99816	0.99877	0.99939
70.00	0.99572	0.99626	0.99738	0.99771	0.99804	0.99836	0.99869	0.99902	0.99935	0.99967
100.00	0.99734	0.99751	0.99767	0.99784	0.99801	0.99817	0.99834	0.99850	0.99867	0.99884
200.00	0.99857	0.99861	0.99865	0.99870	0.99874	0.99878	0.99883	0.99887	0.99891	0.99896
500.00	0.99943	0.99944	0.99944	0.99945	0.99945	0.99946	0.99946	0.99947	0.99948	0.99948
1000.00	0.99971	0.99972	0.99972	0.99973	0.99973	0.99973	0.99973	0.99974	0.99974	0.99974